Reversible enzyme phosphorylation as a mechanism for metabolic adaptation to dehydration in the skeletal muscle of the African clawed frog, *Xenopus laevis*.

by

Christine L. Childers
M.Sc. Carleton University
B.Sc. St. Francis Xavier University

A thesis submitted to the Faculty of Graduate and Postdoctoral Affairs in partial fulfillment of the requirements for the degree of

Doctor of Philosophy

in

Department of Biology

Carleton University
Ottawa, Ontario

The undersigned hereby recommend to the Faculty of Graduate Studies and Research acceptance of this thesis:

Reversible enzyme phosphorylation as a mechanism for metabolic adaptation to dehydration in the skeletal muscle of the African clawed frog, *Xenopus laevis.*

Submitted by

Christine L. Childers

B.Sc., M.Sc.

In partial fulfillment of the requirements for the degree of Doctor of Philosophy

_____

Chair, Department of Biology

_____

Thesis Supervisor

_____

External Examiner

Carleton University

Abstract

Xenopus laevis, although mainly an aquatic frog, lives in seasonally arid regions of southern Africa where well-developed dehydration tolerance is needed when ponds dry up. Frogs can endure about 40% loss of total body water leading to increased hematocrit and blood viscosity that restrict blood and oxygen delivery to tissues, elevate tissue osmolality, and lead to accumulation of lactate and urea. As one response to dehydration, frogs show restricted blood flow to skeletal muscle to preferentially maintain supply to the brain and internal organs. I hypothesized that dehydration stress triggers modifications to cellular energy production in skeletal muscle and could recruit alternative fuel use. This thesis explores metabolic regulation of enzymes (aldolase, CK, IDH), and energy stress signaling (via AMPK) in skeletal muscle of *X. laevis*. A particular focus was put on regulation via protein posttranslational phosphorylation to adapt enzyme activity and substrate affinity to changing physiological needs during dehydration. Analysis of kinetic parameters found that aldolase, CK and IDH all showed reduced maximal velocities and altered substrate affinities during dehydration. Downregulation of aldolase suggested a reduction in glycolytic rate during dehydration, moderating the use of glucose, whereas CK regulation modulates phosphocreatine consumption. Substrate affinities of both CK and IDH were dependent on magnesium concentrations. CK was more active at higher Mg^{2+} concentrations that occur as tissues dehydrate whereas IDH showed increased affinity for Mg^{2+} that could shift the reaction to favor α-KG production during dehydration. I hypothesized that changes to muscle energetics would stimulate the action of AMPK and its downstream effectors to promote a fuel switching from carbohydrates to include fats during dehydration. However,

phosphorylated AMPK (activated) did not increase and the regulation of two key downstream AMPK targets, acetyl-coA carboxylase and Unc-51 like autophagy activating kinase 1, did not indicate recruitment of fatty acid metabolism or autophagy for energy during dehydration in skeletal muscle. Overall, these studies showed that reversible protein phosphorylation has a prominent role in controlling *X. laevis* skeletal muscle enzyme function and reorganization of metabolic pathways during whole animal dehydration.

Acknowledgements

Ken, this has been a process. Thank you for all the opportunities, advice and direction over these several years. I am very grateful for my time here; you've allowed me to grow into something even I could not have dreamt up when I walked in here so many years ago. Almost more importantly, thank you Jan. You are such a critical shelter in the storm for so many of us here. I could not have navigated doctoral studies without your calm advice and savage editing. You are truly one of a kind and everyone should get themselves a Jan if possible.

Thank you to Dr. Tyler Avis and Dr. Tom Moon, for all your support over my masters and doctoral studies. I would not have made it this far without your time and energy and can't thank you enough for the role you've had in my scientific development.

A big thank you to all my friends. Tanya, thanks for sticking it out with me and keeping me in the real world. Thank you, Margie, Jac, Lisa, Amanda and Bailey. You're all nuts and you inspire me constantly. I look forward to more adventures from our endless friendship. Thank you to all of Storey lab and the variety of characters within. You have all taught me something. Thank you for the many coffee breaks and endless support given throughout these years. A special thanks to Bryan. He knows why.

I'd like to say an enormous THANK YOU to my family. You all have endured so many walk-n-talks, struggle busses, bird-like mockery and celebrations throughout this process. Mom thank you for listening to all the changing life plans, struggles and ever fluctuating due dates. Dad, thank you for reminding me to keep the bigger picture in mind and Rob, thanks for setting an epic example of how to be a boss. You always take the right path for you and your bravery constantly impresses and inspires me. The ice cream I need to buy you all is not enough to do this justice. I am so proud to be the second Dr. Childers with you all at my back.

Finally, Jordan, thank you. Thank you for being there for me through the late nights, the tears, the triumphs, the fomo and the yolo. Your kindness and patience are legendary. I would not trade this past year with you for anything.

Table of Contents

List of Abbreviations

- ACC Acetyl-CoA Carboxylase
- ADP Adenosine Diphosphate
- Akt Protein Kinase B
- α-KG Alpha Ketoglutarate
- AMP Adenosine Monophosphate
- AMPK 5' AMP-activated protein kinase
- ATP Adenosine Triphosphate
- β-GP Beta Glycerophosphate
- BWC_i initial body water content
- CAMK Ca2+/calmodulin-dependent protein kinase
- CK Creatine Kinase
- CPT1 Carnitine Palmitoyltransferase
- C-raf proto-oncogene serine/threonine-protein kinase
- DHAP Dihydroxyacetone Phosphate
- DSF Differential Scanning Fluorimetry
- EDTA Ethylene Diamine Tetraacetic Acid
- EGTA Ethylene Glycol Tetraacetic Acid
- ERK extracellular signal–regulated kinase
- $F1,6P_2$ Fructose 1,6-bisphosphate
- F1P Fructose-1-phosphate
- FOXO Forkhead box class O
- G6P Glucose 6 phosphate
- GAP Glyceraldehyde 3-phosphate
- GDH Glutamate Dehydrogenase
- GLUT4 insulin-regulated glucose transporter
- HEPES 4-(2-Hydroxyethyl)-1-piperazineethanesulfonic acid
- HK Hexokinase
- HRP Horseradish Peroxidase
- I_{50} half maximal inhibitory concentration

- IDH1 NADP-dependent isocitrate dehydrogenase (cytosol)
- K_a half maximal activating concentration
- KCl Potassium Chloride
- KH_2PO_4 Monopotassium Phosphate
- K_m Substrate affinity constant
- LC-MS/MS Liquid chromatography–mass spectrometry (2 analyzers)
- LDH Lactate Dehydrogenase
- MAPK Mitogen activated protein kinase
- m_d dehydrated mass
- MES 2-(N-morpholino)ethanesulfonic acid
- $MgCl_2$ Magnesium Chloride
- m_i initial mass
- mTOR mammalian Target Of Rapamycin
- Na_2PO_4 Monosodium Phosphates
- NaCl Sodium Chloride
- NAD Nicotinamide Adenine Dinucleotide
- NADH Nicotinamide Adenine Dinucleotide, reduced form
- NADP Nicotinamide Adenine Dinucleotide Phosphate
- NADPH Nicotinamide Adenine Dinucleotide Phosphate, reduced form
- NaF Sodium Fluoride
- PAGE PolyAcrylamide Gel Electrophoresis
- P-Cr Phosphocreatine
- PEG Polyethylene glycol
- PK Pyruvate Kinase
- PKA Protein Kinase A
- PKC Protein Kinase C
- PKG Protein Kinase G
- PMA Phorbol myristate acetate
- PMSF Phenylmethylsulfonyl Fluoride
- PP1 Protein phosphatase type-1
- PP2A Protein phosphatase 2A

- PP2A Protein phosphatase type-2A
- PP2B Protein phosphatase 2B
- PP2B Protein phosphatase type-2B
- PP2C Protein phosphatase type-2C
- Ppase Protein phosphatase
- PRAS40 Proline-Rich Akt-Substrate 40
- PVDF Polyvinylidene Difluoride
- RSK1 Ribosomal protein S6 kinase alpha-1
- SDS Sodium Dodecyl Sulfate
- SEM Standard Error of the Mean
- Ser Serine
- STAT3 Signal transducer and activator of transcription 3
- TBS Tris-buffered saline
- TBST TBS containing the detergent Tween-20
- TCA Tricarboxylic Acid Cycle
- Thr Threonine
- T_m half maximal unfolding temperature
- TSC2 Tuberous Sclerosis Complex 2
- Tyr Tyrosine
- ULK1 Unc-51 Like Autophagy Activating Kinase 1
- V_{max} Maximal enzyme velocity

List of Definitions

Aldolase	Used in reference to fructose-1,6-bisphosphate aldolase
Medium dehydrated	Used to indicate if the tissue or enzyme is from animals that were dehydrated to ~16% total body water loss.
High dehydrated	Used to indicate if the tissue or enzyme is from animals that were dehydrated to ~30% total body water loss

List of Appendices

List of Figures

.

List of Tables

Chapter 1: General Introduction

1.1 Introduction

Hydration is important to all animals and changes to body water content often have stressful consequences that trigger homeostatic responses to maintain the ionic and osmotic balance in most species. Organisms have developed a defined combination of these mechanisms when in need of protection, particularly against dehydration. It is important to understand the biochemical and physiological interplay in dehydration tolerance of different cells or organisms, in order to apply this knowledge to further biotechnological benefits. Currently research on dehydration resistance ranges from micro fauna that can survive total dehydration (anhydrobiosis) to human research that focuses on the effects of dehydration on physical performance and cognition (Gibbs 2002; Sawka et al. 2015; Pross 2017). As such, dehydration has been extensively examined at a physiological level in many species such as tardigrades (Somme 1993), brine shrimp (Hand and Menze 2015), and salamanders (Stefanski et al. 1989), with tolerances ranging from 15% to total body water lost . Less is known however, about the cellular adaptive responses at the level of protein regulation and cellular metabolic pathways. Amphibians are a useful model for dehydration studies since they are uniquely sensitive to water balance, due to their permeable skin and variable habitats. Many species employ a range of survival strategies for maintaining water balance during periods of dehydration. All dehydrated amphibians accumulate urea to combat water loss and produce a less toxic end point for nitrogen catabolism (Uchiyama and Konno 2006). Some have large urinary bladders to combat water loss and some create a mucus cocoon to shield themselves from the drying environment (Withers 1993; Uchiyama and Konno 2006). *Xenopus laevis* however does not employ these strategies and relies solely on urea

production to combat water loss. Water loss in frogs and toads inevitably induces significant cardiovascular and metabolic change requiring the animals to adapt, often through drastic metabolic rate reductions as seen in *Rana sylvatica* (Sinclair et al. 2013) and *Scaphiopus couchii* (Seymour 1973). *X. laevis* is not know to use this strategy and thus the cellular enzymatic responses to whole-body dehydration in this amphibian is the focus of this thesis. The aim is to study the mechanisms by which *X. laevis* can adapt their metabolic processes to tolerate their changing environments.

1.2 Whole-body dehydration in *X. laevis*

The African clawed frog, *X. laevis*, is a primarily aquatic species but still must deal with annual periods of drought in its native habitat during the dry season of sub-Saharan Africa. The seasonal drying and loss of available water pools forces *X. laevis* to take one of two options: risk a migration to other aquatic habitats or burrow into the mud and enter a state of stasis termed estivation (Alexander and Bellerby 1938; Bellerby 1938; Balinsky et al. 1967; Measey and Tinsley 1998; Eggert and Fouquet 2006). Estivation is classically characterized by whole body water loss, urea accumulation, and entrance into metabolic rate depression that can last for months (Guppy and Withers 1999; Storey and Storey 2012). *X. laevis* is unique amongst dehydration tolerant frogs in that although it accumulates urea and withstands dehydration for an extended period, it has not been demonstrated to lower its metabolic rate. Furthermore, due to the aquatic nature of *X. laevis*, African clawed frogs do not have large urinary bladders that can significantly buffer water loss by drawing on a water reservoir from the bladder (*X. laevis* bladder volume may be only ~1% of body mass) (Hillman 1978a). Ultimately, *X. laevis* must rely

heavily on cellular molecular responses to deal with dehydration, which do enable these frogs to endure a substantial loss of body water (as high as 35%) as their natural habitats get continually drier. These frogs are therefore an interesting model to study the cellular responses to vertebrate whole-body dehydration.

For most of the year, *X. laevis* excretes nitrogenous waste as ammonium ions directly into its aquatic habitat. As these frogs lose that habitat and begin to dehydrate, they reduce ammonia production and instead channel nitrogen into the synthesis of urea, noted by a significant upregulation of urea cycle enzymes (Janssens and Cohen 2003). Certainly, ammonium ion levels do still increase in blood plasma (2-fold), liver (2-fold), and skeletal muscle (3-fold) during dehydration. However, as *X. laevis* dehydrate they show reduced ammonia excretion and urea concentrations in blood plasma (16-fold), red cell (>4-fold), whole blood (>6-fold), liver (22-fold), and skeletal muscle (20-fold) increase dramatically (Balinsky et al. 1961, 1967; Jokumsen and Weber 1980). By elevating this less toxic and non-ionic osmolyte the animal can tolerate the accumulation of urea and use this osmolyte to help resist water loss across the amphibians' water-permeable skin (Balinsky et al. 1961; Jørgensen 1997).

The other notable consequence of dehydration in these frogs is an interruption of usual blood circulation. An analysis of *X. laevis* plasma has shown that concentrations of sodium, potassium, and chloride ions all increase over time, as would be predicted as dehydration proceeds (Hillman 1978b). However, plasma volume appears to decrease faster than expected, and an opposite increase in hematocrit is observed (Hillman 1978b). As blood plasma volume decreases, and hematocrit and blood viscosity increase,

X. laevis show a tissue-specific response with respect to osmoregulatory processes (Hillman 1978a; Hillman and Sommerfeldt 1981). Studies revealed that both the ventricle and gastrocnemius muscle had greater water contents than were predicted from the extent of whole-body dehydration (Hillman 1978a). This indicates a homeostatic mechanism that prioritizes intracellular water maintenance in muscle tissues. This is understandable as it has also been demonstrated that water content maintains tetanic tension development and, therefore, any early dehydration-induced loss of muscle water would hamper muscle function (Hillman 1978a). Further studies using microspheres to track blood circulation during dehydration in *X. laevis* however, demonstrated that skeletal muscle water content is prioritized last among other vital organs (Hillman and Sommerfeldt 1981). In all tissues analyzed, systemic blood circulation did not appear to be affected by dehydration, except for skeletal muscle tissues and the brain. Dehydration was found to increase blood circulation to the brain while microsphere circulation to skeletal muscle tissues decreased as dehydration progressed (Hillman and Sommerfeldt 1981). Ultimately water and blood circulation are regulated in a way that protects higher order tissues such as the brain and vital core organs at the expense of extracellular components and skeletal muscle. Thus, the tissue-specific molecular regulation of skeletal muscle metabolism, and energy homeostasis, during whole animal dehydration in *X. laevis* is particularly interesting.

1.3 Metabolic Enzymes

Unlike some terrestrial amphibians that lower their metabolic rate in response to dehydration, *X. laevis* carefully regulates cellular metabolism to accommodate the tissue-specific homeostatic and circulatory response to dehydration. In accordance with the

tissue-specific physiological changes observed during dehydration in *X. laevis*, various metabolic enzymes are also differentially regulated in a tissue-specific manner (Katzenback et al. 2014; Childers and Storey 2016, 2019). Studies of the properties of purified glycolytic enzymes from hydrated and dehydrated skeletal muscle suggested that reversible changes in enzyme function can occur in *X. laevis* in a manner that appears to modify anaerobic glycolysis in a tissue-specific manner (Katzenback et al. 2014; Childers and Storey 2019). This likely is what allows *X. laevis* to cope with impaired circulation (oxygen delivery) as dehydration and its consequences progresses.

An analysis of skeletal muscle hexokinase (HK), the entry point for glucose into glycolysis, showed a 3.4-fold increase in enzyme maximal activity (V_{max}), as well as changes to the phosphorylation state of the enzyme (increased relative phosphorylation on serine and decreased relative phosphorylation on threonine) that altered HK function in dehydrated frogs (Childers and Storey 2016). Although the K_m of ATP for HK was not significantly altered, there was a 2.4-fold increase in the K_m for glucose from 0.74mM to 1.83mM (Childers and Storey 2016). This suggests that affinity for glucose is suppressed during dehydration but can proceed when there is a higher concentration of glucose. Since it has been demonstrated that plasma glucose levels increase in highly dehydrated *X. laevis* to as much as 5.8 mM it is likely that HK is functioning maximally during dehydration, quickly converting glucose to glucose-6-phosphate (G6P) which locks the substrate into the cell (Malik and Storey 2009a) (Figure 1). However, the efficiency of glucose transport into skeletal muscle cells during dehydration remains unknown, although work has demonstrated that transcript levels of the GLUT4 glucose transporter remain stable (Luu 2018).

At the other end of glycolysis, a characterization of skeletal muscle pyruvate kinase (PK) and lactate dehydrogenase (LDH) provides evidence of a shift towards continued anaerobic glycolysis during dehydration. Although there were no changes in PK kinetic parameters, transcript levels of PK increased in *X. laevis* skeletal muscle during dehydration (Dawson et al. 2018) which may imply a need to maintain PK protein content and overall activity in this tissue. Interestingly, skeletal muscle LDH demonstrated a reduced overall V_{max}, with a 33% lower K_m for pyruvate and a 40% decrease in the K_m for lactate (so increased affinities for both substrates). Interestingly, the affinity changes seen for LDH from dehydrated frogs were sensitive to urea and molecular crowding, with the K_m for pyruvate returning to control levels of approximately 0.18mM while the K_m for lactate was increased to 40mM, which is 1.3-fold higher than the control value when measured under increased levels of urea or PEG (polyethylene glycol). This indicates a shift in affinity that favors the use of the forward substrate, pyruvate, from glycolysis under the physiological conditions of urea and molecular crowding during dehydration. It is argued that this sensitivity allows LDH to regenerate NADH (with the accumulation of lactate) if the TCA cycle cannot proceed normally at higher levels of animal dehydration (Childers and Storey 2019) (Figure 1). However, increases in whole-animal lactate occur when the frogs reach their tolerance point (i.e. a point of dehydration where upon rehydration they cannot recover). The build-up of lactate at the tolerance point may actually be a sign that aerobic glycolysis is no longer possible, leaving only anaerobic metabolism to sustain skeletal muscle energetics during general anoxia; this point is thought to be when cardiovascular strain causes animal death (Hillman 1978a; Childers and Storey 2019).

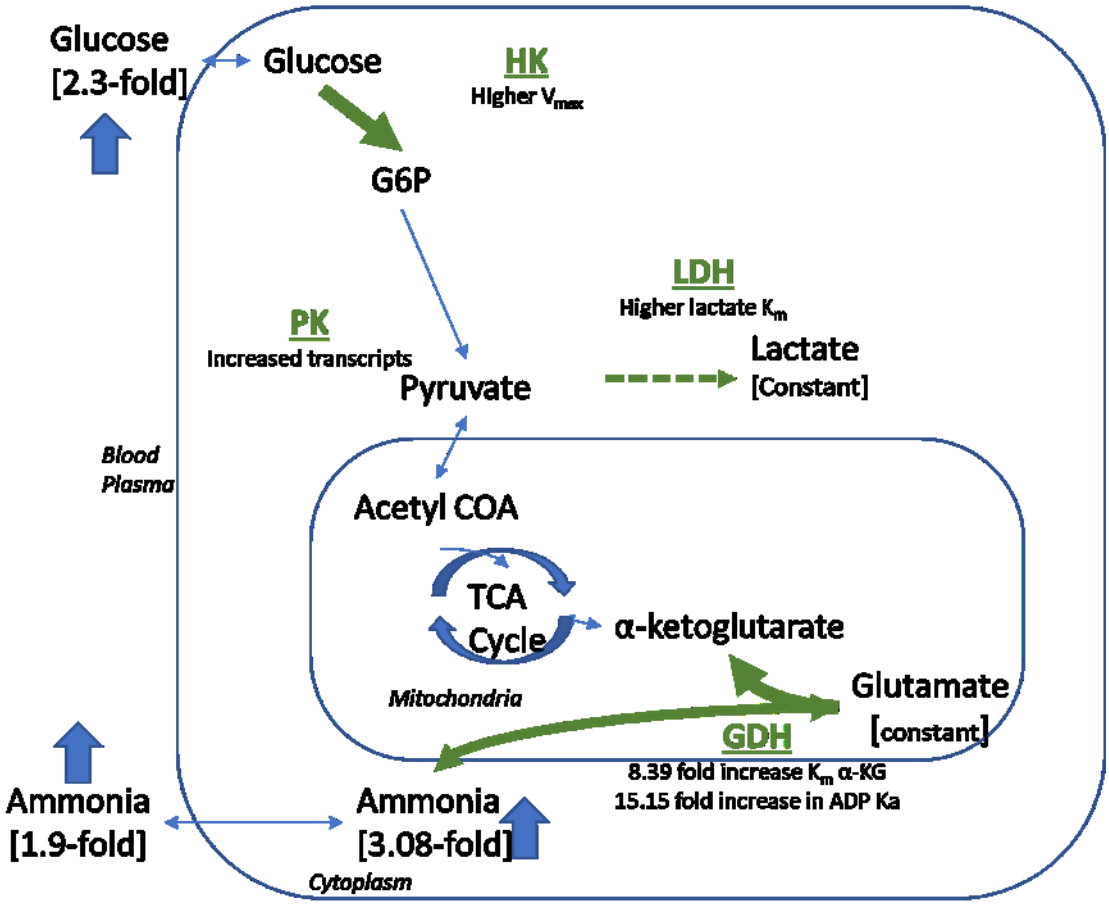

Figure 1.1: Current understanding of metabolic flux in *X. laevis* skeletal muscle during high dehydration. HK: hexokinase (Childers and Storey 2016), LDH: lactate dehydrogenase (Childers and Storey 2019), PK: pyruvate kinase (Dawson et al. 2018), GDH: glutamate dehydrogenase (Appendix 1). Green arrows are the predicted directions of metabolic flux determined from previous experiments. Blue arrows indicate pathways that are not yet confirmed. Glucose, ammonia, lactate and glutamate concentrations are from Balinsky et al. 1967a; Hillman 1978a; Malik and Storey 2009.

In addition to modifications of glycolytic enzymes, glutamate dehydrogenase (GDH) also showed altered properties in response to dehydration. Affinity for α-KG decreased under high dehydration conditions with an 8.39-fold increase in the K_m for α-KG (up to 0.24mM) while also gaining affinity for glutamate with the K_m decreasing down to 3.59mM (Appendix 1). This was coupled by kinetic changes that would favor an increase in flux in the direction of α-KG production, and along with changes in the K_a for ADP (up to 197μM), this suggests that if cell adenylate levels are compromised there can be a compensatory use of glutamate, but only once ADP is dramatically increased (Appendix 1). This could be a mechanism for protein catabolism to support the TCA cycle during dehydration, since α-KG can be transported into the mitochondria to support the TCA cycle intermediate pools by supporting forward α-KG dehydrogenase activity (Smith et al. 1974). Given that blood circulation is compromised to skeletal muscle of dehydrating *X. laevis* these enzyme studies suggest that skeletal muscle anaerobic metabolic enzymes are highly regulated to manage reduced aerobic metabolic capacity. In this way, aerobic cell metabolism is supported to meet energy requirements during dehydration stress, with a linked bonus of providing the ammonium ion precursor for urea synthesis as an osmotic protectant (Figure 1).

1.4 Post-translational regulation by protein phosphorylation

Post-translational modifications of proteins are a major part of the response to dehydration in *X. laevis*. Reversible protein phosphorylation is a well-studied modification that is widely used by animals to reorganize their metabolic priorities to adapt to arid environments (Storey and Storey 1990, 2012). These versatile modifications

control cellular processes ranging from protein kinase signaling cascades, to altering the action of individual proteins such as transcription factors and metabolic enzymes (Storey 2004, 2016; Malik and Storey 2009a, 2011; Storey and Storey 2012). For example, Malik et al. (2009) demonstrated that the ERK pathway is activated in dehydrating skeletal muscle through c-Raf. This was demonstrated through a correlation between c-Raf activation and the phosphorylation of its downstream targets which ultimately led to an increase in STAT3 phosphorylation (regulates translation) and RSK1 phosphorylation (regulates translation) during high dehydration (Malik and Storey 2009a). In addiiton, previous work by Luu (2011, 2018) on *X. laevis,* demonstrated that phosphorylation cascades regulated cell cycle arrest and protein translation signals. Luu demonstrated that in response to whole animal dehydration, Akt protein and phosphorylation levels are reduced in liver and skeletal muscle of *X. laevis* and as a result, the mTORC1 pathway that regulates protein synthesis is dissociated and suppressed. However, dissociation of mTORC1 in *X. laevis* does not appear to follow the same pathway as seen in mammalian models, since TSC2 is poorly conserved. Instead, PRAS40 was discussed as likely deactivating mTORC1 by sequestering Raptor away from mTOR. Unlike protein translation, which was found to be suppressed in both liver and skeletal muscle, cell cycle arrest mechanisms were organ-specific, as they were well conserved in the proliferative liver but poorly conserved in skeletal muscle (Luu 2011). This organ specificity is also clear in the expression of heat shock proteins, where each tissue upregulates a unique pattern to combat dehydration stress (Luu et al. 2018).

Reversible phosphorylation has also been demonstrated to regulate multiple key enzymes involved in *X. laevis* carbohydrate metabolism (Katzenback et al. 2014;

Childers and Storey 2016, 2019; Dawson et al. 2018, Appendix 1). Studies on *X. laevis* LDH have revealed that environmental factors can work in conjunction with phosphorylation to fine tune the kinetic outcomes to the severity of stress. The physiological consequences of dehydration-induced LDH regulation in muscle appear to maintain LDH affinity for pyruvate while strongly reducing the affinity for lactate. In conjunction with an overall reduction in maximal velocity this effectively poises the enzyme towards minimal forward (pyruvate oxidizing) flux during high dehydration in *X. laevis*. This regulation perhaps helps to maintain forward glycolysis under dehydrating conditions whilst providing for the ability to function in the face of increasing lactate (Katzenback et al. 2014; Childers and Storey 2019). Increased phosphorylation of GDH also appears to function to support metabolism through the generation of α-KG (Appendix 1). Therefore, reversible protein phosphorylation appears to be a crucial and ubiquitous response to dehydration in the skeletal muscle of *X. laevis* with the apparent outcome to reduce energy expensive processes such as translation and cell cycle progression, while supporting aerobic metabolism.

1.5 Hypothesis

If skeletal muscle is experiencing compromised circulation during dehydration (thus low oxygen circulation), then there will be a molecular response to adapt muscle metabolism to an increasingly compromised ability to produce cellular energy. Therefore, the protein phosphorylation state of key enzymes and pathways involved in energy balance will be altered in dehydrated *Xenopus* to change their functional output to adjust muscle energy balance.

My hypothesis builds on the current knowledge of skeletal muscle enzyme regulation by phosphorylation in response to whole body dehydration in *X. laevis*, specifically the changes to anaerobic metabolism. Previous work has suggested that most enzymes are regulated to reduce but encourage forward flux through glycolysis and the TCA cycle to support skeletal muscle metabolism during dehydration. To demonstrate whether dehydration is adapting muscle metabolism using protein phosphorylation, this thesis characterizes the phospho-regulation of a glycolytic enzyme that is intermediate in the glycolytic pathway, aldolase, followed by an analysis of creatine kinase (CK), a crucial enzyme that stabilizes the muscle adenylate pool. Following this, this thesis will determine the regulation of AMP-activated protein kinase (AMPK) signalling, the so-called "energy sensor" of the cell, with a focus on two ideas: (a) the phosphorylation state of AMPK itself and (b) the phosphorylation of two downstream pathways that effect energy balance, ACC1 and ULK1, which influence fatty acid synthesis and autophagy as energy sources respectively. The phosphorylation state of these enzymes and some related targets can help determine if these alternative energy sources play a role in maintaining *X. laevis* muscle energetics. Finally, the regulation of cytosolic NADP-dependent isocitrate dehydrogenase (IDH1) is characterized to further assess the fate of α-KG as it is a critical intermediate that bridges amino acid and fatty acid metabolic pathways. Specific objectives of each chapter are described below.

Objective 1: Determine the regulation of aldolase function via protein phosphorylation during dehydration in *X. laevis*.

Control of glycolysis is crucial in *X. laevis* as demonstrated by individual regulation of multiple of its enzymes: HK, PK and LDH. HK is the first enzyme of glycolysis when glucose is the substrate whereas PK and LDH are the terminal enzymes of the pathway. However, inputs or outputs from glycolysis can occur at different points along the pathway and thus to fully understand the global regulation of glycolysis the intermediate steps, such as that catalyzed by aldolase, also need investigation to identify how its regulation influences overall flux through the glycolytic pathway of skeletal muscle.

Specific Hypothesis 1: If previous enzymes are regulated in favor of forward glycolytic flux during *X. laevis* dehydration, then aldolase, an internal regulation point of glycolysis, is likely also regulated by reversible phosphorylation to favor continued forward glycolysis during whole animal dehydration in the skeletal muscle.

In **Chapter 2**, this hypothesis is tested by profiling the phosphorylation state of skeletal muscle aldolase along with a characterization of concurrent kinetic changes. Identification of easily reversible phosphorylation that could regulate the enzymes kinetic output, along with possible effector protein kinases, underscores the importance of tight metabolic control during tissue water loss through an energy inexpensive method. The altered phosphorylation of aldolase demonstrates that the enzyme is specifically regulated during dehydration in *X. laevis*. Aldolase isolated from dehydrated frog muscle had reduced phosphorylation on threonine residues with a larger increase in phosphorylation on serine residues. This accompanied a decrease in both the affinity for its substrate

$F1,6P_2$ and the V_{max} of the forward direction of the enzyme. Chapter 2 also addresses the possible upstream kinase effectors and the influence of some environmental factors that can influence the function of aldolase enzyme activity.

Objective 2: Determine the effect of the phosphorylation of creatine kinase (CK) during dehydration in *X. laevis*.

Control of adenylate levels is critical in *X. laevis* since reduced oxygen circulation can limit established methods of ATP production through the TCA cycle and oxidative phosphorylation. A disruption of the ATP:ADP:AMP ratio is a trigger for many other stress-responsive pathways and must be regulated during dehydration to control cell responses. Therefore the role of CK, the gatekeeper to the phosphocreatine (P-Cr) energy stores, is crucial when skeletal muscle circulation becomes restricted and energy production is compromised. Previous work has shown some glycolytic enzymes undergo posttranslational regulation in order to maintain some anaerobic energy production. The regulation of fast acting homeostatic enzymes like CK however, could also play a large role in the maintenance of cellular energy charge. In order to better understand the potential role of CK during dehydration, this thesis determines if posttranslational regulation through enzyme phosphorylation is occurring to modulate CK activity under dehydrating conditions.

Specific Hypothesis 2: If these frogs are experiencing a compromised ability to produce ATP through oxidative metabolism, then creatine kinase is likely regulated by reversible phosphorylation to increase ATP replenishment from P-Cr stores in skeletal muscle during *X. laevis* dehydration.

In **Chapter 3**, this hypothesis is tested by profiling the phosphorylation of skeletal muscle CK during whole animal dehydration of *X. laevis*. The identification of phosphorylation sites that are altered in response to dehydration shed light on the mechanism of metabolic regulation during water loss. The results from this chapter show that CK is regulated by phosphorylation during dehydration but also demonstrates the possibility of crosstalk between multiple upstream kinases. The phosphorylation of CK demonstrates that this kinase is specifically regulated during dehydration in *X. laevis*. CK from dehydrated frogs demonstrated an increase in affinity for P-Cr and creatine but also a drastic reduction in the V_{max} in both directions. **Chapter 3** also reveals that multiple protein kinases can act on CK to potentially integrate crosstalk from upstream stress signals. The influence of the cellular environment is also discussed through an investigation of the effect of various salts and metabolites on CK activity.

Objective 3: Correlate the influence of AMPK regulation on fatty acid synthesis and autophagy signalling through phosphorylation during whole-body dehydration.

The AMP-activated protein kinase (AMPK) plays a pivotal role in regulating biological processes surrounding energy consumption when ATP availability is limited, and AMPK is often considered to be a main cellular energy sensor. Glucose in blood plasma increases during dehydration yet use of blood-borne fuels and oxygen is thought to be compromised by poor circulation during dehydration. AMPK activates catabolic processes to improve ATP production, while simultaneously inhibiting ATP-expensive anabolic processes. For example, AMPK-mediated phosphorylation inhibits acetyl-CoA carboxylase (ACC) that gates fatty acid synthesis and AMPK directly opposes mTOR-

mediated autophagy inhibition via competing phosphorylation sites on ULK1 (Hardie et al. 2012) [9]. Phosphorylation at Thr172 of the α-subunit of AMPK can trigger a ~100-fold increase in kinase activity (Suter et al. 2006; Hardie et al. 2012). Therefore, the relative amount of phosphorylated AMPKα (p-AMPKα Thr172) is a good indicator of AMPK activity. The phosphorylation of AMPK and its downstream targets can give a strong indication of the state of skeletal muscle metabolism through this energy sensitive pathway.

Specific Hypothesis 3: If *Xenopus* has to adapt to a compromised ability to produce ATP, then the adenylate ratio of skeletal muscle must be in flux, which would stimulate the regulation of AMPK on canonical phosphorylation sites to decrease energy consumption and suppress fatty acid synthesis in skeletal muscle during dehydration.

In **Chapter 4**, this hypothesis is tested by characterizing AMPK subunit protein levels and the phosphorylation state of the catalytic subunit. In addition, the downstream targets of AMPK that are involved in stimulating fatty acid synthesis or autophagy were probed for known regulatory phosphorylation sites. The results of this chapter show that AMPK protein levels remain constant during dehydration along with phosphorylation on Thr172, but there was dephosphorylation on Ser496. This coincided with 1) a decrease in the relative phosphorylation on ACC1, allowing fatty acid synthesis to continue through this enzyme and 2) both the AMPK and mTOR ULK1 relative phosphorylation increasing on their respective amino acid sites, suggesting that autophagy is blocked by mTOR signaling. **Chapter 4** discusses these signal crossovers along with other downstream AMPK signaling regulations during dehydration in *X. laevis*.

Objective 4: Determine the influence of phosphorylation on IDH1 function during whole-body dehydration.

The cytoplasmic form of isocitrate dehydrogenase (IDH1) is often considered as just a mechanism for bolstering NADPH production to support antioxidant systems. Less discussed is the fact that the reversible reaction of IDH1 also uses α-ketoglutarate (α-KG) which could support TCA cycle function during whole animal dehydration in *X. laevis*. *X. laevis* shows an increase in skeletal muscle ammonium ion concentrations during dehydration that seems to be due to upregulated processing of glutamate by GDH (or other amino acids catabolized via GDH). The GDH conversion of glutamate to ammonia creates an equal amount of α-KG, which can be transported to the cytosol from the mitochondria or vice versa. Therefore, the regulation of α-KG using enzymes could reveal if α-KG is being used for fatty acid synthesis in the cytosol through a production of isocitrate by IDH1 or if cytosolic isocitrate is being converted to α-KG to be used in the mitochondria. The regulation of IDH1 is critical as it sits at this branch point of amino acid metabolism and fatty acid metabolism.

Specific Hypothesis 4: If the reduction in blood circulation during *Xenopus* dehydration causes reduced oxygen delivery then muscle tissue may require IDH1 to be regulated by reversible phosphorylation to favor α-KG production in *X. laevis* skeletal muscle during whole animal dehydration.

In **Chapter 5**, this hypothesis is tested by profiling the phosphorylation of IDH1 during whole animal dehydration of *X. laevis*. The identification of phosphorylation sites that are altered on IDH1 in response to dehydration can shed light on TCA cycle support

during water loss in *X. laevis*. The results from this chapter show that IDH1 is dramatically downregulated by phosphorylation during dehydration. However, this downregulation is accompanied by an increase in magnesium affinity, potentially driving the reaction towards α-KG production during high dehydration. Chapter 5 discusses the implications on fatty acid synthesis and investigates possible upstream kinases effectors that may be responsible for the regulation of IDH1.

Chapter 2: Purification and characterization of fructose 1,6 bisphosphate aldolase from the African clawed frog, *Xenopus laevis*: enzyme role in amphibian dehydration.

2.1 Introduction

Living animals are faced with a variety of environmental stresses that can challenge normal life, such as water and oxygen availability or food restriction. Water restriction is a commonly experienced variation in the environment that many animals must endure, arising from seasonal changes in conditions including temperature, rainfall and other factors. The main issue arising from this environmental change is the loss of total body water to a degree that compromises the circulation of blood and oxygen due to hypovolemia. Indeed, dehydration in *X. laevis* is known to affect circulation to their skeletal muscle tissue as blood volume and oxygen delivery is prioritized towards the head (Hillman and Sommerfeldt 1981). A restriction of oxygen availability necessitates a greater reliance on glycolysis for ATP production and the presence of modified regulatory mechanisms to fine tune glycolysis to energy needs. Certainly, glycolysis in *X. laevis* has been demonstrated to be strictly regulated through protein phosphorylation of key enzymes under high levels of dehydration exposure (Katzenback et al. 2014; Childers and Storey 2016, 2019; Dawson et al. 2018). These studies have documented significant changes in both enzyme maximal velocities and substrate affinities upon whole animal dehydration that appear to maintain forward flux through the pathway. This is further supported by glucose levels that increase in skeletal muscle during whole animal dehydration in *X. laevis* without an increase in lactate until the animal reaches their tolerance point where they can no longer survive (Balinsky et al. 1967; Malik and Storey 2009a). The regulation of HK to have an elevated V_{max} supports metabolism by allowing more glucose to be trapped by muscle tissue, while the regulation of LDH to

have a reduced V_{max} indicates that the overall glycolytic rate may be decreased during dehydration in *X. laevis* (Hillman 1978b; Childers and Storey 2016, 2019).

Commonly, metabolic rate depression is used by dehydration tolerant animals to survive the restriction of water in their normal environment (Storey 2004; Storey and Storey 2012). Still, *X. laevis* has not been shown to undergo global metabolic rate depression in response to dehydration. However, the stress to *X. laevis* skeletal muscle is more severe than in other tissues and the impact on its tissue-specific metabolism has not been fully elucidated (Hillman and Sommerfeldt 1981). The regulation of HK and LDH suggest anaerobic carbohydrate metabolism is favored, but it is unknown if the entire glycolytic pathway is set up to increase glucose use, in a similar manner to HK, or if there are points of downregulation during this stress exposure to limit the use of energy reserves. Fructose-1,6-bisphosphate aldolase (aldolase) is an intermediate step of glycolysis that cleaves fructose 1,6-bisphosphate ($F1,6P_2$) to glyceraldehyde-3-phosphate (GAP) and dihydroxyacetone phosphate (DHAP) as follows:

$$F1,6P_2 \rightleftharpoons DHAP + GAP$$

It is thought that the continual depletion of GAP by later steps in glycolysis facilitates the flow of $F1,6P_2$ toward GAP production and ultimately allows the forward flow of glycolysis to continue. Work on animals that face environmental stress has demonstrated that aldolase is typically regulated to alter substrate affinity during environmental stress (Storey 1980; Holden and Storey 1994; MacDonald and Storey 2002; Dawson et al. 2013). However, changes to posttranslational modifications however have not been previously documented. Aldolase is a ubiquitous and abundant enzyme in

skeletal muscle and through post translational regulation could be a critical point of regulation for carbohydrate metabolism. The importance of structure and stability to the function of aldolase has been previously demonstrated with enzyme resolution (Sygusch et al. 1987) and with the use of mutants of the aldolase protein (Rellos et al. 2000). Alterations in aldolase structure have been shown to impact both the kinetic parameters (Cox et al. 1983) and the stability of the catalytically active dimer, ultimately affecting its catalytic ability (Rellos et al. 2000). Due to the importance of aldolase for overall carbohydrate metabolism, this chapter aims to explore changes in aldolase protein phosphorylation and the regulation that may confer advantageous changes in enzyme function in *X. laevis.* Particular attention is paid to the role that reversible phosphorylation might have in mediating the maximal velocity of aldolase during dehydration in *X. laevis* muscle tissue.

2.2 Methods

Animals

Adult male African clawed frogs (*X. laevis*) were purchased from a colony from the University of Toronto and upon delivery, the frogs were acclimatized in tanks of de dechloraminated water at 22 ± 1 °C for 3 weeks prior to the start of experiments according to Carleton Committee for Animal Care guidelines (protocol # 106936). Frogs were fed 3–4 pellets of CU Adult Frog diet (PMI Nutrition International) three times/week and water was changed the day after each feeding. Frogs were then randomly divided into groups of control, medium dehydration, and high dehydration conditions, where they were not fed again. For the dehydration experiments, the frogs were weighed

and placed into dry containers at 22 ± 1 °C where water was lost through evaporation over time. Animals were weighed at approximately 12-h intervals to determine body water loss due to evaporation. To quantify the extent of dehydration, the percentage of total body water lost was calculated as follows: %water lost=$(m_i-m_d)(m_i-BWC_i)\times100\%$ where m_i, m_d, and BWC_i are the initial mass, dehydrated mass, and initial body water content of *X. laevis* frogs, respectively. For the purpose of this study, BWC_i of *X. laevis* frogs was 0.74 ± 0.02 g H_20 per gram body mass as previously determined (Malik and Storey 2009). Animals in the medium and high dehydration groups were sampled when mean total body water loss reached ~16 and ~30%, respectively. The final mean percentages for total body water loss were 16.43 ± 0.33% SEM for medium dehydration and 31.18 ± 0.83% SEM for high dehydration. These levels of water loss were not lethal and prior testing showed that dehydrated frogs that were returned to aquatic conditions all recovered. All frogs were sacrificed by pithing and all major tissues including sartorius, triceps femoris and gastrocnemius muscles from the legs were rapidly dissected and quickly frozen in liquid nitrogen before being stored at −80 °C until use.

Aldolase Assay

Sephadex G-25 columns were used to remove ions and small molecular weight metabolites from the crude extracts. A 5 ml syringe barrel plugged with glass wool was used to prepare the column and the G-25 resin was equilibrated in buffer A. A bench-top centrifuge was used to centrifuge the column at 500×g for 2 min to remove excess buffer. A 500-µl aliquot of skeletal muscle extract was then loaded on the G-25 and spun again

for 1 min. The final eluent was pooled. Aldolase activity was assayed by a coupled enzyme assay. The change in absorbance at 340 nm as a result of NADH oxidation was monitored with a Biotek Synergy HT multimode microplate reader (Biotek). Standard assay conditions for frog muscle aldolase were 20mM imidazole–HCl (pH 7.0 at 22℃), 0.2 mM NADH, 1.5 mM F1,6,P_2, 0.55 mg/ml triosephosphate isomerase, and 25 mg/ml of a-glycerophosphate dehydrogenase in a 200-uL assay volume. All reactions were initiated with the addition of isolated aldolase.

Aldolase purification

Frozen leg muscle samples, taken from sartorius, triceps femoris and gastrocnemius, were homogenized 1:5 w:v in ice-cold homogenization buffer A (25 mM HEPES buffer, pH 8.0 with 25 mM NaF, 2.5 mM EDTA, 2.5 mM EGTA 10 % v:v glycerol, 5 mM 2-mercaptoethanol) with 1 mM PMSF added immediately before homogenization. Muscle homogenates were centrifuged at 13,500×g at 4 °C for 30 min and the supernatant was decanted. The supernatant was then mixed with 1.5:1 with 40% PEG 8000, vortexed for 1min before a second centrifugation at 13 500xg at 4 °C for 30 min. The resulting supernatant was removed, and the pellet was resuspended to 2x the initial volume in buffer B (Buffer A with 25mM MES pH 6.0). The re-suspended pellet was then loaded onto a 2 cm x 3 cm hydroxyapatite column previously equilibrated in buffer B. To remove unbound proteins the column was washed with 30 ml of buffer B before the enzyme was eluted with 30 mls of 250 mM Na_2PO_4. Fractions of ~1 ml were collected and assayed and those with the highest aldolase activities were pooled. Pooled peak fractions were loaded into a 1.5 cm × 3 cm Cibacron Blue affinity column

equilibrated in buffer B. Any unbound proteins were again removed with a 30 ml wash with buffer B. Elution of aldolase was then carried out with a KCl gradient (0–2 M) in buffer B.

SDS–polyacrylamide gel electrophoresis

SDS-PAGE was used to assess the results of the aldolase purification procedure. Samples from each of the purification steps were mixed 1:1 v:v with 2x SDS loading buffer (100 mM Tris buffer, pH 6.8, 4% w/v SDS, 20% v/v glycerol, 0.2% w/v bromophenol blue, 10% v/v 2-mercapotethanol), boiled for 5 min and stored at -20°C until use. Lanes of 10% (w/v) acrylamide separating gel and a 3.5% stacking gel were loaded with 15 µl of sample and electrophoresis was carried out at 180 V for 60 min in running buffer (0.05 M Tris, 0.5 M glycine, 0.05% w/v SDS, pH 8.0). The gel was stained for 2 h in 0.25% w/ v Coomassie brilliant blue R250/50% v/v methanol/7.5% v/v acetic acid, and then de-stained in 25% v/v methanol/ 10% v/v acetic acid until protein bands were visible with little background. A ChemiGenius instrument was used for imaging with gels placed on a white opaque background for imaging (SynGene, Frederick, MD).

Mass Spectroscopy Identification

The isolated protein band from an aldolase preparation from control *X. laevis* muscle was cut out of the SDS-PAGE, destained and sent directly for LC-MS/MS analysis. Protein digestion and mass spectrometry experiments were performed by the Proteomics platform of the CHU de Quebec Research Center, Quebec, Canada.

Protein Quantification

Total protein concentrations were measured using the Coomassie blue dye-binding method with the BioRad prepared reagent (Cat #500-0006; BioRad Laboratories, Hercules, CA) with bovine serum albumin as the protein standard (Bradford 1976). A PowerWave HT microplate spectrophotometer (Biotek) was used to measure protein concentration at 595 nm.

Immunoblotting

For total protein determination, total protein extracts were prepared as previously described (Zhang & Storey, 2015). In short, samples of frozen skeletal muscle weighing approximately 100 mg were powdered for the control, 15% and 30% dehydration conditions under liquid nitrogen. Samples were homogenized in 1:2 w/v of homogenization buffer C (20 mM HEPES, 200 mM NaCl, 0.1 mM EDTA, 10 mM NaF, 1 mM Na3VO4, 10 mM β-glycerophosphate at a pH of 7.5) with 1 mM PMSF (Bioshop) and 1 µL of Sigma protease inhibitor (cat. No. P1Coo1.1; Sigma, Burlington, ON, Canada) using a Polytron PT10 homogenizer for ∼15–20 s. All the homogenates were then centrifuged at 10,000 rpm at 4 °C for 10 min and the resulting supernatants containing the soluble proteins were collected. The concentrations of the supernatants were determined using a BioRad reagent (Cat #500-0006; BioRad Laboratories, Hercules, CA) at 595 nm on a MR5000 microplate reader. Afterwards, all the samples were normalized to 5 µg/µL using buffer C. Then aliquots were combined 1:1 v:v with 2x SDS loading buffer and the samples were then boiled for 5 min. The final protein samples at their respective concentrations were stored at −20 °C until use.

Equal amounts (25 μg) of prepared protein homogenate and 4–5uL of 10.5–175 kDa PiNK Plus pre-stained protein ladder (#PM005-0500; FroggaBio, Toronto, Canada) were loaded onto 10% SDS-PAGE gels and electrophoresis was carried out at 180 V for 50 min. Proteins were transferred to polyvinylidene difluoride membrane at 160 mA for 90 min. Membranes were then blocked with 2.5% non-fat dried milk in Tris–buffered saline containing Triton-X (TBST) for 40 min and washed three times with TBST. Membranes were incubated with aldolase goat primary antibody (Abcam Cat#: ab78339) overnight at 4°C. After washing with TBST, membranes were incubated with secondary antibody (mouse anti-goat IgG) for 30 min and then washed. Immunoreactive bands were visualized with enhanced chemiluminescence (H_2O_2 and Luminol) using a ChemiGenius Bioimaging System (Syngene, Frederick, MD) band intensities were quantified using the associated Gene Tools program. Each PVDF membrane was stained using Coomassie brilliant blue staining to visualize the total amount of protein in each lane. Immunoblot band density in each lane was standardized against the summed intensity of a group of Coomassie blue stained protein bands in the same lane. Finally, the mean band density for the dehydrated condition was standardized against the mean control band density, such that the relative band density of control would be 1 for graphing purposes.

For determination of posttranslational modifications purified aldolase samples were combined 1:1 v:v with 2x SDS loading buffer (see above), boiled for 5 min and frozen at −20 °C until use. Aliquots of 15 ug of purified aldolase was loaded onto 10% polyacrylamide gels and were run at 180 V for 60min. Proteins were transferred to PVDF membranes at 160 mA for 90 min. Membranes were blocked with 2.5 % non-fat dried milk in Tris-buffered saline containing Triton-X (TBST: 20 mM Tris base, pH 7.6, 140

mM NaCl, 0.05 % v/v Tween-20) for 30 min and washed three times with TBST. Membranes were then left to mix with antibody overnight at 4 °C. Antibodies used in this study were made in rabbits or mice and diluted 1:1000 (v:v) in TBST before use: rabbit anti-phosphoserine (Cat #618100), rabbit anti-phosphothreonine (Cat. #718200), and mouse anti-phosphotyrosine (Cat #700286) were all from Invitrogen (Carlsbad, CA, USA). To remove unbound primary antibody membranes were washed three times for 5 min with TBST before they were incubated with HRP-conjugated anti-rabbit or anti-mouse secondary antibody (BioShop, diluted 1:5000 v:v in TBST) for 30 min. To remove unbound secondary antibody the membranes were washed again three times for 5 min in TBST. Enhanced chemiluminescence was used to visualize immunoreactive bands, which were visualized on the ChemiGenius Bioimaging System (Syngene, Frederick, MD). Band intensities were quantified using GeneTools software. Aldolase band intensities were standardized against the Coomassie brilliant blue re-stained band to account for any discrepancy in sample loading. Finally, the mean band density for the dehydrated conditions was standardized against the mean control band density, such that the relative band density of control would be 1 for graphing purposes.

Kinetic Studies

Substrate affinity constants (K_m values) were determined from the Michaelis-Menten equation using a non-linear least squares regression computer program (Brooks 1992). The concentrations of inhibitors that decrease enzyme velocity by 50% (I_{50} values) were determined using plots of initial velocity vs [inhibitor]. Plots were constructed for frog aldolase by measuring enzyme activities under standard assay conditions (20mM

HEPES, pH adjusted to 7.2 at 23 ℃, 0.2 mM NADH, 1.5 mM F1,6P_2). All kinetic parameters are means ±SEM for n =4–5 determinations.

In vitro incubation to stimulate protein kinases

To assess the effects of reversible phosphorylation on CK, incubations were prepared under conditions that facilitated the activities of selected endogenous protein kinases. Crude muscle extracts, prepared as previously described in buffer A, were centrifuged through Sephadex G25 columns equilibrated in incubation buffer (25 mM HEPES buffer, pH 7.0 with 10 % v:v glycerol, 5 mM 2-mercaptoethanol) that lacks kinase and phosphatase inhibitors. Aliquots of the filtered supernatant were then incubated for 24 h at ~4°C with specific stimulators of protein kinases as described in Macdonald and Storey (1999). Each aliquot was mixed 1:3 v:v with the appropriate additions that were designed to stimulate different protein kinases: AMP-activated protein kinase (AMPK), Ca^{2+}-calmodulin protein kinase (CAMK), protein kinase A (PKA), protein kinase C (PKC) and general endogenous kinases activity. The tested conditions were as follows (made in incubation buffer pH 7.0):

A. OPEN conditions (control for unaccounted changes to the enzyme during the incubation period): no additions to incubation buffer.
B. STOP condition (same as Buffer A) was designed to inhibit all protein kinases and phosphatases. incubation buffer plus 25 mM NaF, 2.5 mM EDTA, 2.5 mM EGTA.
C. Endogenous Protein Kinases: buffer B plus 5 mM Mg·ATP, 30 mM β-GP and either:

a. 1mM AMP to stimulate AMPK
b. 1.3 mM $CaCl_2$ + 7 µg/mL phorbol myristate acetate (PMA) to stimulate protein kinase C (PKC)
c. 1 U of calmodulin + 1.3 mM $CaCl_2$ to stimulate calcium–calmodulin kinase activity (CaMK)
d. 1 mM cAMP, to stimulate protein kinase A (PKA)
e. 1 mM cGMP (to stimulate PKG) plus all of the components in (a)-(d) above to stimulate total kinases.

After incubation overnight, samples were mixed 1:1 with STOP buffer to halt kinase reactions before the samples were assayed as above with varying $F1,6P2_2$ concentrations to determine the changes to the K_m or relative V_{max} of the preparations. Open and Stop conditions were compared for any unaccounted-for changes in aldolase activity over the incubation period. These values were not found to be different and thus were averaged and used for comparison to the treated values under the title 'OPEN'.

Kinase in silico predictions and homology modelling

The aldolase FASTA sequence (Accession #: BAA19524) taken from the NCBI database was used to predict the most likely kinase interactions through the online software from Netphos3.1 server (http://www.cbs.dtu.dk/services/NetPhos/). Serine, threonine and tyrosine residues were selected individually with threshold values set to 0.75. The same aldolase sequence was then run through a simple homology modelling server (https://swissmodel.expasy.org/), using 1ald.1.pdb from human muscle as a

template (Gamblin et al. 1991), to view the location of the predicted phosphorylation sites and compare *X. laevis* aldolase structure to the human template.

Data and Statistical Analysis

To analyze enzyme rates a Microplate Analysis (MPA) Program was used, kinetic parameters were calculated using a nonlinear least squares regression program, Kinetics 3.51 (Brooks 1992). Statistical analysis of two conditions (control vs. dehydrated) were carried out with a Student's t test (SigmaPlot 12.0 statistical package) with a P value < 0.05 considered significant. For immunoblotting, data are expressed as means ± SEM, n = 3-4 independent samples from different animals for immunoblot analysis. Differences between control and dehydrated protein samples were analyzed using SigmaPlot software and considered statistically significant when the one-way ANOVA with the Tukey's post-hoc test yielded a result of $p < 0.05$.

2.3 Results

The typical scheme for the purification of aldolase is summarized in Table 2.1. The specific activity of aldolase in crude muscle extracts was 0.37 U/mg protein. The PEG precipitation retained 63.3% of aldolase activity in the pellet. The re-suspended aldolase was then bound and eluted from hydroxyapatite using a Na_2PO_4 wash, which recovered 58.6 % of the aldolase activity, and resulted in a specific activity of 2.92 U/mg. Activity was inhibited due to a noted inhibition by Na_2PO_4 but activity was still present. The active fractions were pooled and diluted 1:1 with buffer B before being applied to a Cibacron blue column where aldolase was eluted with a 0-2 M KCl gradient. Finally,

aldolase was bound and eluted from a Cibacron Blue column where 26.5% of activity was retained with a specific activity of 5.11 U/mg of protein. The peak activity eluted at 0.75 M KCl. Peak fractions were pooled and desalted using an Ultra-15 Centrifugal Filter Concentrator (Millipore Sigma UFC910008 Amicon®). The resulting preparation provided a 13.9-fold purification of aldolase (Table 2.1).

Both control and dehydrated muscle aldolase preparations were analyzed on a 10% SDS-PAGE gel. The enzymes purified from both conditions were judged to be homogeneous and neither contained any apparent contaminating enzymes, which could interfere with the basic assay or alter any of the added metabolites. The subunit molecular mass was approximately 45 kD (Figure 2.1) which is comparable to other known examples of aldolases (Pasha and Salahuddin 1977; Holden and Storey 1994). This is higher than the predicted molecular weight using ExPASy (https://www.expasy.org/) which predicted the molecular weight to be 39.4 kD from the *X. laevis* gene sequence (Accession #: BAA19524). However, this might be accounted for by the presence of posttranslational modifications.

Immunoblotting for total protein levels of aldolase was used to determine the relative abundance of aldolase between control and dehydrated conditions. High and medium dehydrated skeletal muscle had 38.7% ($p<0.05$) and 35.8% ($p<0.05$) less aldolase than control frog skeletal muscle samples (Figure 2.2). Immunoblotting was also used to assess relative differences in the posttranslational modifications of muscle aldolase purified from control versus high dehydrated frogs. Phosphorylation on serine residues was 2.14-fold higher ($P < 0.05$) for dehydrated aldolase as compared to control

aldolase whereas phosphorylation of threonine residues of aldolase from dehydrated muscle was 52.7% lower compared to control aldolase ($P < 0.05$) (Figure 2.3). Relative phosphorylation of tyrosine residues was also measured and although both aldolases were demonstrated to be phosphorylated on these residues, they were not significantly different between the conditions (Figure 2.3).

In order to validate the identity of the purified protein band on SDS PAGE (Figure 2.1) mass spectrometry (MS) analysis was carried out on the purified band. The excised band revealed only one protein with 60 exclusive unique peptides, 119 exclusive unique spectra and 314/364 amino acids (86% coverage) identified as *X. laevis* fructose-bisphosphate aldolase with a molecular weight of 39,386 Da. This molecular weight correlated well with the unmodified amino acid sequence molecular weight calculated from Expasy (https://web.expasy.org/cgi-bin/compute_pi/pi_tool).

Kinetic parameters of frog aldolase were assessed for $F1,6P_2$ and fructose-1-phosphate (F1P) as substrates to determine potential changes in substrate affinity during control and dehydrated conditions. The dehydrated muscle enzyme showed no change in K_m for $F1,6P_2$ (0.024 mM) however demonstrated a significant drop in V_{max} as the control maximal velocity was 7.8±0.21 U/mg and the dehydrated muscle value dropped to 5.53±0.06 U/mg (Figure 2.4A). The relationship between aldolase activity and $F1,6P_2$ substrate concentrations were hyperbolic for both conditions. The K_m value for F1P did not change significantly between control and stressed conditions (Figure 2.4B). As with $F1,6P_2$, there was a significant drop in V_{max} as the control maximal velocity was 0.34±0.05 U/mg and the dehydrated muscle value dropped to 0.21±0.02 U/mg (Figure

2.4B) The ratio between $F1,6P_2$/F1P aldolase activity was found to be 22.94 for control frogs and 26.33 for high dehydrated frogs. This suggests that frog muscle aldolase increasingly favors $F1,6P_2$ as a substrate during high dehydration conditions.

Various metabolites and salts were tested for allosteric effects on aldolase using an optimal concentration of $F1,6P_2$ that was above the V_{max} at 23°C. Although several metabolites exhibited inhibitory effects on aldolase activity, no enzyme activators were found. I_{50} values were determined for various inhibitors of *X. laevis* aldolase at saturating levels of $F1,6P_2$ (1.25mM). Aldolase from dehydrated animals was more sensitive to all inhibitors except for F1P. Inorganic phosphates were more effective inhibitors than the chloride salts. I_{50} values for Na_2PO_4 and K_2PO_4 were 0.1±0.01 M and 0.1±0.004 M for control and 0.04±0.003 M and 0.05±0.002 M for the enzyme from dehydrated muscle (Figure 2.5) whereas NaCl and KCl were 0.47±0.04 M and 0.43±0.05 M for control and 0.17±0.04 M and 0.21±0.02 M for aldolase from dehydrated frog muscle (Figure 2.6). Dehydrated frog muscle aldolase was also 59% more sensitive to urea than control muscle aldolase (Figure 2.7). The I_{50} of lactate was not significantly different between control and dehydrated values although the relative activity of the control significantly dropped when above 100mM lactate (Figure 2.8).

To determine if *X. laevis* muscle aldolase was subject to reversible protein phosphorylation and whether this could account for the stable kinetic differences between control and dehydration conditions, *in vitro* incubation studies were conducted. Crude muscle extracts of control muscle were incubated with small molecule activators of specific endogenous protein kinases and the effects of these incubations on the K_m and

relative V_{max} value for $F1,6P_2$ was analyzed (Table 2.2). Incubation conditions that inhibited both kinases and phosphatases (STOP) and the OPEN control were not significantly different (indicating no changes due to the incubation procedure). The crude homogenates resulted in a higher K_m $F1,6P_2$ for control aldolase (0.07±0.01mM) than what was seen in the purified samples (0.024mM). In the incubated extracts of control skeletal muscle, the K_m of $F1,6P_2$ decreased significantly by 57% when AMPK was stimulated along with a 2.15-fold increase in V_{max}. When CAMK was stimulated there was no significant change to the V_{max} of $F1,6P_2$ but the K_m decreased by 42.8% (Table 2.2). The stimulation of PKC resulted in a significant decrease in the K_m of $F1,6P_2$ (42.8%) with no change in the V_{max} while the stimulation of PKA lowered both the K_m $F1,6P_2$ and the V_{max} by 42.8% and 29.2% respectively (Table 2.2). The stimulation of total kinases resulted in a significant decrease in the K_m (50%) but no significant change in the V_{max} $F1,6P_2$ (Table 2.2, $P<0.05$).

Using protein kinase binding site prediction tool on the NetpPhos3.1 server and the *X. laevis* aldolase protein sequence, PKC and PKA were the only protein kinases that met the threshold for phosphorylating aldolase (Table 2.3). PKC had the highest score (0.81) for phosphorylating aldolase at Thr241, followed by PKA on Ser46 and PKC on Thr255 both with a score 0.78 (Table 2.3). The same aldolase sequence was then run through a simple homology modelling server using a human muscle aldolase (Gamblin et al. 1991) as the template which resulted in a sequence identity of 88.3%. The three sites predicted to be phosphorylated by PKA and PKC were highlighted to demonstrate their surface exposure on the quaternary structure (Figure 2.9).

2.4 Discussion

X. laevis muscle aldolase was purified to apparent electrophoretic homogeneity by using a combination of ion-exchange and affinity chromatography (Figure 2.1). The apparent monomer subunit molecular weight (~45 kDa) determined by SDS-PAGE corresponded well with the rabbit skeletal muscle aldolase standard and the subunit molecular weight reported for aldolase from various other vertebrate species (MacDonald and Storey 2002; Dawson et al. 2013). This purification scheme produced enzyme preparations that were apparently purified 13.9-fold with a specific activity of 5.11 U/mg (Table 2.1). Mass spectrometry validation confirmed that the purification had isolated aldolase with 86% sequence coverage. Thus, the purification procedure presented here indicates an effective way of purifying aldolase from frog muscle.

Immunoblotting analysis revealed that there was significantly less aldolase in *X. laevis* skeletal muscle samples from both medium and high dehydrated frogs as compared to control animals (Figure 2.2). Kinetic analysis demonstrated a dramatic decrease in V_{max} of skeletal muscle aldolase from highly dehydrated animals as compared to controls (Figure 2.3). Further studies were done to assess the inhibition of aldolase from control and highly dehydrated frogs by salts that naturally increase in concentration during dehydration. In the face of all salts tested, aldolase from dehydrated frogs was more susceptible to inhibition when compared to aldolases isolated from control frogs, as indicated by significantly reduced I_{50} values (Figure 2.4-7). This could indicate that the physiological condition of increasing ion concentrations also contributes to aldolase inhibition during dehydration. Considered together, the reduced aldolase protein levels

and the greater sensitivity to inhibition suggests a decrease in aldolase activity during whole animal dehydration in *X. laevis*.

Through the immunoblot analysis of isolated aldolase from *X. laevis* muscle, the present study also demonstrates that aldolase from highly dehydrated frogs is differentially phosphorylated when compared to aldolase isolated from hydrated frogs. Phosphorylation on serine residues increased whereas threonine phosphorylation was reduced (Figure. 4). It is well known that reversible phosphorylation of enzymes is a major mechanism in the plasticity of metabolic reactions (Storey 2004; Humphrey et al. 2015). In this case, reversible phosphorylation may be mediating the overall decrease in activity of aldolase, which further supports the decrease in its maximal activity caused by the reduction in relative protein amounts (Figure 2.2). Furthermore, the stimulation of endogenous protein kinases in a crude muscle extract confirmed the effect of phosphorylation on aldolase since several kinases, once stimulated, resulted in changes to both the K_m and V_{mas} of the enzyme (Table 2.2). Of the kinases tested, PKA most closely mimicked the natural changes caused by aldolase serine phosphorylation during dehydration *in vivo,* as stimulation of this kinase significantly lowered the V_{max} of control aldolase (Table2). Further evidence points to PKA as the likely effector kinase since an *in silico* kinase prediction software showed that PKA and PKC scored with the highest probability as being the kinases involved in the serine and threonine phosphorylation changes on aldolase (Table 2.3). Since PKA is predicted to act on Ser46 this could be the site of regulation that dramatically decreased aldolase activity. Furthermore, data by (Cortright et al. 2000) on human skeletal muscle has demonstrate that certain PKC inhibitors augment insulin-mediated glucose uptake. The removal of phosphorylation on

threonine sites that are potentially mediated by PKC, in *X. laevis* then might be part of an insulin signalling response that correlates well with glucose levels measured in the animals' plasma. Further studies investigating the responses of these specific phosphorylation sites are required to elucidate the relationship between aldolase and upstream insulin signalling.

In conclusion, the activity of aldolase from the muscle of dehydrated *X. laevis* is severely depressed. Since it is known that HK has an increased V_{max} this may be a source of metabolic rate depression to avoid rampant use of energy stores as more G6P is created (Childers and Storey 2016). Thus, aldolase regulation would allow HK to secure glucose energy in the cells as G6P while preventing immediate depletion through glycolysis (Kong et al. 1994). G6P is not going to rise to unreasonable levels however, as glycogen synthesis is shown to not occur during dehydration in *X. laevis*. So, as dehydration continues, forward glycolytic flux inevitably will continue. The reversible regulation of aldolase in *X. laevis* skeletal muscle then could be a form of glycolytic rate depression used in skeletal muscle to adapt to the curtailment of circulation during whole animal dehydration. However, future studies on the regulation of aldolase from other tissues is required.

2.5 Figures

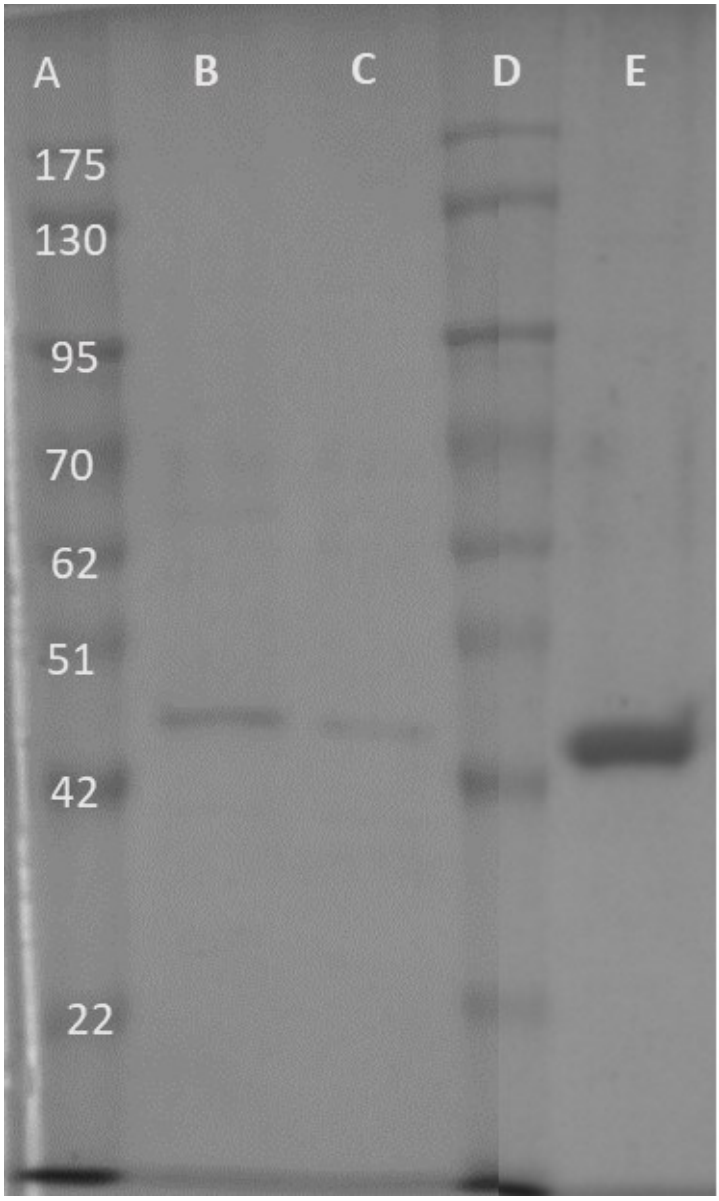

Figure 2.1: Electrophoretic analysis on 10 % SDS-PAGE gels showing typical isolations of aldolase from control and high dehydrated skeletal muscle. Lane A is the molecular weight ladder, lane B is aldolase from control frogs and lane C is aldolase isolated from dehydrated frog skeletal muscle. Lane D is the molecular weight ladder and lane E is rabbit muscle aldolase standard.

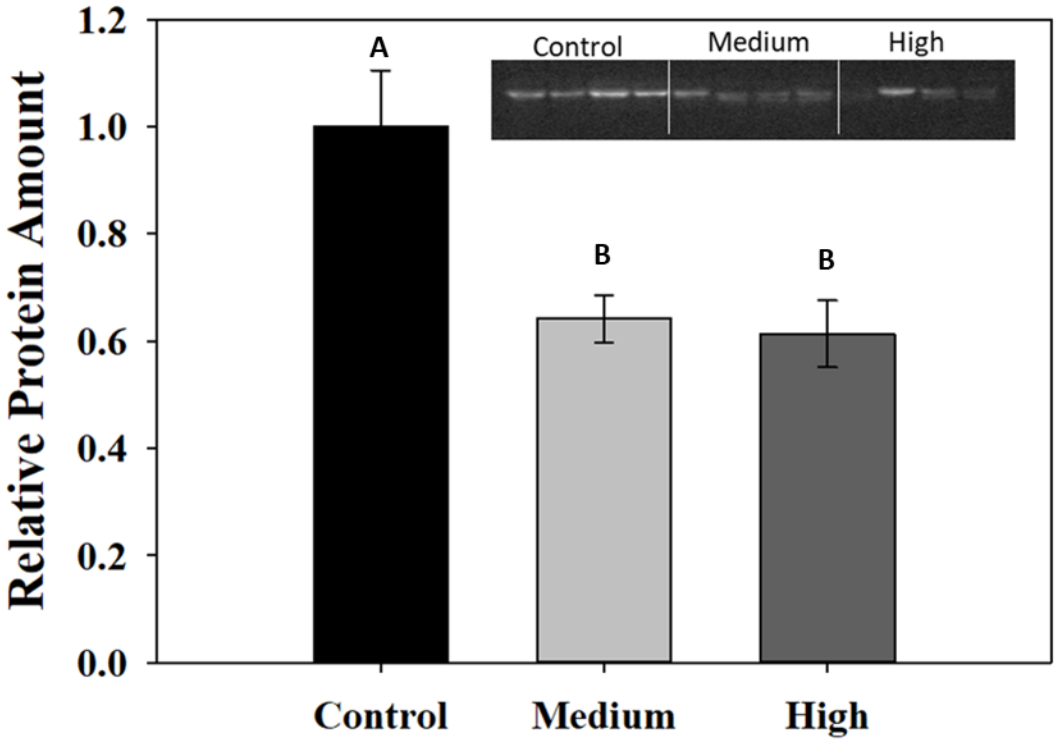

Figure 2.2: Relative total aldolase protein in crude extracts of skeletal muscle from control, medium and high dehydrated *X. laevis* skeletal muscle as assessed by immunoblotting. Chemiluminescent bands are inset. Data are means ± SEM, n = 4 independent determinations. *Significantly different from the control value, $p < 0.05$.

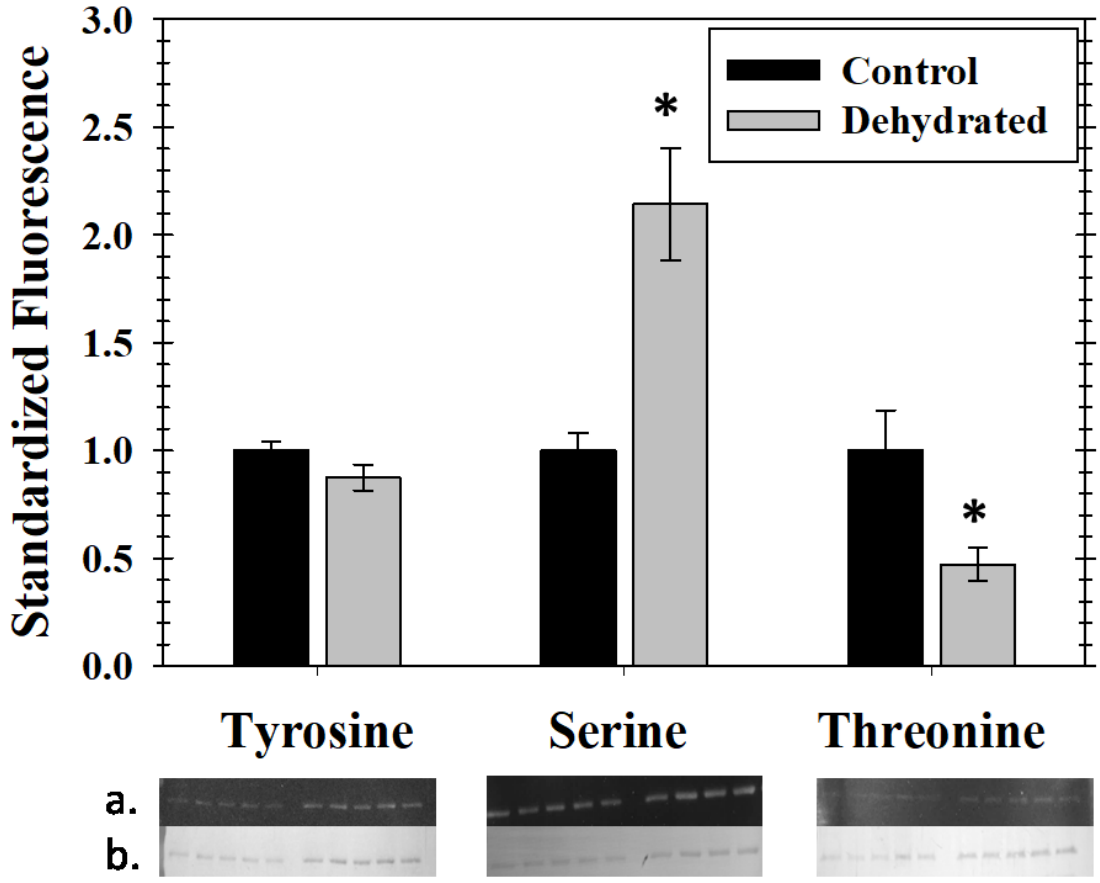

Figure 2.3: Immunoblot analysis of phosphorylation on threonine, serine or tyrosine residues of purified *X. laevis* muscle aldolase from control and high dehydrated frogs. Chemiluminescent images (a) and subsequent Coomassie stained images of the same blots (b) are imbedded below the histogram bars. Relative amounts of phosphorylated residues were standardized against the corresponding Coomassie blue stained bands. Data are relative intensities, means ± SEM, n = 3. *Significantly different from the corresponding control value, $p < 0.05$.

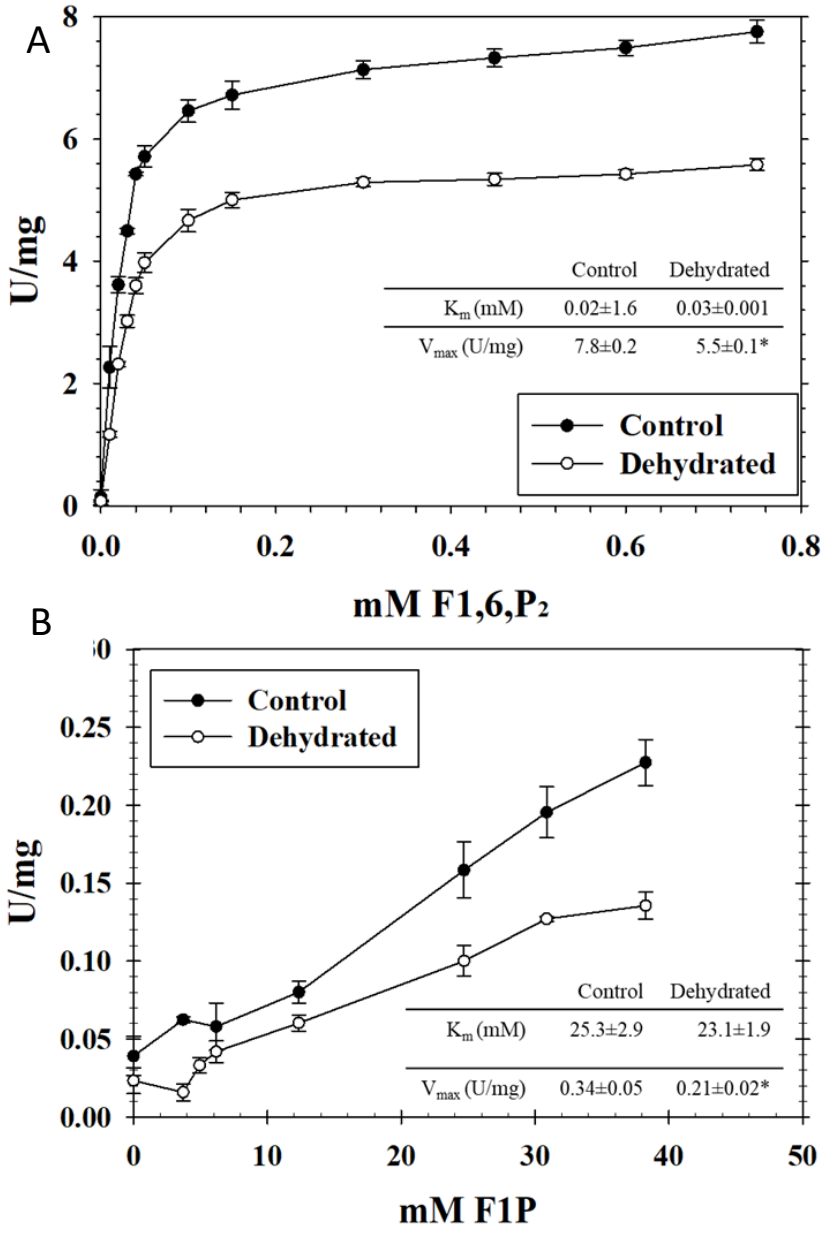

Figure 2.4: Graphical results of kinetic analysis of substrate affinities for purified aldolase from control and high dehydrated frogs. Non-linear regression lines of untransformed initial rates with increasing amounts of $F1,6P_2$ (A) and F1P (B), with $MgCl_2$ held at constant concentrations. Velocity points are means ± SEM n=4.

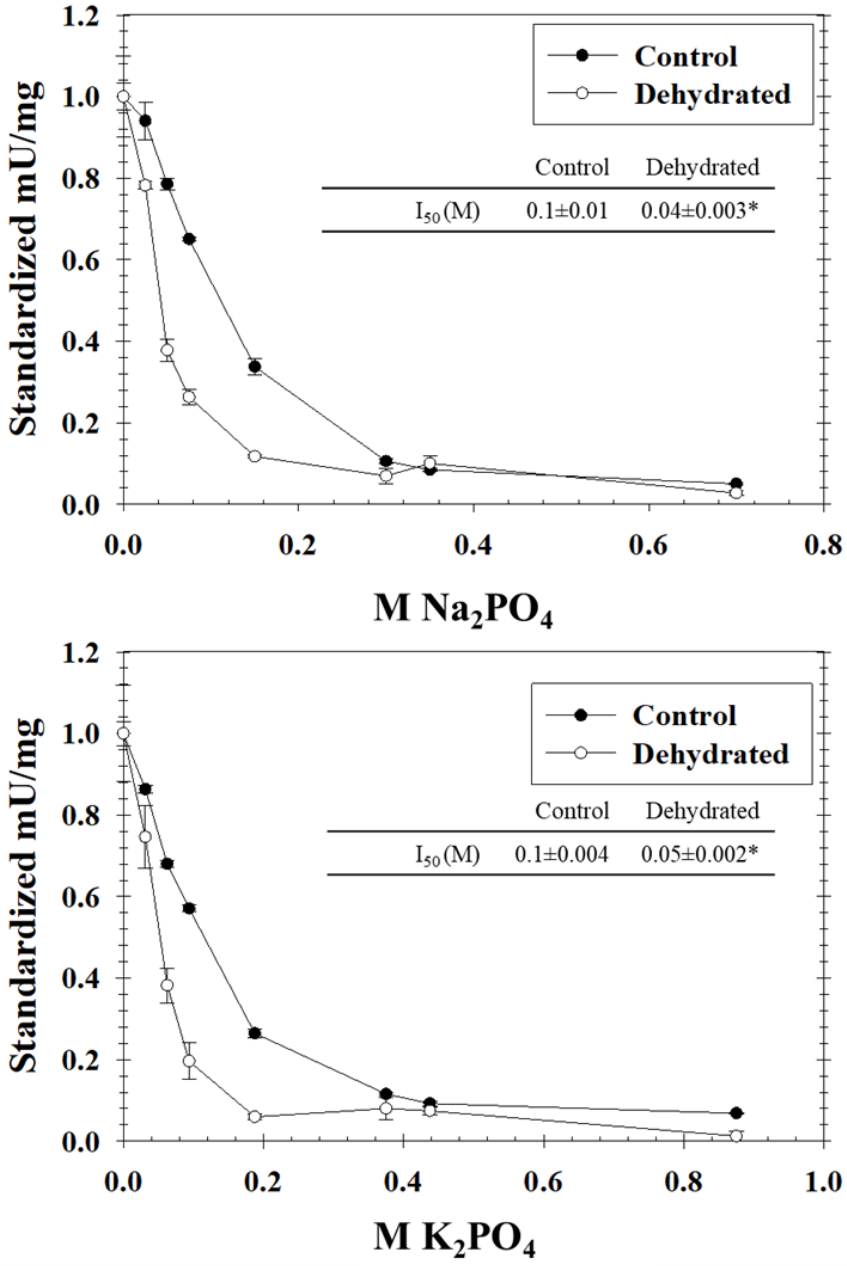

Figure 2.5: Graphical results assessing inhibition of purified aldolase by Na_2PO4 and KPO_4. Graphs show velocity vs [salt] with increasing amounts of inhibitor assayed at saturating substrate concentrations are presented along with the calculated I_{50} values. Velocity points are means ± SEM for n=3-4.

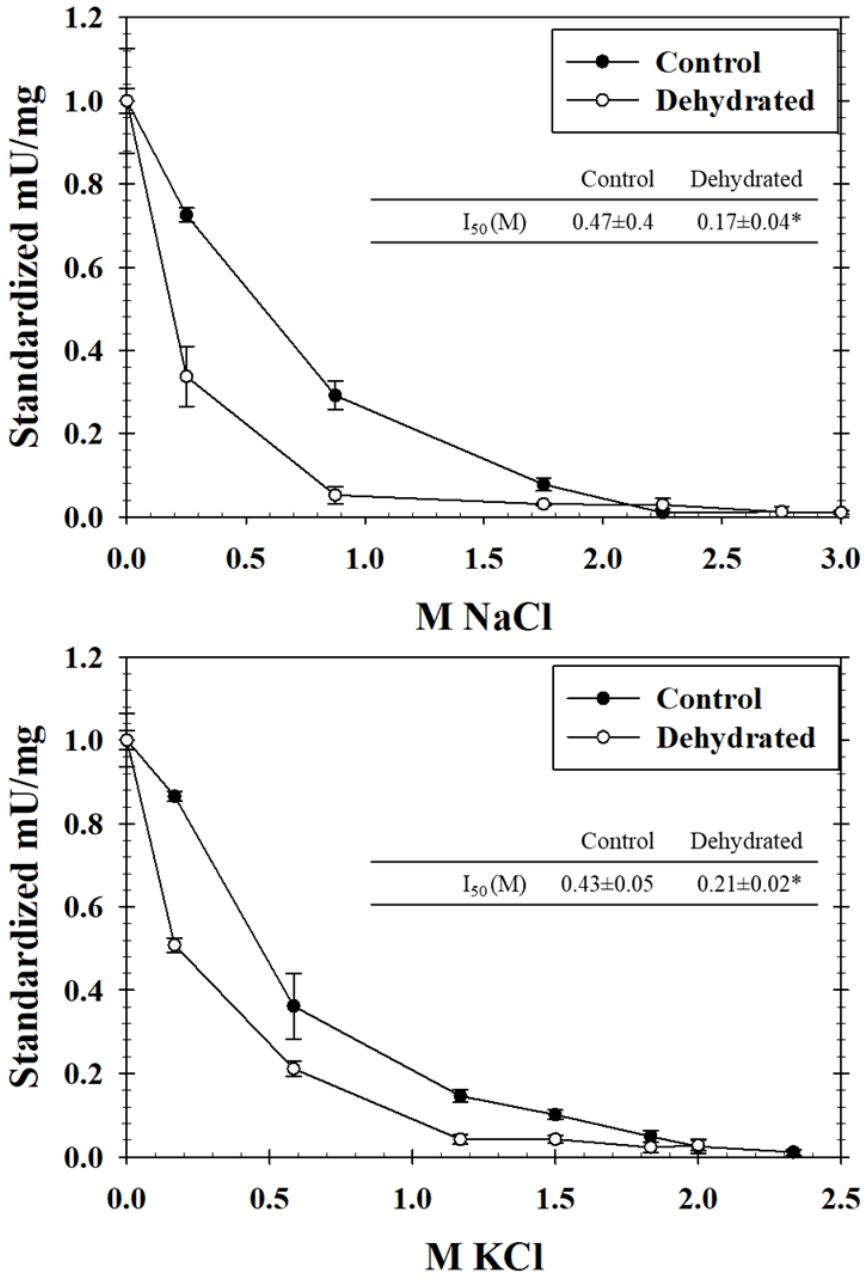

Figure 2.6: Graphical results assessing inhibition of purified aldolase by NaCl and KCl. Graphs show velocity vs [salt] with increasing amounts of salt assayed at saturating substrate concentrations are presented along with the calculated I_{50} values. Velocity points are means ± SEM for n=3-4.

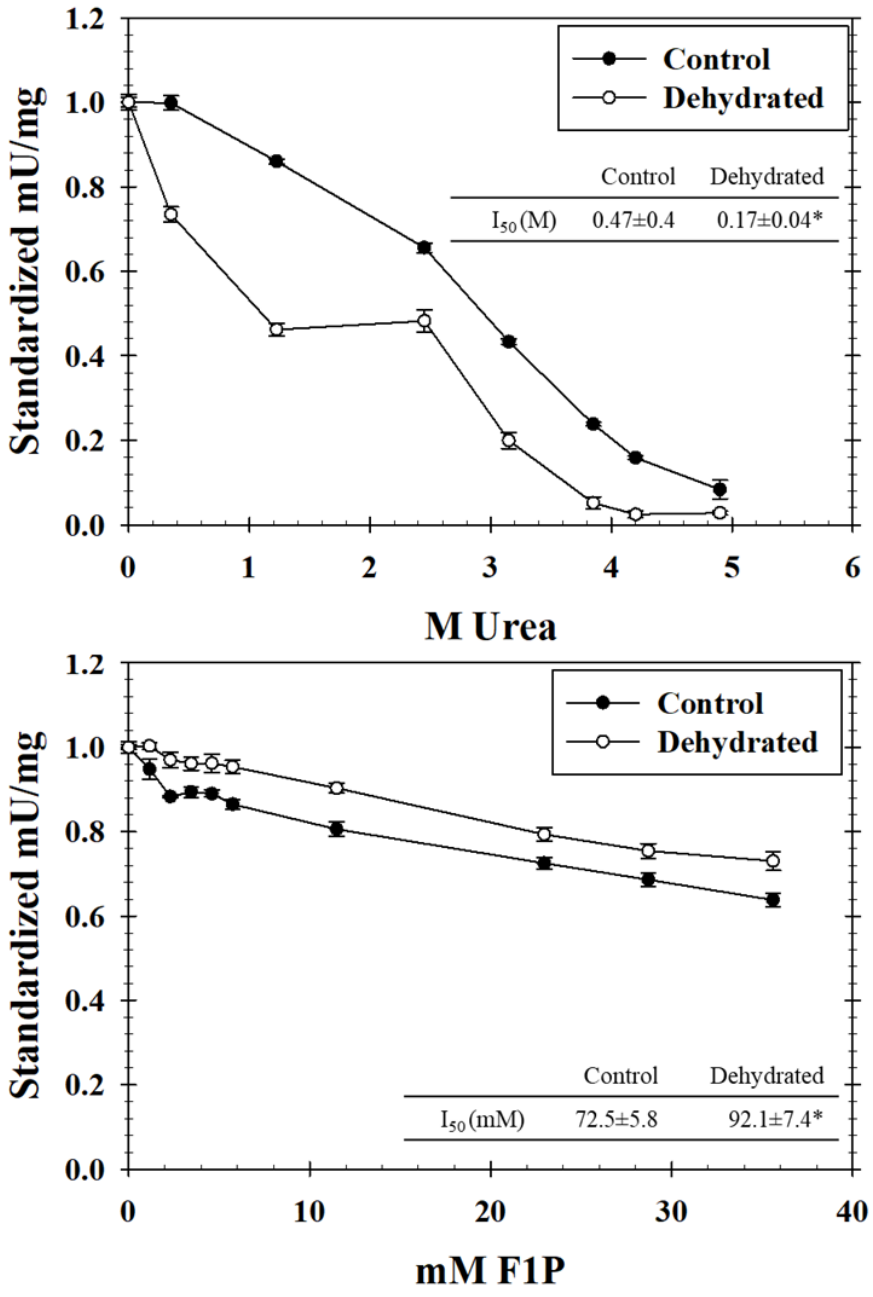

Figure 2.7: Graphical results assessing inhibition of purified aldolase by urea and F1P. Graphs show velocity vs [salt] with increasing amounts of salt assayed at saturating substrate concentrations are presented along with the calculated I_{50} values inset. Velocity points are means ± SEM for n=3-4.

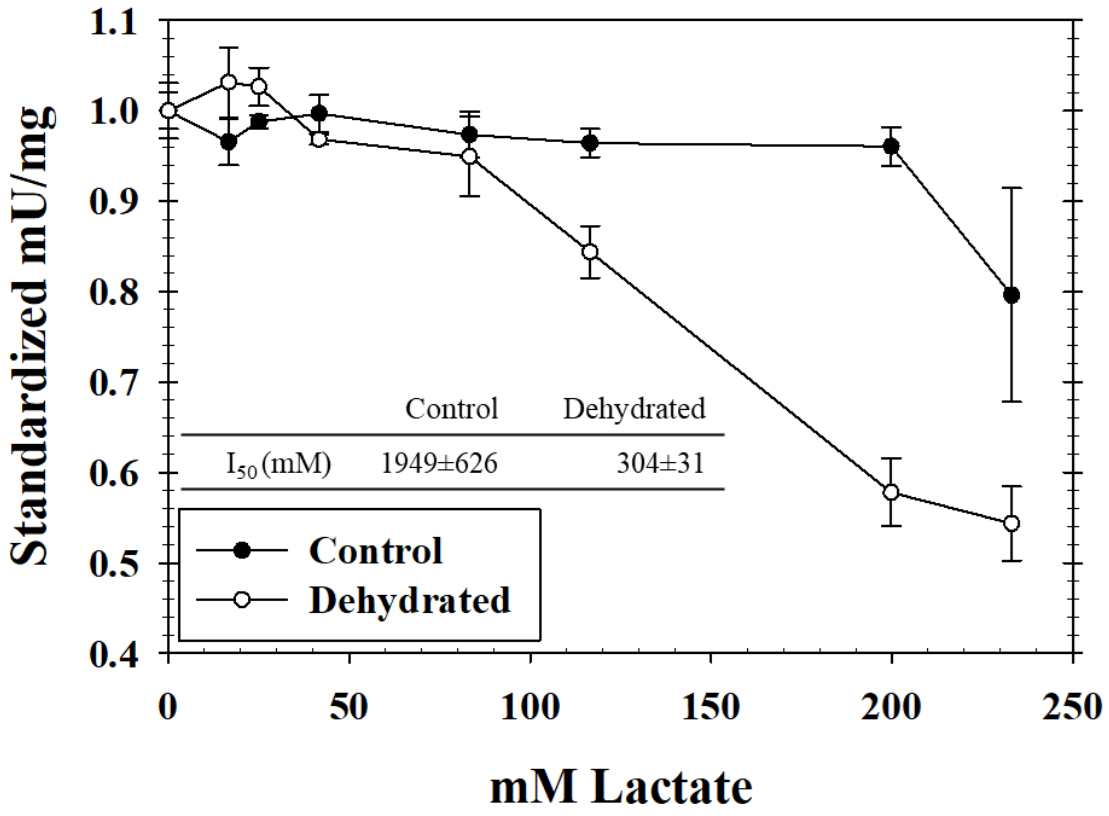

Figure 2.8: Graphical results assessing inhibition of purified aldolase by L-lactate. Graphs show velocity vs [lactate] with increasing amounts of lactate assayed at saturating substrate concentrations are presented along with the calculated I_{50} values inset. Velocity points are means ± SEM for n=3-4.

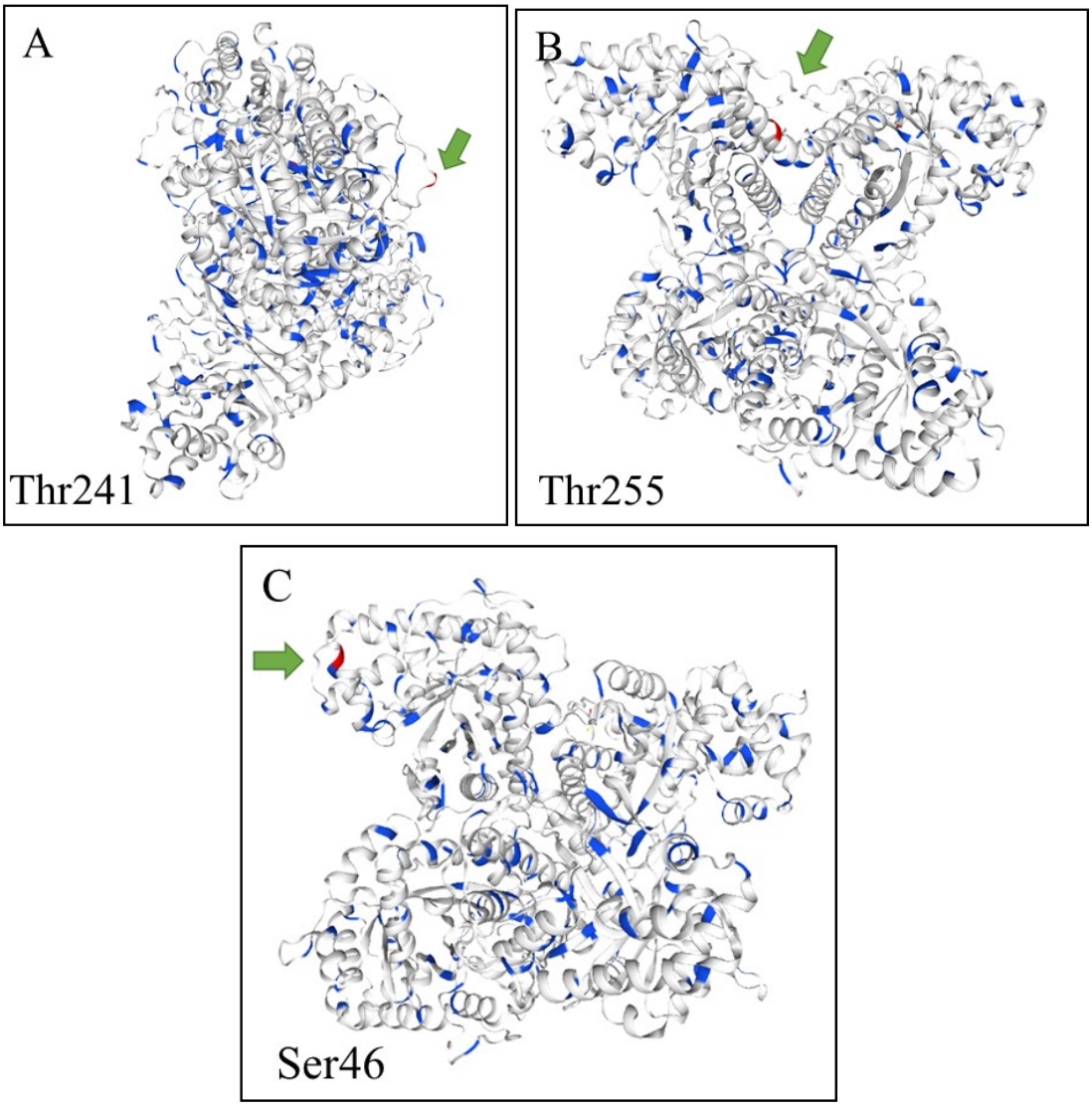

Figure 2.9: Homology models of *X. laevis* muscle aldolase indicating the predicted phosphorylation sites (green arrows) from NetPhos3.1. A) Thr241, B) Thr255, C) Ser49.

2.6 Tables

Table 2.1: Outline of aldolase purification from muscle of *X. laevis*. The scheme for dehydrated muscle is shown; the control purification scheme was very similar but with a total activity yield of 21%.

	Total Activity (U)	Total Protein (mg)	Specific Activity (U/mg)	Activity Yield (%)	Fold Purification
Crude	14.36	39.06	0.37		
PEG Precipitation	9.09	-	-	63.32	-
Hydroxyapatite	8.41	2.88	2.92	58.58	7.95
Cibacron Blue	3.82	0.75	5.11	26.63	13.91

*The pellet from the PEG precipitation could not be accurately measured for protein content so that data was omitted for clarity.

Table 2.2: Kinetic values of control aldolase assayed after the *in vitro* stimulation of endogenous kinases. Data are means ± SEM, n = 4 technical preparations of enzyme. *- indicates statistically a significant difference from the OPEN condition using the Students t-test, $p<0.05$.

	K_m (mM)	V_{max} (mU/ul)
OPEN	0.07±0.01	3.8±0.4
AMPK	0.03±0.01*	8.1±0.9*
CAMK	0.04±0.0001*	5.5±0.4*
PKC	0.04±0.01*	3.2±0.3
PKA	0.04±0.0001*	2.7±0.2*
Total Kinases	0.035±0.01*	3.9±0.5

Table 2.3: *In silico* kinase binding site prediction from the NetPhos 3.1 server for *X. laevis* aldolase (Accession#: BAA19524).

Residue	Context	Score	Kinase
Ser46	KRLS**S**IGAE	0.780	PKA
Thr241	GHAC**T**KKYP	0.809	PKC
Thr255	MATV**T**AL66	0.779	PKC

Chapter 3: Purification and characterization of creatine kinase from the skeletal muscle of the African clawed frog, *Xenopus laevis*

3.1 Introduction

Creatine kinase (CK; EC 2.7.3.2) catalyzes the reversible transfer of an N-phosphoryl group from phosphocreatine (P-Cr) to ADP to produce creatine and ATP via the following reaction (Wallimann et al. 1998).

$$P\text{-}Cr^{2-} + Mg^{2+} + ADP^{-} + H^{+} \leftrightarrow Creatine + Mg\text{-}ATP^{2-}$$

The P-Cr and CK system in cell bioenergetics is manifold and its regulation can have implications for many cellular functions. As an enzyme notably responsible for buffering and transporting cellular ATP during burst activity, CK is primarily in tissues with high and/or fluctuating ATP demands such as skeletal muscle, heart, and brain (Wyss et al. 2000). In muscle tissue, CK constitutes ~20% of the total soluble protein (Wyss et al. 2000; Lipskaya 2001; McLeish and Kenyon 2005) and is specifically located in these cells both near sites of ATP production, i.e. mitochondria, and by sites of ATP use, e.g. myosin ATPases, plasma membrane Na^{+}, K^{+}-ATPase and Ca^{2+}-ATPase (Brewster, 2018). However, although CK is primarily thought of as a transport and buffering system for ATP there are larger implications to its function. ATP replenishment is crucial for Na^{+}, K^{+}-ATPase driven salt retention in processes that require the membrane potential to be maintained such as in the sarcoplasmic reticulum for calcium membrane transport (Wyss et al. 2000; Wallimann 2015; Brewster 2018). The conversion of ADP to ATP also takes up H^{+}. The activity of CK can therefore prevent cell acidification which would affect many cell functions since many metabolic processes are not only controlled by the ADP:ATP ratio but also by pH. Therefore, CK could have a central role in global

cellular homeostasis and the regulation of CK activity could profoundly alter cellular metabolism (Brewster 2018).

Reversible protein phosphorylation has been repeatedly demonstrated as the main source of CK regulation when under cells are under energy stress. For example, in hibernating ground squirrels, CK is phosphorylated during hibernation which reduces its overall activity and lowers its affinity for ATP and creatine (Abnous and Storey 2007). When euthermic squirrel muscle CK was phosphorylated by stimulating endogenous PKA, PKC and PKG the activity was similarly decreased. However, ground squirrel CK, was not affected by the AMP-activated protein kinase (AMPK) and muscle CK from hibernating squirrels was not affected by activation from any of the protein kinases tested. Conversely, the CK from the muscle of the freeze-tolerant wood frog*, Rana sylvatica*, showed increased activity when the animal was frozen which also correlated to a highly phosphorylated form of CK (Dieni and Storey 2009). Other work in *R. sylvatica* revealed that P-Cr levels remained stable throughout freezing and that ATP levels declined slowly whereas liver lost 50% of its ATP quickly in the frozen state which was attributed to a lack of P-Cr reserves (Storey and Storey 1986). Wood frog muscle CK from both control and frozen muscle conditions showed increased activity after stimulation of endogenous kinases, including AMPK (Dieni and Storey 2009). This indicates that there may be multiple sites for phosphorylation that can create specific kinetic outcomes to tailor the activity of CK to the cellular needs of the animal and upstream kinase signalling. As demonstrated through these two species, AMPK phosphorylation has a variable influence on CK activity. Other work demonstrated the importance of the effects of various protein kinases on CK such as in differentiated skin

cells, where the inhibition of protein kinase C (PKC) also decreased CK activity whereas stimulation of calcium–calmodulin dependent protein kinase (CAMK) had no effect (Chida et al. 1990b, a). However, CAMK does phosphorylate CK in some cases but there are few reports of an effect on activity. However, CK is found to interact with CAMK at the sarcoplasmic reticulum and has been immuno-precipitated with CAMK along with other glycolytic enzymes such as aldolase, GAPDH, PK and LDH (Singh et al. 2004).

The African clawed frog, *Xenopus laevis*, is an aquatic species that endures seasonal drying and loss of aquatic habitat. This forces *X. laevis* to either migrate to find other bodies of water or to burrow into the mud of the drying pond and enter a resting state termed aestivation. Aestivation is characterized by whole body water loss, urea accumulation, and an entrance into a dehydrated state that can last for months (Hillman 1978a; Tinsley and Kobel 1996; Storey and Storey 2012). A major consequence of dehydration in frogs such as *Xenopus* is the thickening of blood that causes poor circulation of oxygen to some tissues. This places an energy stress on tissues like skeletal muscle, the function of which is often compromised (Hillman 1978b; Gatten 1987). Unlike *R. sylvatica*, *X. laevis* is not known to reduce its metabolic rate to conserve fuel/energy stores, suggesting that another mechanism must be in use to stabilize cellular energetics and help maintain viability to endure long-term dehydration. For skeletal muscle, the pool of P-Cr and the appropriate regulation of CK is a likely source of the stabilization of muscle bioenergetics. Indeed, as mentioned previously for wood frogs, the slow consumption of P-Cr has been shown to fully sustain the adenylate pool in skeletal muscle for at least 4 days of freezing whereas others organs without significant phospho-creatine reserves (e.g. liver) showed a strong decline in ATP and adenylates

over the same time (Storey and Storey 1984). Hence, CK control over the phosphagen pool can be a muscle-specific protective mechanism during times of stress. The present study analyzes the pattern of CK regulation through reversible phosphorylation that could be involved in enzyme control with respect to the energetic needs for dehydration survival by the African clawed frog.

3.2 Methods

Animals

See Chapter 2

Creatine Kinase Assay

CK activity was assayed using a Thermo Labsystems Multiskan Spectrum microplate spectrophotometer and Multiskan software. CK activity was measured by monitoring the consumption or production of NAD(P)H at 340 nm at room temperature (23°C). The optimum assay conditions for the creatine phosphorylating forward reaction for muscle CK from both the control and dehydrated frogs were 2.5 mM ATP-$MgCl_2$, 42 mM creatine, 0.3 mM NADPH, 4 mM PEP, 1 unit of LDH, 1 unit of pyruvate kinase, and 50 mM Tris buffer pH 7.5 in a total volume of 200 µl with 10 µl of purified enzyme used per assay. Optimum assay conditions for the P-Cr dephosphorylating reverse reaction were determined to be 6.5 mM phosphocreatine, 1.5 mM ADP, 1.7 mM $MgCl_2$ (4 mM for dehydrated animals), 40 mM glucose, 1 mM NADP, 0.3 units of hexokinase, 1 unit of glucose-6-phosphate dehydrogenase, and 50 mM Tris pH 7.5 in a total volume of 200 µl with 30 µl of purified enzyme used per assay. Maximal activity was measured as mU/mg

soluble protein. For the determination of enzyme K_m values for substrates, co-substrate concentrations were held constant at optimal concentrations. I_{50} values for urea (the concentration reducing V_{max} by 50%) were determined for the creatine phosphorylating direction using optimal concentrations of both substrates.

Creatine Kinase Purification

CK was purified from muscle of both control and dehydrated frogs using a combination of ion-exchange and dye ligand affinity column chromatography. Skeletal muscle samples (previously stored at -80 °C) were homogenized 1:5 w:v, using a Diamed Pro 200 homogenizer, in cold buffer A containing 10 mM K_2PO_4, 5 mM 2-mercaptoethanol, 1 mM EGTA, 1 mM EDTA, 20 mM β-glycerophosphate and 10% v:v glycerol, pH 8.0. A few crystals of PMSF were added at the time of homogenization. Homogenates were centrifuged for 30 min at 13,500 × g at 4 °C. The resulting supernatant was decanted and held on ice until use. A sample of crude muscle extract was applied to a DEAE Sephadex A-25 (1.5 cm x 7 cm) column equilibrated in buffer A. The column was washed with 15 ml of buffer A and CK activity eluted in the wash. The initial fractions were collected, assayed, and those with high CK activity were pooled. The pooled fractions were then added to a Cibacron blue column (1.5 cm x 4 cm) pre-equilibrated in buffer A and eluted with 40 ml of 100 mM creatine in buffer A. The fractions (~1.4 mL) were collected and assayed (in the creatine + ATP direction). Fractions with high activity were pooled for further studies, remaining in the eluate buffer A that contained creatine. For subsequent kinetic analysis, aliquots of CK preparation

were first subjected to a low speed centrifugation through a G25 spun column equilibrated in buffer A to remove creatine.

SDS–polyacrylamide gel electrophoresis

SDS-PAGE was used to assess the results of the CK purification procedure as done in Chapter 2. In brief, samples from each of the purification steps were mixed 1:1 v:v with SDS loading buffer, boiled for 5 min and stored at -20 °C until use. Lanes of 12% SDS-PAGE gels were loaded with 15 µl of sample and electrophoresis was carried out at 180 V for 60 min in running buffer. Gels were stained with Coomassie blue and imaged using a ChemiGenius instrument (SynGene, Frederick, MD).

Mass Spectroscopy Identification

The isolated protein band from a CK preparation of control *Xenopus* muscle was cut out of the SDS-PAGE gel, destained and sent directly for LC-MS/MS analysis. Proteins digestion and mass spectrometry experiments were performed by the Proteomics platform of the CHU de Quebec Research Center, Quebec, Canada.

Protein Quantification

Total protein concentrations were measured using BioRad reagent (Cat #500-0006; BioRad Laboratories, Hercules, CA) with bovine serum albumin as the protein standard (Bradford 1976).

Western blotting

Total protein determination of CK from control, medium and high dehydrated frogs was performed as in Chapter 2. Equal amounts (25 µg) of prepared protein homogenate and 4–5uL of 10.5–175 kDa PiNK Plus pre-stained protein ladder (#PM005-0500; FroggaBio, Toronto, Canada) were loaded onto 10% SDS-PAGE gels and electrophoresis was carried out at 180 V for 50 min. Proteins were transferred to PVDF membranes at 160 mA for 90 min. Membranes were then blocked with 2.5% non-fat dried milk in Tris–buffered saline containing Triton-X (TBST) for 40 min and washed three times with TBST. Membranes were incubated with CK goat primary antibody (Abcam Cat#: ab174672) overnight at 4°C. After washing with TBST, membranes were incubated with secondary antibody (mouse anti-goat IgG) for 30 min and then washed. Immunoreactive bands were visualized and quantified as in Chapter 2.

Dot Blotting

For assessment of post-translational modifications, aliquots of purified CK were loaded as dots onto nitrocellulose membranes and allowed to run through the membrane until dry (~40min) (Abboud and Storey 2013). Membranes were then washed three times with TBST for 5 min each before a primary antibody was applied. Antibodies used were: (1) rabbit anti-phosphothreonine (Cat. # 718200, Invitrogen, Carlsbad, CA, USA); (2) mouse anti-phosphotyrosine (Cat # 700286, Invitrogen, Carlsbad, CA, USA); or (3) rabbit anti-phosphoserine (Cat #618100, Invitrogen, Carlsbad, CA, USA). The primary antibody was left to incubate at 4°C overnight. Unbound primary antibody was removed with 3×5 min washes with TBST and the membrane was then incubated with HRP-

conjugated anti-rabbit secondary antibody or anti-mouse secondary antibody (BioShop, both diluted 1:4000 v:v in TBST) for 40 min and then washed again with 3×5 min washes of TBST. Immunoreactive dots were visualized by enhanced chemiluminescence, as above, and dot intensities were quantified using GeneTools software. CK dot intensities were standardized against the corresponding Coomassie blue-stained dot to correct for any variations in sample loading.

Kinetic Studies

Substrate affinity constants (K_m values) were determined from the Michaelis-Menten equation using a nonlinear least squares regression computer program (Brooks 1992). The concentrations of inhibitors that decrease enzyme velocity by 50% (I_{50} values) were determined using plots of initial velocity vs [inhibitor]. Plots were constructed for frog CK by measuring enzyme activities under standard assay conditions (50 mM Tris buffer pH adjusted to 7.5 at 23°C, with 2.5 mM ATP-$MgCl_2$, 42 mM creatine, 0.3 mM NADH, 4 mM PEP, 1 unit of LDH, 1 unit of PK). All kinetic parameters are means ± SEM for n = 4–5 determinations.

In vitro incubations to stimulate endogenous kinases

To assess the effects of reversible phosphorylation on CK incubations were prepared under conditions that facilitated the activities of selected endogenous protein kinases or of total protein phosphatases. Crude muscle extracts, prepared as previously described in buffer A, were centrifuged through Sephadex G25 columns equilibrated in incubation buffer (10 mM K_2PO_4, 5 mM 2-mercaptoethanol, and 10% v:v glycerol, pH

7.5.) that lacked kinase and phosphatase inhibitors. Aliquots of the filtered supernatant were then incubated for 24 h at 4°C with specific stimulators of protein kinases or protein phosphatases as described in Macdonald and Storey (1999). Aliquots of spun crude extracts were then mixed 1:3 v:v with the appropriate additions that were designed to stimulate different protein kinases: AMP-activated protein kinase (AMPK), Ca^{2+}-calmodulin protein kinase (CAMK), protein kinase C (PKC). Comparable incubations tested effects of stimulating total endogenous protein kinases activities or total protein phosphatases activities. Test conditions were as follows (all in incubation buffer pH 7.5):

D. OPEN conditions (control for unaccounted changes to the enzyme during the incubation period): no additions to incubation buffer.

E. STOP condition (same as Buffer A) was designed to inhibit all protein kinases and phosphatases. “Open” buffer plus 1 mM EGTA, 1 mM EDTA, 20 mM β-glycerophosphate.

F. Endogenous Protein Kinases: incubation buffer plus 5 mM Mg·ATP, 30 mM β-GP and:

   a. 1 mM AMP to stimulate AMPK

   b. 1.3 mM $CaCl_2$ + 7 μg/mL phorbol myristate acetate (PMA) to stimulate protein kinase C (PKC)

   c. 1 U of calmodulin + 1.3 mM $CaCl_2$ to stimulate calcium–calmodulin kinase activity (CAMK)

   d. 1 mM cAMP (to stimulate PKA) + 1 mM cGMP (to stimulate PKG) plus all the components in (a)-(c) above to stimulate total kinases.

After overnight incubation, samples were mixed 1:1 with STOP buffer to halt kinase reactions before the samples were assayed as above with varying [creatine] to assess changes to K_m or relative $V_{max.}$ under the following conditions: 0-21 mM creatine, 2.5 mM ATP, 0.3 mM NADH, 4 mM PEP, 1 unit of LDH, 1 unit of pyruvate kinase, and 50 mM Tris buffer pH 7.5 in a total volume of 200 µl with 5 µl of purified enzyme used per assay. Open and Stop conditions were compared for any unaccounted-for changes in CK activity. These values were not found to be different and thus were averaged and used for comparison to the treated values under the title 'OPEN'.

Kinase in Silico predictions and homology modelling

The FASTA sequence for muscle CK from *X. laevis* (NP_001080073) taken from the NCBI database was used to predict the most likely kinase interactions through the online software from Netphos3.1 server (http://www.cbs.dtu.dk/services/NetPhos/). Serine, threonine and tyrosine residues were selected individually with threshold values set to 0.75. The same CK sequence was then run through a simple homology modelling server (https://swissmodel.expasy.org/) using the 1qh4.1.A.pdb template structure from chicken brain type creatine kinase (Eder et al. 2008), to view the location of the predicted phosphorylation sites and compare the *Xenopus* CK structure to the chicken template.

Differential Scanning Fluorimetry

CK protein unfolding was assessed using a Bio-Rad IQ PCR instrument. Purified CK that was concentrated with a Centricon (Ultracel-10 K regenerated cellulose 10,000 NMWL, REF: UFC801024) to greater than 0.02 g/l and was combined with DSF buffer

(as per Biggar et al. 2012), 40× diluted SYPRO orange dye (Invitrogen) and any additional reagents to a 20 µl final volume in thin-walled PCR plates. The plates were placed in the IQ and fluorescence was measured as described by Bigger et al. (2012). OriginPro 8.5., using the Boltzmann distribution curve, was used to determine the mid-point transition temperature where the protein is unfolding and there is an increase in fluorescence intensity. This calculated the mid-point transition temperature (T_m) at which time half the protein is unfolded (Niesen et al. 2007).

Data and Statistical Analysis

A microplate analysis program (MPA) was used to acquire enzyme rates and then data were processed using a nonlinear least squares regression computer program, Kinetics 3.51 to calculate values for kinetic parameters (Brooks 1992). Enzyme kinetic values were computed as means ± SEM and significance testing used either a Student's T-test or analysis of variance (ANOVA) followed by a Tukey's test. Statistical significance was accepted as $P<0.05$.

3.3 Results

The steps for the purification of CK from control and dehydrated *X. laevis* were as follows (summarized in Tables 1a and b). The first step in the purification was ion-exchange chromatography on DEAE Sephadex; CK eluted in the wash from this column but much other protein was left behind. The peak DEAE Sephadex fractions with high CK activity were pooled and loaded onto a Cibacron Blue column that was then eluted with 100 mM creatine in homogenization buffer. Fractions with high CK activity were

pooled resulting in a final specific activity for control CK of 26.1 U/mg and a final fold purification of 6.9 (Table 3.1a) and a final specific activity for CK from dehydrated animals of 186.4 U/mg with a final fold purification of 15.2 (Table 3.1b)

Aliquots from different steps in a control CK purification scheme were run on 12 % SDS-PAGE while the final step of dehydrated was run on a 10% SDS page (Figure 3.1). Figure 3.1 shows that considerable protein was removed during the DEAE Sephadex step (lane 3) and that the pooled fractions eluted from the Cibacron blue column provided purified aldolase from control (Figure 3.1, lane 4) and dehydrated (Figure 3.1, lanes 6 and 7) animals. The single bands for purified CK from both preparations, (at ~41 kDa) agrees with the predicted subunit molecular weight of CK calculated from its sequence, 42.9 kDa (NCBI Reference Sequence: NP_001080073.1: https://web.expasy.org/compute_pi/).

Western blotting was used to evaluate the relative amount of CK protein in muscle from control, medium (16.4% body water lost) and high (31.2%) dehydrated *Xenopus*. Antibodies detecting mammalian CK showed no significant change in CK protein content as a result of dehydration (Figure 3.2). Dot blotting was used to assess relative differences in posttranslational modifications on muscle CK purified from control versus dehydrated frogs. Data in Figure 3.3 show dot blot images for immunodetection of phosphorylated residues (left; a) and corresponding total protein from Coomassie staining (right; b). The histogram shows the relative immunofluorescence of muscle CK from dehydrated frogs compared with controls. Phosphorylation on serine residues was 25.7% lower ($p<0.05$) for dehydrated CK as compared to control CK. Phosphorylation on

threonine and tyrosine residues was not significantly different between control and dehydrated CK (Figure 3.3).

To validate the identity of the purified protein band seen on the SDS PAGE immunoblot (Figure 3.1), mass spectrometry (MS) analysis was carried out on the purified control samples. The isolated band was excised and sent for MS analysis. The peptide results revealed a protein with 29 exclusive unique peptides, 32 exclusive unique spectra and 193/381 amino acids (51% coverage) and was identified as *Xenopus laevis* creatine kinase muscle type with a molecular weight of 42,906.7 Da. This correlated to the unmodified amino acid sequence molecular weight calculated from Expasy (https://web.expasy.org/cgi-bin/compute_pi/pi_tool).

Kinetic constants for substrates were measured for purified CK from skeletal muscle of both control and dehydrated *X. laevis*. The K_m P-Cr for control CK was 6.6±0.9 mM when measured at 0.78 mM $MgCl_2$ (Figure 3.4A and Table 3.2) which was not significantly different from the comparable K_m for P-Cr of 6.3±0.9 mM for the enzyme from dehydrated skeletal muscle (Figure 3.4B and Table 3.2). $MgCl_2$ concentrations affected control and dehydrated CK differently (Figure 3.4). At 0.78 mM $MgCl_2$ the V_{max} of control CK was 1.4-fold higher than the V_{max} of CK from dehydrated frogs (Figure 3.4, Table 3.2). However, control CK was maximally activated by 1.78 mM $MgCl_2$ (V_{max} of 25.8±2.5 mU/ug) and was inhibited by 46% when $MgCl_2$ was increased to 4 mM (V_{max} of 14.0 ±1.0 mU/ug) whereas dehydrated frog CK was maximally activated by 4 mM $MgCl_2$ (52.8±2.5 mM) (Figure 3.4). The V_{max} for dehydrated CK was then 3.8-fold higher than the V_{max} for control CK at 4 mM $MgCl_2$ (Figure 3.4).

The K_m for creatine was lower for CK from dehydrated frogs compared with controls with K_m values of 11.54±0.37 and 19.24±0.832 mM, respectively (Figure 3.5 and Table 3.2). The K_m values for ATP were not significantly different between the two states with control being 1.0±0.15 mM ATP and dehydrated being 0.86±0.06 mM ATP (Figure 3.5 and Table 3.2). The CK V_{max} in the creatine + ATP direction for the enzyme from dehydrated frogs (128.9±4.6 mU/ug) was just 5.5% of the V_{max} from control frogs (2373.6±156.6 mU/ug) (Table 3.2). The effects of urea as an inhibitor/denaturant were also tested (Figure 3.6). The I_{50} value for urea inhibition of CK from dehydrated muscle CK was 0.91±0.03 M urea which was 87% of the control skeletal muscle I_{50} (1.04±0.03 M, $p<0.05$) (Figure 3.6 and Table 3.2). DSF was used to test the thermal stability of purified CK from control and dehydrated frogs. The T_m value, the temperature that resulted in 50 % unfolding of the enzyme, was determined. CK from dehydrated muscle showed a T_m value of 49.5 °C which was 1.8 °C higher than the value for the control enzyme (T_m = 47.7 °C, n = 6 $p<0.0001$)) (Figure 3.7).

Incubation studies were used to test the effects of stimulating three individual protein kinases (PKC, AMPK or CAMK) or of stimulating total protein kinase or total protein phosphatase activities on K_m creatine (Table 3.3) or V_{max} (Table 3.4) values for CK from dehydrated frogs. Unstimulated dehydrated CK (OPEN condition) had a creatine K_m (5.86 mM) (Table 3.3) that was not significantly different from the purified dehydrated CK (6.6 mM, Table 3.2) from dehydrated frog muscle. The stimulation of CAMK resulted in the K_m creatine value being increased by 2.25-fold (Table 3.3) and the V_{max} becoming increased by1.89-fold (Table 3.4). AMPK did not affect the K_m creatine but significantly increased the maximal velocity of CK by 1.4-fold (Table 3.3 and 4).

PKC action led to a significant decrease in the K_m creatine of dehydrated CK by 61.6% but did not alter the maximal velocity. Stimulation of total kinases or total phosphatases did not significantly alter either K_m or V_{max} values of the enzyme (Table 3.3 and 4). In the case of kinase action this may be a consequence of opposing actions of PKC and CAMK on the K_m.

The CK protein sequence was analyzed via the NetPhos3.1 program to predict binding sites for protein kinase phosphorylation on the protein. PKC was the only kinase that met the threshold for phosphorylating CK (Table 3.5). PKC had the highest score (0.86) for putative phosphorylation of CK at Thr103, followed by Thr133 (0.84), S128 (0.83) and then finally S129 (0.77). The same CK sequence was then run through a simple homology modelling server using chicken brain-type creatine kinase (Eder et al. 2008) as the template which resulted in a sequence identity of 83.4%. The four sites predicted to be phosphorylated by PKC are highlighted to demonstrate their exposure on the quaternary structure, which implicates them as potential binding sites for the protein kinase (Figure 3.8).

3.4 Discussion

X. laevis muscle CK was purified to apparent homogeneity through a combination of ion-exchange and affinity column chromatography (Figure 3.1). The subunit molecular weight (~41 kDa) of CK (a dimer in its native state), corresponded well with the predicted molecular weight (42.9 kDa) calculated from the CK amino acid sequence as well as the subunit molecular weights reported for CK from various other species (Abnous and Storey 2007; Dieni and Storey 2009). This purification scheme typically

produced enzyme preparations that were purified 15.2-fold from dehydrated animals with final specific activities of 186.4 U/mg (Table 3.1).

The velocity vs [substrate] measurements indicated that the substrate affinities and maximal velocity of *Xenopus* skeletal muscle CK change significantly between control and dehydrated conditions (Table 3.2). CK maximum activity decreased significantly by 94.6% in the creatine phosphorylating direction between the two physiological conditions but was $MgCl_2$-dependent in the reverse direction. If assayed at 0.78 mM $MgCl_2$, the P-Cr V_{max} decreased by 30% in dehydrated frogs, as compared with control frogs (Figure 3.4). However, when assayed at 4 mM $MgCl_2$ the V_{max} of CK from dehydrated frogs increased by 3.8-fold over the comparable control value (Figure 3.4). This occurred with no significant change in the relative protein amount of CK in the cells (Figure 3.2). Interestingly, substrate affinities for P-Cr increased (ie. K_m decreased) as $MgCl_2$ concentrations increased when assaying CK from control animals (Figure 3.4). The opposite occurred when CK from dehydrated animals was assayed (Figure 3.4). This indicates a decrease in CK sensitivity to low concentrations of magnesium concentrations while also allowing for an increase in the capacity of this salt to activate CK. Furthermore, CK affinity for creatine followed an opposite trend with a reduced V_{max} but a 40% decrease in the K_m for creatine in muscle from dehydrated frogs (Table 3.2). Hence, during high dehydration, CK appears to be regulated to reduce the use of creatine and favor the use of P-Cr. A response that is amplified as $MgCl_2$ concentrations are increased.

Maintaining muscle energetics during estivation or under stressful environmental conditions is important for long-term viability. High P-Cr reserves in skeletal muscle can maintain ATP pools for prolonged times under stress conditions whereas other tissues that lack P-Cr reserves (e.g. liver) show a much more rapid decline in ATP and total adenylate pools in response to stress (Storey 1987). Thus, in addition to buffering ATP demands during exercise, P-Cr and CK can maintain a high energy state in muscle under stresses imposed by hypoxia, hibernation, freezing and now, dehydration. The increase in maximal activity of the dehydrated enzyme suggests that the enzyme undergoes a stable modification that functionally activates CK only when $MgCl_2$ concentrations are high (note that dehydration of muscle cells would, by default, elevate cytoplasmic Mg^{2+} levels). This modification is likely a mechanism to reduce its role in buffering ATP levels in dehydrated muscle perhaps to save phospho-creatine stores for a when dehydration is reaching its upper limits. This conditional activation occurred simultaneously with an increase in thermal stability of the enzyme, which suggests that a modification may be altering the enzyme's overall structure (Figure 3.7). Increased thermal stability is an indication that CK is more structurally stable in muscle under high dehydration conditions and implies that enzyme regulation may also be reducing protein turnover during high dehydration. Protein turnover is an energetically costly cellular event that many organisms suppress when faced with environmental stress (Storey and Storey 2004).

Subsequent experiments evaluated post-translational modification as the possible mechanism responsible for dehydration-induced changes to CK. Reversible protein phosphorylation typically alters kinetic parameters of enzymes such as substrate affinities

or effects of inhibitors/activators by creating conformational changes in the protein structure (Humphrey et al. 2015). There is considerable prior evidence that CK undergoes protein phosphorylation that serves various outcomes. For example, in hibernating ground squirrels, phosphorylated CK showed a lower activity than the dephosphorylated form (Abnous and Storey 2007). Threonine autophosphorylation near the active site is known to regulate CK activity and the direction of the reversible reaction whereas the phosphorylation by PKC inactivates BB-CK (Chida et al. 1990b). However, *Xenopus* CK did not show a change in threonine phosphorylation in response to dehydration. In rat skin, CAMK phosphorylates CK with no effect on CK activity whereas AMPK phosphorylation leads to inactivation (Chida et al. 1990a, b). During dehydration, CK in *Xenopus* muscle showed a decrease in total serine phosphorylation (Figure 3.3) that correlated with changes in the V_{max} in the P-Cr utilizing direction (Figure 3.4 and Table 3.2) that may suggest that the dephosphorylation of CK could be the mechanism used in muscle to regulate the use of its P-Cr pool in the dehydrated state. Previous work with *Rana sylvatica* revealed that when these frogs freeze, which causes anoxia due to an ice-induced halt to blood flow, muscle CK became more phosphorylated leading to an increase in enzyme maximal velocity and substrate affinity (Dieni and Storey 2009). It is of interest that *Xenopus* responded differently since the conditions experienced by the two species are comparable with both experiencing reduction in blood flow under the stress condition. Freezing at low temperatures slows metabolism whereas dehydration stress is often accompanied by hotter conditions, making the reduction of enzyme activity more critical as the environmental factors do not assist in metabolic rate depression. However, *Xenopus* CK having different magnesium sensitivities under hydrated versus

dehydrated conditions may help tailor the use of P-Cr to the physiological requirements in these two states.

In order to assess which specific protein kinase activity may mediate dehydration-induced changes in CK, incubations that stimulated the activities of different endogenous protein kinases were conducted using crude muscle extracts from dehydrated frogs that displayed the lower phosphate form of the enzyme (Figure 3.3). The crude extracts did not differ significantly from the purified enzyme with respect to K_m for creatine. Stimulation of AMPK caused an increase in CK V_{max} for the enzyme from dehydrated frogs without a change in K_m creatine (Table 3.4). The recovery of the maximal velocity with no change in substrate affinity suggests that the dehydration-related reduction in serine phosphorylation that occurs *in vivo* (Figure 3.3) might be linked to AMPK phosphorylation sites (Tables 3 and 4). Incubations that stimulated CAMK activity increased CK V_{max} (Table 3.4) as would be predicted if this kinase restored the enzyme to control conditions but CAMK action on dehydrated CK also elevated K_m creatine, that was opposite to expectations for a return to the control state (Table 3.2 and Table 3.3). PKC action on dehydrated CK reduced K_m creatine but did not significantly change V_{max} (Tables 3 and 4). The actions of these three protein kinases indicate that they are probably physiological regulators of the frog CK enzyme, which is consistent with the known regulatory sites on CK (Chida et al. 1990b). However, their actions did not fully mimic the kinetic changes in CK that would be required to restore the enzyme parameters of the control enzyme. Potentially, a combination of two or more protein kinases is involved the recovery of control CK properties when frogs are rehydrated. The incubations to stimulate endogenous kinases suggests that AMPK is a likely kinase that acts on CK in

muscle and the removal of this phosphorylation regulates CK activity during dehydration. *In silico* studies pointed to PKC as the most likely protein kinase to act on frog muscle CK (Table 3.5, Figure 3.8). However, incubations to stimulate PKC did not show a significant impact on the V_{max} of CK which could indicate that PKC phosphorylation sites on the enzyme are not involved in kinetic regulation but perhaps instead regulate cellular localization or stability. AMPK is known to play a significant role in the stress response and is known to be regulated by the ATP:AMP ratio (Ponticos et al. 1998; Hardie et al. 2012; Gowans et al. 2013). Ponticos et al., (1998) demonstrated that AMPK is also activated by a decrease in the P-Cr:Cr ratio making its interaction with CK a potential feedback loop to regulate muscle energetics. The impact of different phosphorylation sites on CK regulation would require knockout studies to determine their individual roles in dehydration survival.

In conclusion, the present data show that CK from *X. laevis* muscle undergoes a stable modification that regulates the maximal velocity of this enzyme in response to magnesium concentrations during high dehydration. The low phosphate (dehydrated) form of CK showed a different magnesium sensitive V_{max}, along with an increased tolerance for thermal unfolding and increased sensitivity to urea unfolding (Figure 3.6, 7 and Table 3.2). The physiological consequences of dehydration-induced CK regulation appear to be to limit the use of P-Cr until magnesium concentrations naturally increase during high dehydration in *Xenopus laevis*. CK has a crucial role to play in mediating muscle responses to exercise or environmental stress since the enzyme mediates a very fast-acting response to declining ATP levels in the cell by replenishing ATP from the rapid transfer of the phosphate group of P-Cr to ADP (Wallimann et al. 1992). Typically,

P-Cr mobilization is near-instantaneous and supports ATP levels during the longer time that it takes for ATP production by glycolysis or by oxidative phosphorylation to be activated. Since glycolysis appears to be downregulated during dehydration stress at the intermediate and final enzymatic steps (Chapter 2 and Childers et al., 2019), the magnesium dependent use of P-Cr by CK may help to ration these reserves until dehydration reaches a crucial level. Posttranslational modifications are known to contribute to CK regulation by altering its enzymatic activity but the response to various environmental stresses have not been fully characterized (Abnous and Storey 2007; Dieni and Storey 2009). The structural and functional modifications of CK revealed by this study indicate a level of CK control via reversible protein phosphorylation that provides a mechanism for reducing the use of P-Cr during whole animal dehydration until physiological signals reach critical levels.

3.5 Figures

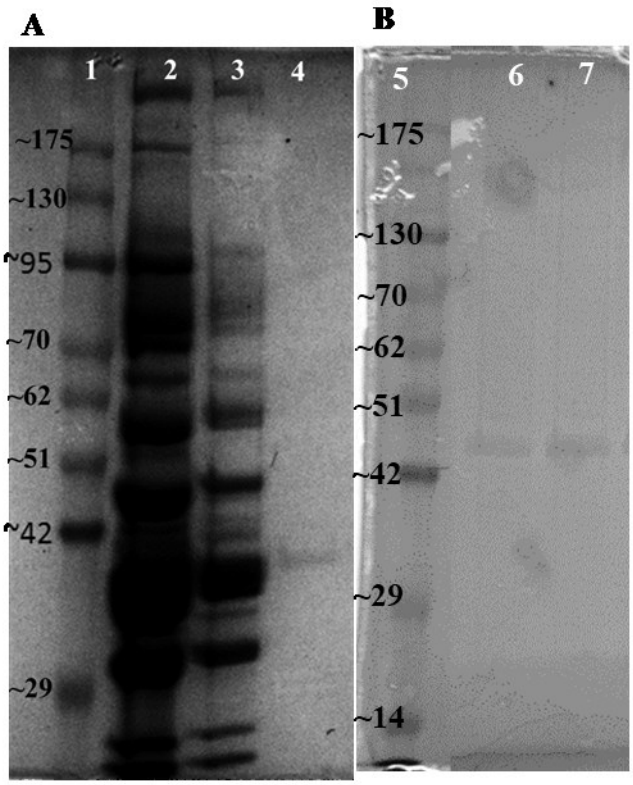

Figure 3.1: Isolated muscle CK from control and dehydrated *X. laevis*.

Electrophoretic analysis on 12% and 10% SDS-PAGE gels shows the different steps in the purification scheme of A) control CK and B) the final purification step of dehydrated CK. A) Lane 1: molecular weight ladder with kDa sizes indicated on the left. Lane 2: crude control supernatant, Lane 3: pooled fractions from DEAE Sephadex chromatography, Lane 4: final desalted CK fractions after Cibacron Blue chromatography. B) Lane 5: molecular weight ladder with kDa sizes indicated on the left. Lane 6 and 7: top two elution fractions from Cibacron Blue chromatography.

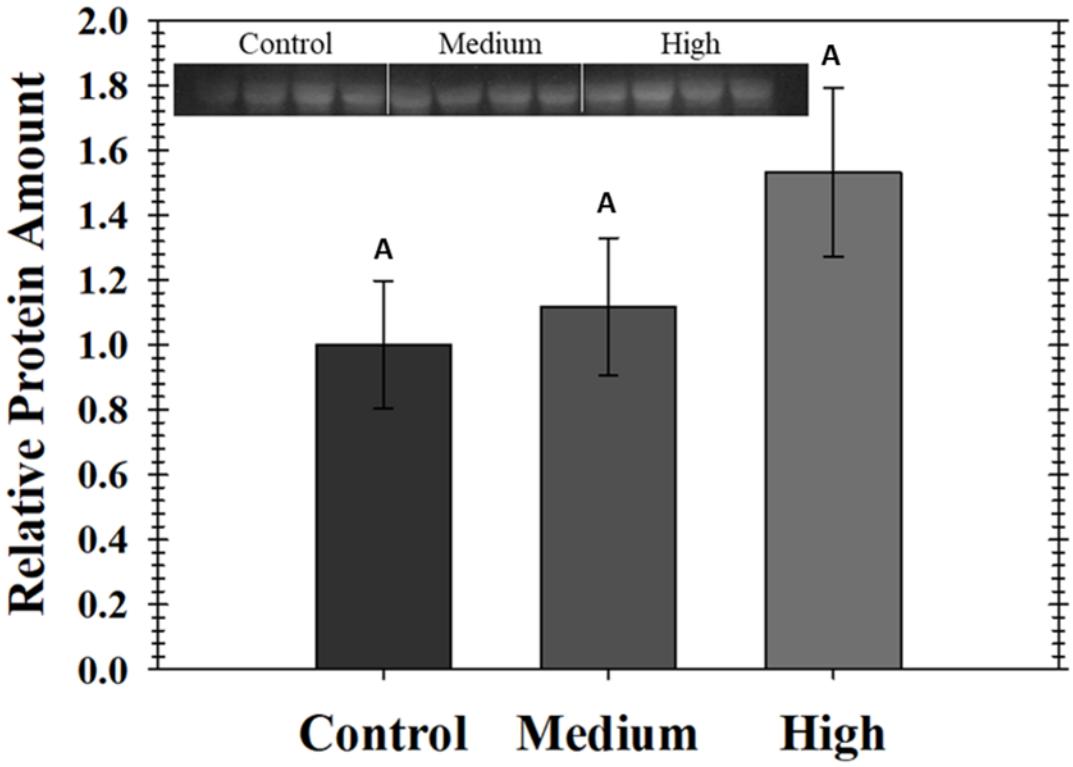

Figure 3.2: Standardized total CK protein content in skeletal muscle extracts of control, medium and high dehydrated *Xenopus*, as determined by immunoblotting. Data are means ± SEM, n = 4 independent determinations on different preparations of enzyme.

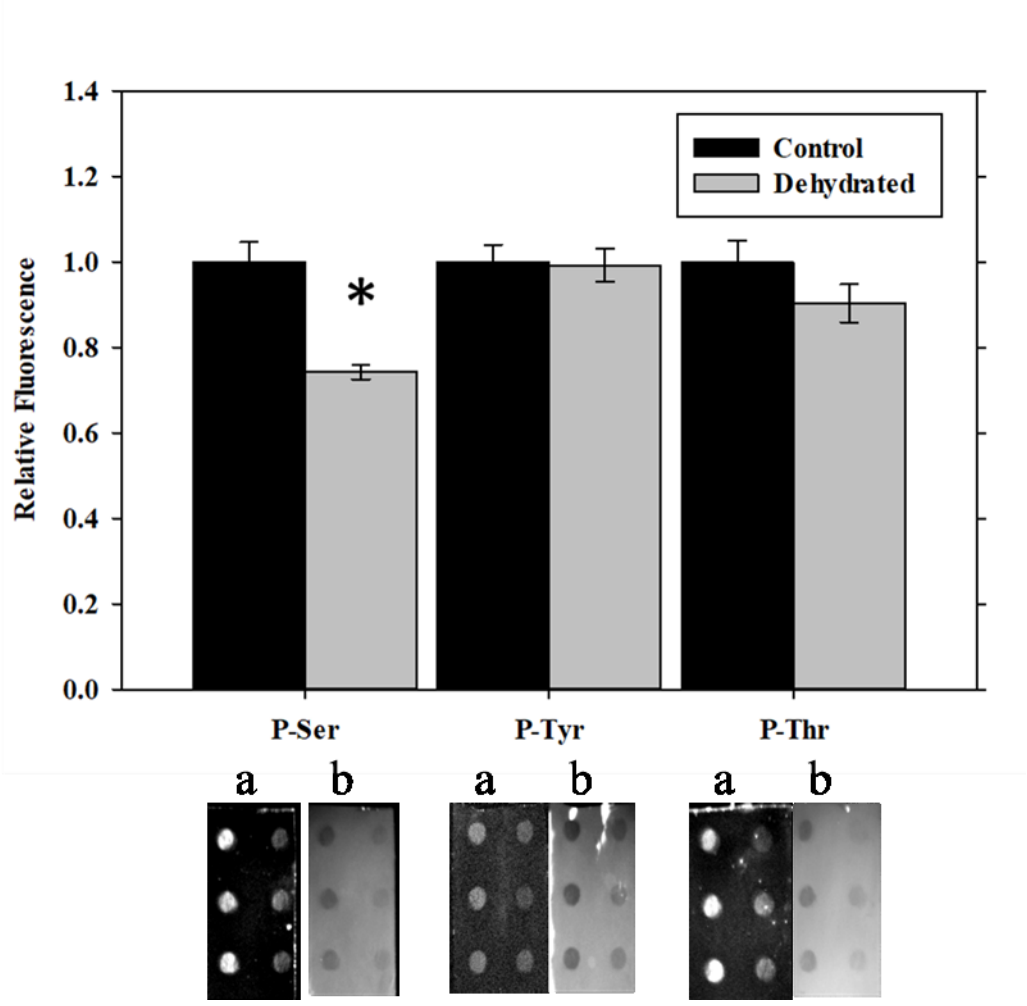

Figure 3.3: Dot blot analysis of posttranslational phosphorylation (serine, threonine, tyrosine) of purified *X. laevis* muscle CK from control and dehydrated frogs. Paired chemiluminescent images (left) and Coomassie stained dots (right) are shown below the corresponding histogram bars (a, control; b, dehydrated). Data are relative intensities, means ± SEM, n = 6. The Student's t-test was used for statistical analysis and the asterisk indicates a significant change from the corresponding control value, $p < 0.05$.

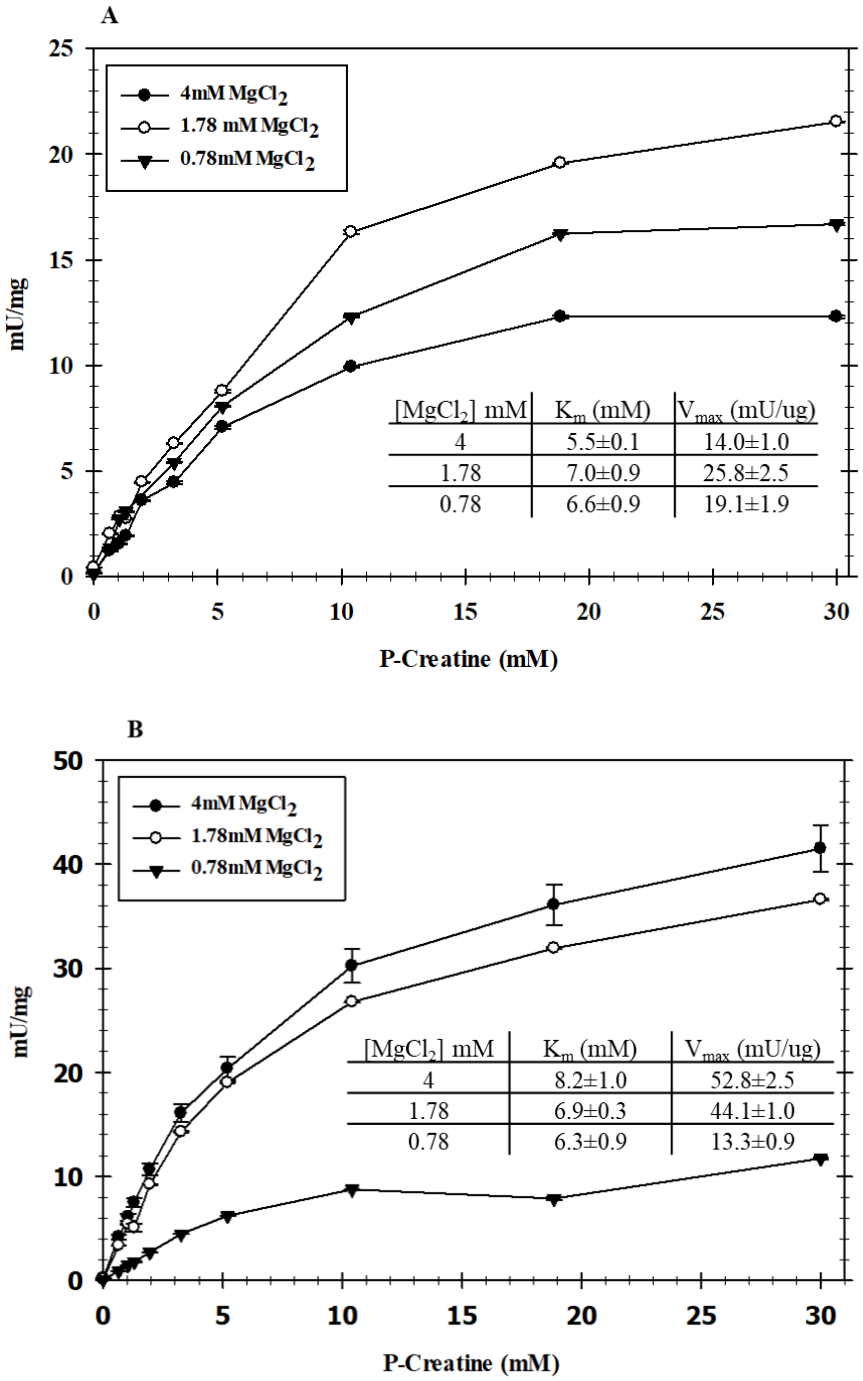

Figure 3.4: P-Creatine kinetics for (A) Control, and (B) Dehydrated CK at various concentrations of $MgCl_2$. Plots are [P-Cr] vs initial enzyme velocity points with data being means ± SEM, n = 4 individual enzyme determinations. K_m and V_{max} values for each $MgCl_2$ concentration are shown in the inset table.

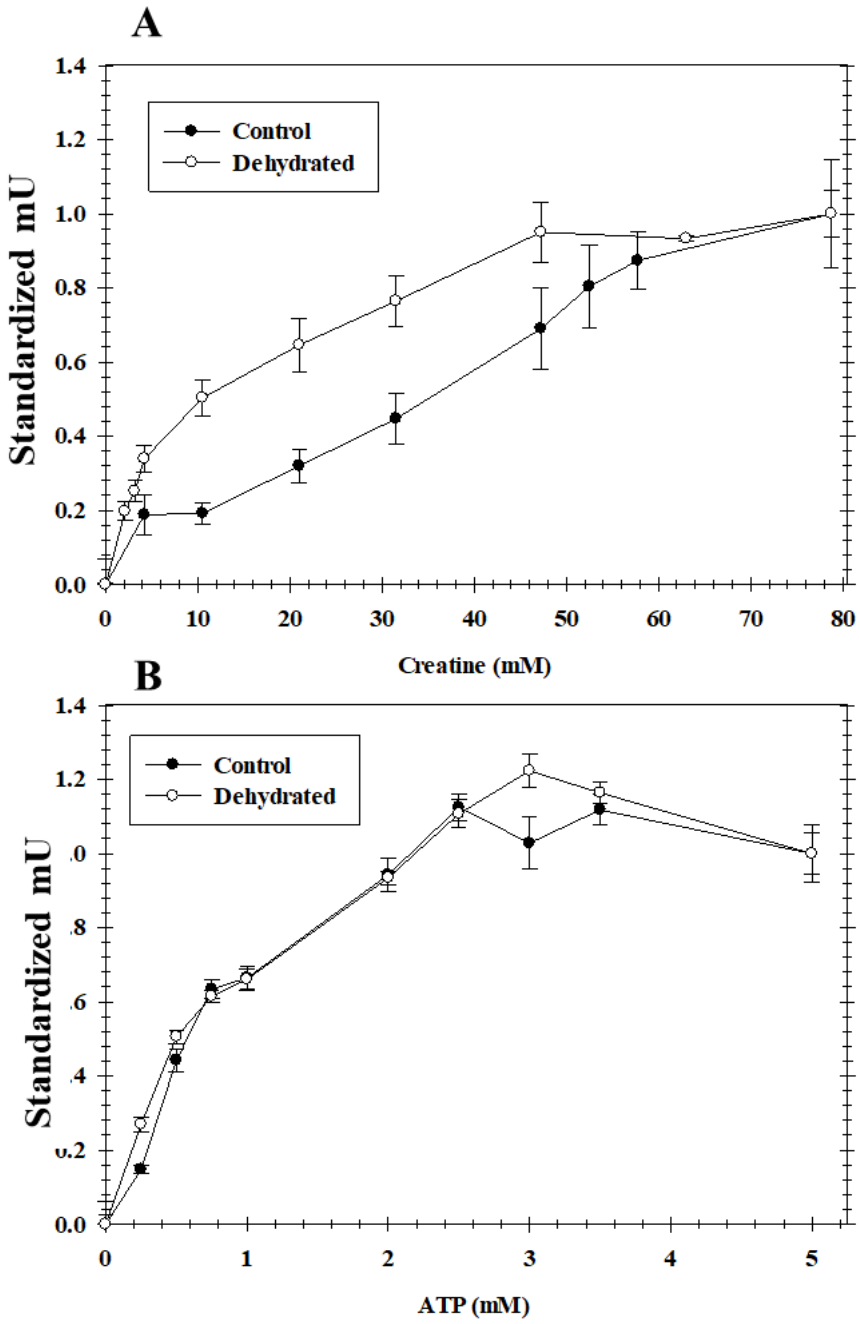

Figure 3.5: Normalized basic kinetics of control and dehydrated CK in *Xenopus* skeletal muscle. Data has been normalized to a V_{max} value of 1 to highlight changes in K_m. See Table 3.2 for the calculated I_{50} values. Individual velocity points are means ± SEM, n = 4.

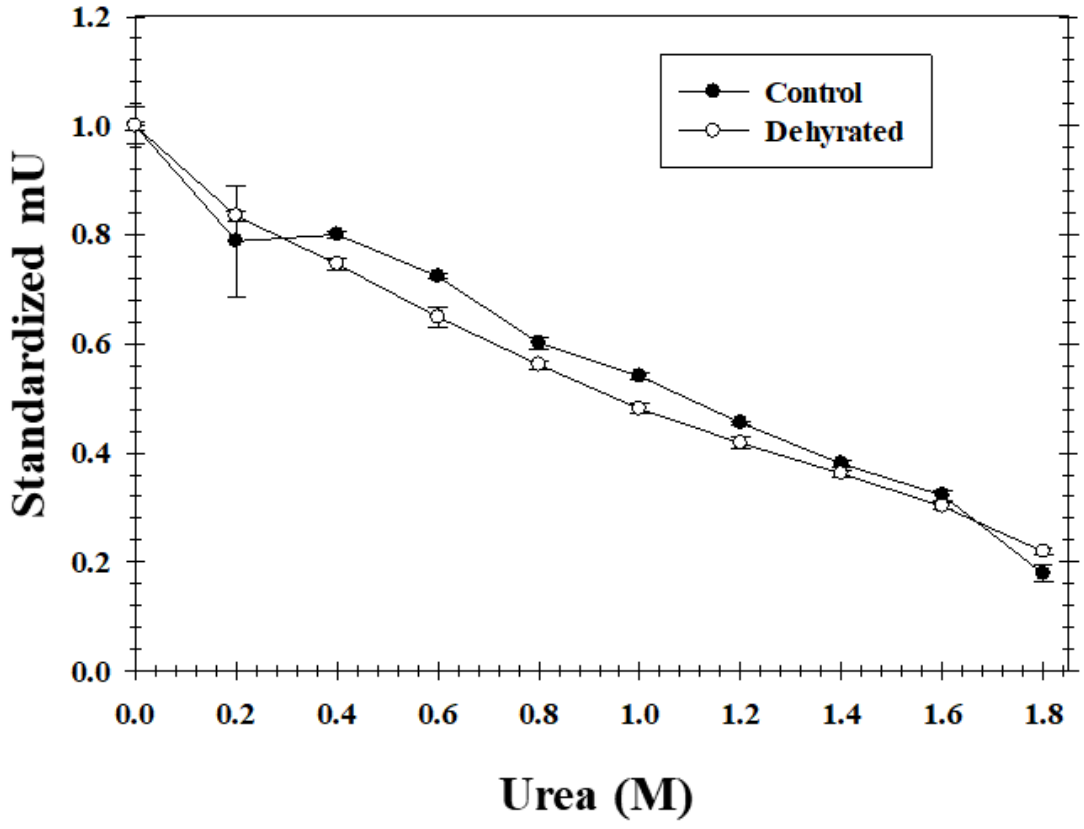

Figure 3.6: Graphical results assessing inhibition of purified CK by urea. Graphs show velocity vs [urea] with increasing amounts of urea assayed at saturating substrate concentrations are presented. See Table 3.2 for the calculated I_{50} values. Velocity points are means ± SEM for n=3-4.

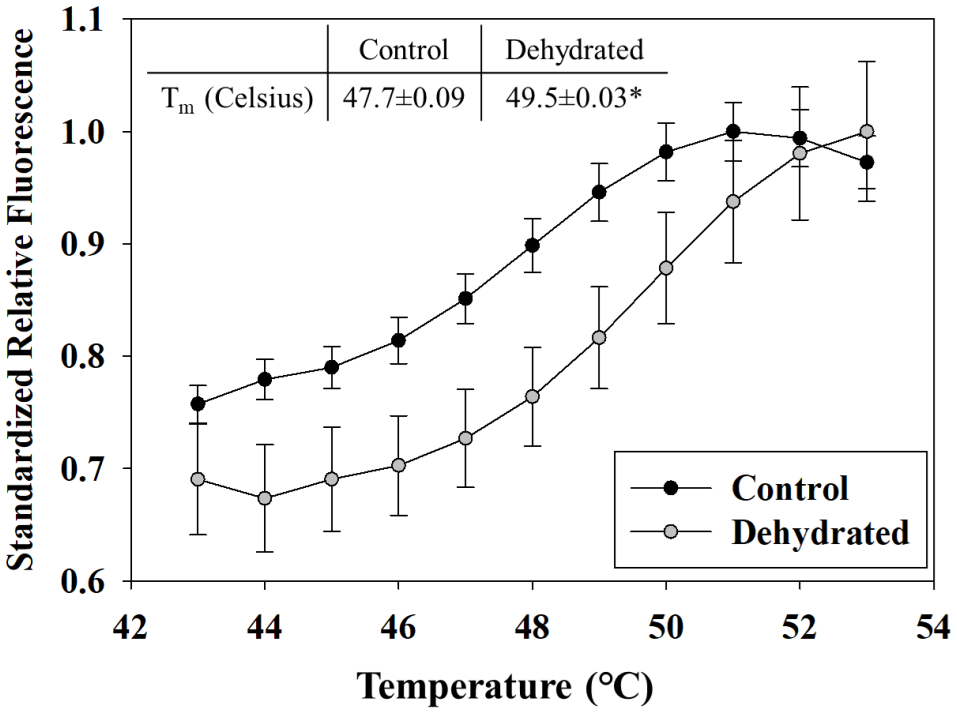

Figure 3.7: Thermal stability of control and high dehydrated CK as measured by differential scanning fluorimetry. The melting curves of control (black dots) and dehydrated (white dots) CK are shown with standardized relative fluorescence plotted against temperature. Data are means ± SEM, n = 4 individual enzyme determinations. T_m values are shown in the inset table.

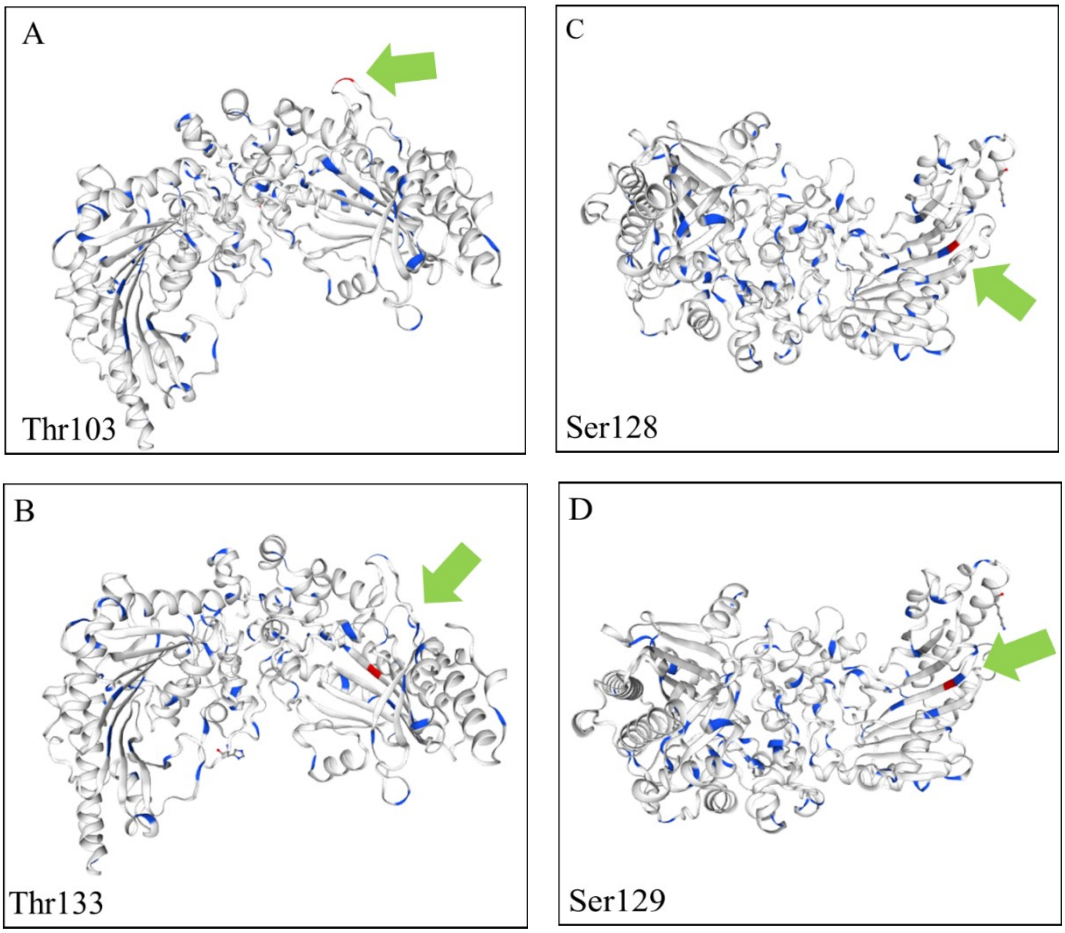

Figure 3.8: Homology models of *Xenopus* muscle creatine kinase indicating the predicted phosphorylation sites from NetPhos3.1. A) Thr103, B) Thr133, C) Ser128, D) Ser129.

3.6 Tables

Table 3.1 (a): Purification table for CK from control frog muscle. Assayed at 0.78 mM $MgCl_2$.

Step	Total protein (mg)	Total activity (U)	Yield (%)	Fold purification	Specific activity (U/mg)
Crude	13.6	51.5	-	-	3.8
DEAE	9.5	53.6	104.0	1.5	5.6
Cibacron Blue	0.6	15.1	28.1	6.9	26.1

Table 3.1(b): Purification table for CK from dehydrated frog muscle. Assayed at 2.5 mM Mg^{2+}.

Step	Total protein (mg)	Total activity (U)	Yield (%)	Fold purification	Specific activity (U/mg)
Crude	12.1	149.6	-	-	12.3
DEAE	7.4	144.0	96.6	1.6	19.6
Cibacron Blue	0.1	24.5	17.0	15.2	186.4

Table 3.2: **Summary of kinetic parameters for purified CK from skeletal muscle of control and dehydrated frogs assayed at 23 °C. K_m and I_{50} values for P-Cr, creatine and ATP were determined at constant co-substrate concentrations, 4 mM ADP, 4 mM ATP or 10 mM creatine**. The P-Cr K_m and V_{max} was measured at 0.78 mM $MgCl_2$. All ATP/ADP stock solutions were prepared as a 1:1 molar mix with $MgCl_2$. Data are mean ± SEM (n = 4-6). *Significantly different from the corresponding control condition using the Student's t-test ($p < 0.05$).

Parameter	Control	Dehydrated
K_m P-Cr (mM)	6.6±0.9	6.3±0.9
P-Cr V_{max} (mU/ug)	19.1±1.9	13.3±0.9*
K_m Creatine (mM)	19.2±0.8	11.5±0.4*
K_m ATP (mM)	1.0±0.2	0.86±0.1
Creatine V_{max} (mU/ug)	2373.6±156.6	128.9±4.6*
I_{50} Urea (M)	1.04±0.03	0.91±0.03*

Table 3.3: Kinetic values of dehydrated CK assayed for the creatine K_m after the incubated with additives that stimulated individual protein kinases (PKC, AMPK, CAMK) or that stimulated total protein kinase or total protein phosphatase action. Data are mean creatine K_m ± SEM (n = 4-6). *Significantly different from the "OPEN" condition using the Student's t-test ($p < 0.05$).

	Creatine K_m (mM)	p-values
OPEN	5.86±0.98	
PKC	2.55±0.99*	0.02
AMPK	6.32±0.73	0.72
CAMK	14.97±0.41*	0.00
Total Kinase	4.92±0.25	0.40
Total PPase	7.37±0.50	0.22

Table 3.4: **Effects on the CK V_{max} in the creatine-using direction when crude muscle extracts from dehydrated frogs were incubated with additives that stimulated individual protein kinases (PKC, AMPK, CAMK) or that stimulated total protein kinases or total protein phosphatases.** Data are mean V_{max} ± SEM (n = 4-6) with the data standardized to the OPEN condition which has been set to 1 U/g. *Significantly different from the "OPEN" condition using the Student's t-test, $p < 0.05$.

	Standardized Creatine V_{max} (U/g)	p-value
OPEN	1.00±0.08	
PKC	0.84±0.07	0.15
AMPK	1.39±0.1*	0.01
CAMK	1.89±0.09*	0.001
Total Kinase	0.96±0.07	0.73
Total PPase	1.31±0.001	0.35

Table 3.5: *In silico* kinase binding site prediction from the NetpPhos 3.1 server for *Xenopus* CK (Accession#: NP_001080073.1).

Residue	Context	Output Score	Kinase
Thr103	GYKP**T**DKHK	0.861	PKC
Thr133	GYKP**T**DKHK	0.809	PKC
Ser128	NYVL**S**SRVR	0.833	PKC
Ser129	YVLS**S**RVRT	0.777	PKC

Chapter 4: Fatty acid synthesis and autophagy: the role of AMP-activated protein kinase on fuel use during dehydration in *Xenopus laevis*

4.1 Introduction

All eukaryotes possess mechanisms for assessing the status of energy reserves and energy demand, and when required, making compensatory adjustments (Hardie et al. 1998; Ross et al. 2016). AMP-activated protein kinase (AMPK) is the main protein kinase sensitive to low cellular energy status that stimulates energy producing pathways to restore homeostasis during times of stress (Hardie and Carling 1997; Hardie et al. 2012) . AMPK is a heterotrimer built of a catalytic α subunit and two regulatory subunits, β and γ (Ross et al. 2016; Wang et al. 2016; Rider 2016). The α subunit has two isoforms, α1 and α2, that both consist of an N-terminal kinase domain that is most commonly activated through the phosphorylation of Thr172 (Horman et al. 2005; Wang et al. 2016). High concentrations of AMP and ADP promote AMPK activity through allosteric stimulation of activity or by preventing the dephosphorylation of AMPK at Thr172 (Horman et al. 2005; Oakhill et al. 2011; Xiao et al. 2011; Gowans et al. 2013). Typically, low energy stress and the stimulation of AMPK leads to a decrease in energy-consuming biosynthetic pathways. One of these pathways is fatty acid synthesis that is gated via acetyl-CoA carboxylase 1 (ACC1). ACC1 catalyzes the irreversible carboxylation of acetyl-CoA to produce malonyl-CoA, the building block for fatty acid chains (Winder et al. 2003; Horman et al. 2005; Wang et al. 2015; Craig et al. 2018). AMPK-induced phosphorylation of ACC1 inhibits its activity and thereby halts fatty acid synthesis. Malonyl-CoA also inhibits carnitine palmitoyltransferase I (CPT1), a key enzyme in the process of fatty acid β-oxidation (Figure 4.1). Therefore, AMPK can promote or inhibit the use of fatty acids as fuel through this interaction with ACC1 (Hardie and Pan 2002; Wang et al. 2015; Rider 2016). Previous evidence has suggested

that β-oxidation is downregulated in *X. laevis* during high dehydration, therefore the interaction between AMPK and ACC1 is of interest since ACC1 phosphorylation can influence the fat catabolic pathway and help to conserve or alter fuel use in the face of environmental stress (Luu, 2018, Hardie and Carling 1997).

AMPK also sits at a critical branchpoint between cell growth and autophagy signaling (Hardie 2011; Sanchez et al. 2012). Canonically, autophagy is used to balance protein levels in muscle tissue and AMPK has been shown to interact with the mammalian target of rapamycin complex 1 (mTORC1), which in opposition, supports muscle mass. The ULK1 (unc-51 like autophagy activating kinase 1) serine/threonine protein kinase is a key regulator of the initial event in autophagy, the formation of the autophagosome (Hardie 2011; Alers et al. 2012). In this thesis, the interaction at ULK1 is of interest since AMPK (activated during low energy/nutrient conditions) can directly phosphorylate ULK1 at multiple sites including Ser555 to promote autophagy (Egan et al. 2011; Bach et al. 2011). Activated mTOR, which is a regulator of cell growth and is an inhibitor of autophagy, opposes AMPK when it phosphorylates ULK1 at Ser758 which inhibits its action (Shang and Wang 2011; Egan et al. 2011; Alers et al. 2012). Therefore, the interaction between these two signals details the crosstalk between AMPK and mTORC1 signaling on ULK1 (Egan et al. 2011). The signaling through adenylate ratios and the activation of AMPK in *X. laevis* skeletal muscle is unknown, although mTOR signals have previously been reported to be downregulated (Luu, 2018).

Previous work on *X. laevis* has demonstrates that, during whole animal dehydration, skeletal muscle undergoes a remodelling of its molecular signaling.

Importantly, high nutrient signalling through the AKT/mTOR pathway is decreased through the dephosphorylation and reduction in AKT and mTOR total protein levels during high dehydration (Luu 2011; Childers and Storey 2016, 2019). This reduced signalling through AKT and mTOR is coupled with the apparent increased dependence on glycolytic ATP production and a reduction in access to P-Cr reserves through reduced CK activity (Childers and Storey 2016, 2019, Chapter 2 and 3). It is reasonable to assume that ATP levels may be compromised by these changes and lead to elevated AMP, which would alter the activity level of AMPK. This is especially interesting since AMPK is sensitive to AKT/mTOR signalling, adenylate ratios and, as recent research suggests even the P-Cr:Cr ratio (Ponticos et al. 1998; Xiao et al. 2011; Oakhill et al. 2012). Therefore, the current chapter investigates the phosphorylation state of AMPK and the phosphorylation of two key downstream proteins involved in regulating the energy balancing pathways of fatty acid synthesis and autophagy. Both ACC1 and ULK1 gate these processes through reversible phosphorylation and could indicate the likely state of energy balance during high dehydration in *X. laevis.*

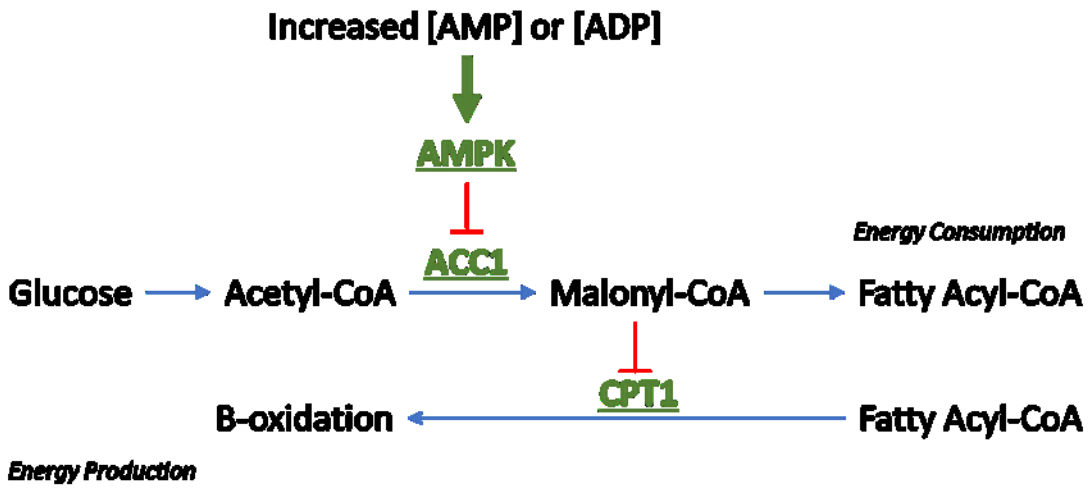

Figure 4.1: Activated (Thr172) AMPK phosphorylates ACC1 to decrease malonyl-CoA production and *de novo* fatty acid synthesis. This also stimulates β- oxidation through the removal of malonyl-CoA inhibition on carnitine palmitoyltransferase I (CPT1). Adapted from (Rider 2016).

4.2 Methods

Animals.

See Chapter 2

Protein Extractions

See Chapter 2.

Western blotting

Immunoblotting was done as described in Chapter 2. In short, equal amounts (25 µg) of prepared protein homogenate and 4–5uL of 10.5–175 kDa PiNK Plus pre-stained protein ladder (#PM005-0500; FroggaBio, Toronto, Canada) were loaded onto 10% SDS-PAGE gels and electrophoresis was carried out at 180 V for 50-90 min. Proteins were transferred to PVDF membrane at 160 mA for 90 min (2h for ACC1). Membranes were then blocked with 2.5% non-fat dried milk in Tris–buffered saline containing Triton-X (TBST) for 30 min and washed three times with TBST. Membranes were incubated with primary antibodies (antibodies are listed in Table 4.1; all were a 1:1000 dilution) overnight at 4°C. After washing with TBST, membranes were incubated with secondary antibody (mouse anti-goat IgG) for 30 min and then washed. Immunoreactive bands were visualized with enhanced chemiluminescence (H_2O_2 and Luminol) using a ChemiGenius Bioimaging System (Syngene, Frederick, MD) and band intensities were quantified using the associated Gene Tools program. Each PVDF membrane was then stained using

Coomassie brilliant blue (see Chapter 2) to visualize the total amount of protein in each lane.

Quantification and Statistics

Immunoblot band density in each lane was standardized against the summed intensity of a group of Coomassie-stained protein bands in the same lane; this group of bands was chosen because they were not located close to the protein band of interest but were prominent and constant across all samples. This method of standardizing against a total protein loading control has been suggested to be more accurate in comparison with standardizing against housekeeping proteins such as tubulin (Eaton et al., 2013). Western blot band densities were normalized at each condition relative to control. Immunoblot data are expressed as means ± SEM, n = 4 independent samples from different animals. Statistical testing used the one-way ANOVA and the Tukey's post-hoc functions from the SigmaPlot 12.0.

4.3 Results

AMPK subunit protein levels were investigated to determine the isozyme composition present in *X. laevis* skeletal muscle and to assess whether these changed during dehydration. Total protein levels of the three AMPK subunits (AMPKα1, α2 and 2β) did not change significantly in skeletal muscle in response to either medium or high dehydration of the frogs (16.43 ± 0.33% and 31.18 ± 0.83% respectively of whole body water lost) (Figure 4.2). The activation loop sequence containing Thr172 of the human AMPK α1/α2-subunit (DFGLSNMMSDGEFLR**T**SCGSPNYAAPE) is extremely well

conserved across eukaryotic evolution (Figure 4.3) and the whole protein was 75.4% conserved when the *X. laevis* sequence (NP_001088426) was compared to human (AAB32732) by the Clustal 2.1 program. Hence, it is not surprising that the anti-human p-Thr172 AMPK α-subunit antibody cross reacted with the frog AMPK sequence where the phosphorylation site was identified at Thr183 (Figure 4.3 and 4.4). Relative phosphorylation levels of the p-Thr172 catalytic α-subunit activation loop were not significantly elevated in response to dehydration in *X. laevis* (Figure 4.4). However, another known and well-conserved phosphorylation site on mammalian AMPK, p-Ser496 (Figure 4.3), which corresponded to p-Ser516 (QAK**S**SDGSG) in *X. laevis*, showed a significant reduction in relative phosphorylation by 73% and 63% during medium and high dehydration, respectively (Figure 4.4).

ACC1 phosphorylation is the main point of AMPK regulation of fatty acid synthesis. ACC1 was 91% conserved between human (NP_942131) and *X. laevis* (XP_018104903) sequences when compared with Clustal 2.1. The sequence surrounding the Ser79 phosphorylation site of human ACC1 was also well conserved in *X. laevis* (RPSM**S**GLHLV) explaining the cross-reaction of the frog protein with the anti-rabbit p-Ser79 ACC1 antibody (Figure 4.3). Immunoblotting revealed a decreasing trend (by 29%) in ACC1 Ser79 phosphorylation under the medium dehydrated condition, compared to control frogs. This changed to a very strong and significant decrease of 89% ($p<0.05$) in ACC1 phosphorylation under the high dehydration condition, as compared to control frogs (Figure 4.5).

AMPK regulates autophagy signalling through an interaction with the ULK1 protein. The ULK1 sequence was 70% conserved between human (AAC32326) and *X. laevis* (AAI54696) when compared with Clustal 2.1 and the peptides containing the human ULK1 p-Ser758 (GSRLH**S**APNL) and p-Ser555 (FTVG**S**PPDG) residues are well conserved in the *X. laevis* protein explaining the good cross-reactivity of the frog protein with the mammalian antibodies (Figure 4.3). Immunoblotting to assess total ULK1 protein levels showed an increased trend in ULK1 protein in medium dehydrated frogs (but not significantly different from the control). Under high dehydration, however, ULK1 total protein showed a downward trend (not significantly different from control) but that was significantly different from the medium dehydration value, an overall 70% decrease between medium and high dehydration in ULK1 total protein levels in frog muscle ($p<0.05$, Figure 4.6). Phosphorylation of ULK1 was also examined. Protein levels of p-Ser758 were significantly increased by 1.78-fold between control and high dehydrated conditions (Figure 4.7). Phosphorylation on ULK1 Ser555 also increased by 1.68-fold and 1.84-fold in medium and high dehydrated frogs, respectively (Figure 4.7).

Beclin1 is a downstream autophagy-related protein whose expression is stimulated by AMPK phosphorylation. Beclin1 was 88% conserved between human (AAD27650) and *X. laevis* (AAH73292) sequences when compared with Clustal 2.1. The sequence containing the human beclin1 p-Ser93 (TDGV**S**RRL) site was also well conserved in *X. laevis* explaining the reaction of frog beclin1 with mammalian antibodies (Figure 4.3). Immunoblotting for total protein content revealed no significant change in beclin1 total protein in medium or high dehydration as compared to control (Figure 4.8). However, a 37% and 36% decrease in phosphorylation on beclin1 Ser93 occurred under

medium and high dehydration conditions compared to control, indicating a substantial sensitivity of this protein to changes in tissue water content (Figure 4.8, $p<0.05$).

FoxO3a transcription factor activation by AMPK induces the expression of various downstream autophagy-related proteins. The FoxO3a sequence was 72% conserved between human (NP_963853) and *X. laevis* (NP_001086418) when compared using Clustal 2.1. The sequence surrounding the human FoxO3a p-Ser318 site (PRRRAV**S**MDNSNKYTKTTE) was partially conserved in *X. laevis* with Ser317 being the probable phosphorylation site whereas the p-Ser253 site (RRRAV**S**MDNSNK) was fully conserved in the *X. laevis* protein (Figure 4.3). Immunoblotting for total FoxO3a protein revealed no significant change in medium or high dehydration situations as compared to control (Figure 4.9). However, a 2.9-fold increase in phosphorylation on Ser318 was observed under high dehydration conditions compared to control but phosphorylation on FoxO3a Ser253 did not significantly change during dehydration (Figure 4.9).

4.4 Discussion

AMPK is often considered to be a master regulator that acts as a sensor of low energy to trigger metabolic readjustments to maintain energy homeostasis in cells (Pelosse et al. 2016). Given its sensitivity to the energy state of the cell and the whole organism, AMPK is highly relevant to energy homeostasis in *X. laevis* skeletal muscle when frogs undergo restricted circulation and limited oxygen delivery as dehydration progresses (Hillman 1978b; Hardie et al. 2012). These animals have been shown to adjust their signaling pathways in skeletal muscle to selectively suppress various energy

expensive functions, such as transcription and translation, while also adjusting carbohydrate metabolism to combat the limitations of circulation and oxygen availability in this dehydrated state (Hillman 1978b; Malik and Storey 2009a; Childers and Storey 2016). AMPK can be activated by phosphorylation via upstream kinases or through the elevated levels of AMP and ADP under environmental stress conditions (Hardie et al. 1998, 2012). Thus, AMPK phosphorylation is a key marker of cells experiencing low energy stress (Horman et al. 2005; Storey and Storey 2012).

In this study the relative total protein expression levels of AMPK subunits remained stable along with phosphorylation at Thr172 in response to medium or high dehydration conditions (Figure 4.2 and 4.4). Since phosphorylation at Thr172 stimulates the catalytic activity of AMPK, these data suggest that AMPK is equally active in skeletal muscle during dehydration as under control conditions with respect to this phosphorylation site. This is understandable since phosphorylation at this site is maintained when Mg-ATP is not available to bind to the protein and expose p-Thr172 to phosphatases (Carling et al. 2012). Another site, Ser496 (Ser516 in *X. laevis*) in the activation loop of AMPK showed decreased phosphorylation during medium and high dehydration (Figure 4.4). This could be an indication of activation, as it has been demonstrated that the removal of AMPK phosphorylation on a related site (Ser491) increases its activity in hypothalamic tissue (Dagon et al. 2012). Phosphorylation at Ser491 has also been linked to the kinase p70 s6k, which is known to increase in skeletal muscle during high dehydration (Luu 2011), and also to PKC action as previously demonstrated in myotube cell cultures (Dagon et al. 2012; Coughlan et al. 2016). In pituitary adenomas, however, AMPK Ser496 dephosphorylation was associated with

reduced AMPK activity and attenuated glycolysis (Zhao et al. 2019). The mechanism of this regulation in *X. laevis* must be further investigated, but it is interesting that the reduction in AMPK Ser496 relative phosphorylation supports glycolytic attenuation since reduced glycolysis has been repeatedly demonstrated in skeletal muscle during high dehydration through the regulation of aldolase (Chapter 2) and LDH (Childers and Storey 2019). Thus, a reduced AMPK activity follows with trends already presented in *X. laevis*.

The phosphorylation responses of AMPK downstream targets further indicate that AMPK action has not been activated during dehydration. ACC1 is a good substrate for AMPK and any changes in AMPK activity would likely lead to alterations in ACC1 phosphorylation. Phosphorylation of ACC1 on Ser79 significantly decreased throughout dehydration, which suggests that the activity of AMPK is decreased overall (Figure 4.5). This may suggest that the phosphorylation on Thr172 is not enough on its own to support AMPK stress signalling. Furthermore, the dephosphorylation of ACC1 is activating of its catalytic activity. ACC1 synthesizes malonyl-CoA that can inhibit fatty acid delivery into the mitochondria through malonyl-CoA inhibition of CPT1 and thus β-oxidation (see Figure 4.1) (Hardie and Pan 2002; McGee and Hargreaves 2010). Overall then, AMPK does not appear to be activated during *X. laevis* dehydration, as the inhibition of ACC1 through phosphorylation, that would support β-oxidation to produce energy, is not maintained during dehydration. Fatty acid synthesis is not known to occur in abundance in skeletal muscle, so the removal of this AMPK-mediated phosphorylation on ACC1 is likely a mechanism to prevent or reduce β-oxidation. The primary isoform of ACC in human skeletal muscle is ACC2, which is similar to its more widely expressed counterpart ACC1 with an N-terminal sequence targeting it to the mitochondrial

membrane (Thomson and Winder 2009). A comparison of the predicted *X. laevis* amino acid sequences reveals that the ACC1(XP_018104903.1) and ACC2 (XP_018104904.1) sequences are 100% identical in *X. laevis* barring a small 8-amino-acid section excised from ACC2 at amino acid 1189, with the Ser79 phosphorylation site remaining unchanged. The reduced phosphorylation detected here therefore is likely representative of both isoforms. It is known that *X. laevis* have fat bodies that are used up after 6 months of natural estivation (Merkle and Hanke 1988b). The lack of AMPK/ACC response during the presently used relatively short-term dehydration suggests that this stress may not be enough to trigger gross energy stress signaling and trigger a switch to fats as an alternative fuel in skeletal muscle.

AMPK and mTORC1 directly phosphorylate ULK1 and are known to have opposing effects on autophagy signalling (Egan et al. 2011; Roach 2011). Indeed, previous work has determined that mTORC1 phosphorylation of human ULK1 at Ser757 (Ser758 in *X. laevis*) disrupts the interaction between ULK1 and AMPK (Egan et al. 2011). Interestingly, phosphorylation on both these sites increases during high dehydration with ULK Ser555 phosphorylation (the AMPK site) increasing under medium dehydration conditions as well (Figure 4.7). This could indicate that AMPK is more sensitive to changes in water content but is quickly stifled by mTOR signalling if nutrient signalling is high enough. Previous results indicate that ULK1 has unique and tissue-specific roles but mainly functions in starvation-induced autophagy. The increases in Ser555 and Ser758 phosphorylation may set up these frogs to use autophagy if high dehydration continues over the many weeks of their natural estivation, as needed to support energy production. It is known mTOR phosphorylation (thus its activity) is

reduced during high dehydration in this model of *X. laevis* dehydration but the degradation of mTOR-mediated phosphorylation on its target proteins may be delayed. Studies on ULK during starvation note the importance of the removal of Ser758 phosphorylation for the initiation of autophagy. The upregulation of phosphorylation on both sites indicates that there is enough signalling to begin activating the AMPK/ULK interaction, but not enough to signal the removal of phosphorylation at the mTOR regulatory site. More studies are needed to determine if this conflicting phosphorylation pattern shifts over longer periods of dehydration or starvation during natural estivation that can last for many months.

Further analysis of cell energy regulating targets supported the decrease in autophagy through beclin1 dephosphorylation and further suggested a potential maintenance of growth signalling by the nuclear export and inhibition of FoxO3a (Figure 4.8 and 4.9). Some evidence has suggested that AMPK can stimulate autophagy by directly phosphorylating the central scaffold protein, beclin1, at Ser93 (Kim et al. 2013). Beclin 1 can assemble proteins to either promote or inhibit autophagy, with the phosphorylation of Ser93 required for maximal autophagy (Fujiwara et al. 2016). During medium and high dehydration, beclin1 total protein levels remained stable while the relative phosphorylation on Ser93 significantly decreased (Figure 4.8). This indicates that autophagy in *X. laevis* muscle is inhibited not only upstream at ULK1 but also through inhibition of its induction by beclin1 (Kim et al. 2013; Fujiwara et al. 2016). This dephosphorylation of beclin 1 and ULK1 might be water content sensitive since both dephosphorylations occur strongly in the medium dehydration condition and are maintained through high dehydration (Figure 4.7 and 4.8). The coordinated

dephosphorylation of both ULK1 and beclin1 further support a downregulation of autophagy signals during dehydration.

Forkhead transcription factors are a highly conserved family of proteins involved in the regulation of various signalling processes, including energy metabolism and apoptosis, that are regulated through phosphorylation-dependent nuclear shuttling (Mammucari et al. 2007; Chiacchiera and Simone 2010). Insulin and growth factor stimulation causes Akt-dependent phosphorylation that reduces the DNA-binding ability of FoxO, promotes FoxO export to the cytoplasm, and enhances FoxO degradation, which all reduce its DNA binding ability (Lam et al. 2006; Salih and Brunet 2008).The FoxO subfamily has considerable involvement in responses to environmental stress (Malik and Storey 2011; Storey and Storey 2012; Krivoruchko and Storey 2013; Wu and Storey 2014). For example, in the thirteen-lined ground squirrel, *Ictidomys tridecemlineatus*, the phosphorylation of FoxO3a suggests a predominantly cytoplasmic localization of FoxO3a in skeletal muscle throughout torpor when metabolic pathways are depressed during hibernation (Wu and Storey 2014). Furthermore, FoxO1 was demonstrated to be removed from the nucleus in the muscle of *X. laevis* while liver tissue demonstrated an increase in nuclear content (Malik and Storey 2011). *X. laevis* therefore demonstrates a tissue-specific response with an apparent increase in its transcriptional activity of FoxO1 in liver but not in muscle during dehydration. FoxO3a is also known to be phosphorylated at Ser253 by Akt kinase in response to growth factor stimulation. This phosphorylation, along with interactions with other proteins, promotes the nuclear exclusion of FoxO3a inhibiting its influence on transcriptional activities. In this thesis, the relative Ser253 phosphorylation on FoxO3a remained constant suggesting that

although Akt is downregulated during dehydration its influence on FoxO3a has not been reversed (Luu, 2018). In C2C12 myoblasts, Tong et al. (2009) demonstrated that insulin growth factor treatment enhanced cytoplasmic FoxO3a phosphorylation at Thr318/321 and reduced nuclear FoxO3a contents. Here, FoxO3a Ser318 was highly phosphorylated, which strongly promotes its nuclear export and likely limits its inhibitory effects on transcription (Figure 4.9) (Tong et al. 2009). Therefore, this downregulation of energy stress signaling through FoxO3a seems to be translated through many phosphorylation cascades, to tightly control energy signaling.

In conclusion, the regulation of phosphorylation appears to play an important role in signal transduction in response to dehydration stress in *X. laevis* muscle. Future studies should focus on phosphatase action since various upstream kinases become downregulated, and yet their targets are not always similarly dephosphorylated. Overall, signaling through AMPK to regulate energy stress suggests that although these experimental frogs are experiencing high dehydration, they may not have reached an energy stress point where fat stores or autophagy are needed as sources of energy and nutrients to maintain cell processes. Therefore, although upstream signals demonstrate some competing crosstalk through AKT/mTOR and AMPK phosphorylation, there does not seem to be an overall recruitment of AMPK signalling during frog dehydration. Further studies of AMPK signalling should focus on the long-term influences of estivation over the weeks or months of dormancy that *X. laevis* is known to naturally endure (Merkle and Hanke 1988b).

4.5 Figures

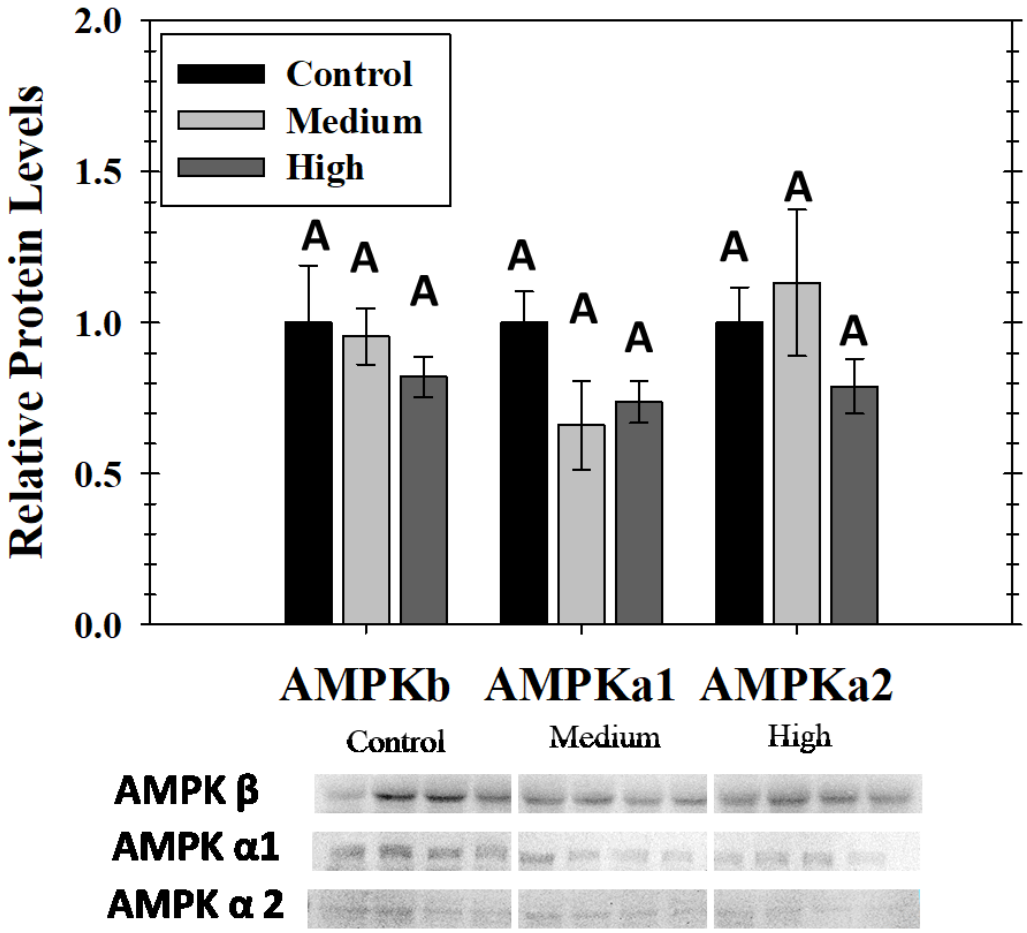

Figure 4.2: Relative protein expression levels of AMPKα1, α2 and 2β in *X. laevis* skeletal muscle under control, medium dehydration, and high dehydration conditions. Protein levels were obtained from western immunoblot signal normalized against total protein loaded represented by an average of Coomassie blue-stained proteins on the membrane from a non-quantified region. Data are presented in the histogram as relative means ± SEM, n =3-4 independent biological replicates. Statistically significant differences compared to the control were determined with a one-way ANOVA, followed by a post hoc Tukeys's test; values that share the same letter notation are not significantly different from one another ($p < 0.05$).

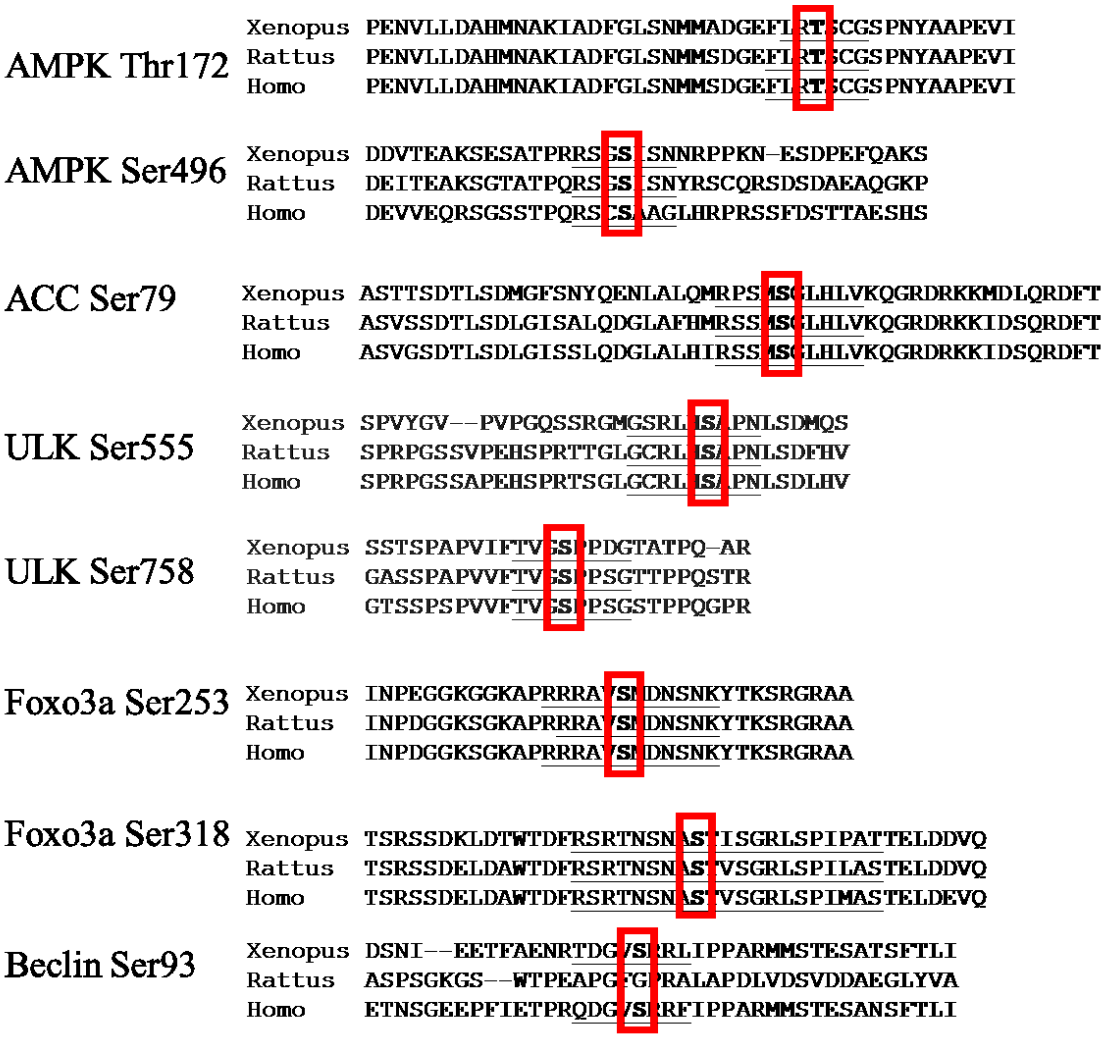

Figure 4.3: The Clustal 2.1 alignments of human, rat and *X. laevis* amino acid sequences demonstrating the conservation of the sequences around the phosphorylation sites on frog AMPK, ACC, ULK, FoxO3a and beclin1.

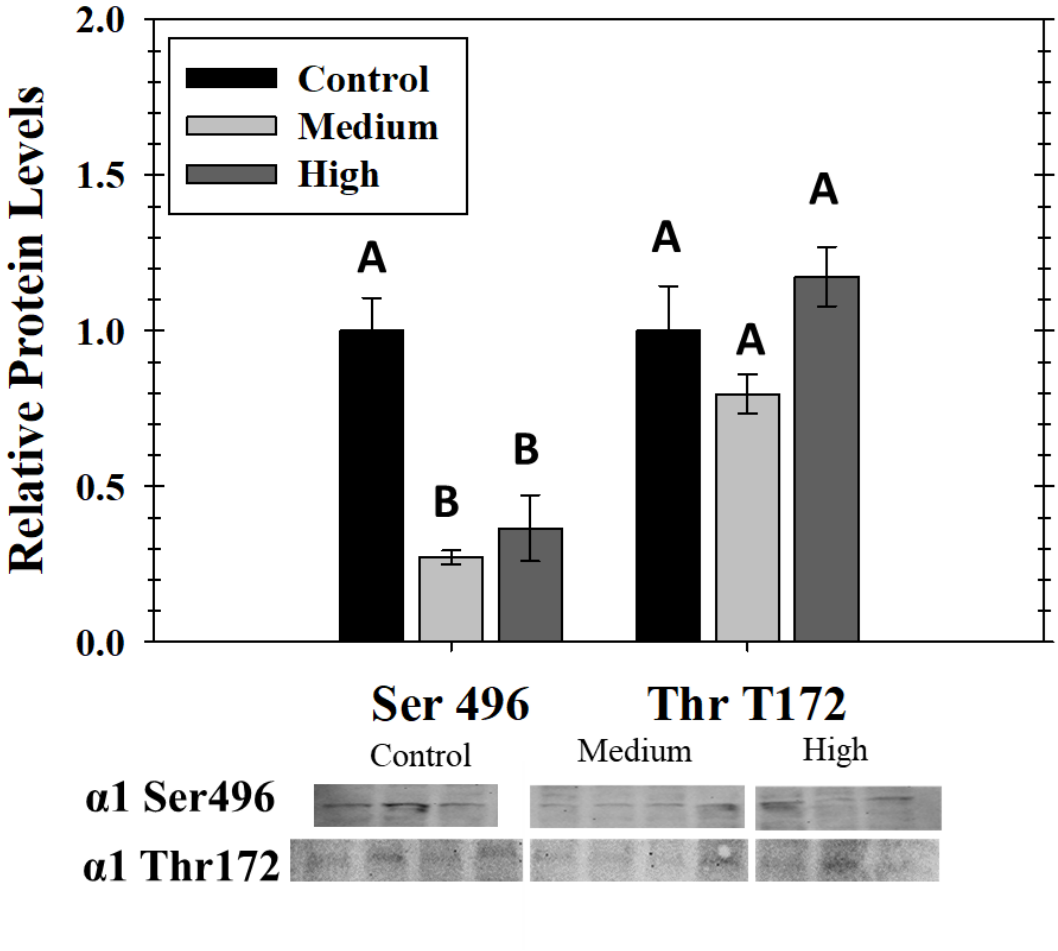

Figure 4.4: Relative protein expression levels of AMPK phosphorylation on Ser 496 and Thr172 in *X. laevis* skeletal muscle under control, medium dehydration, and high dehydration conditions. Other information as in Figure 4.2.

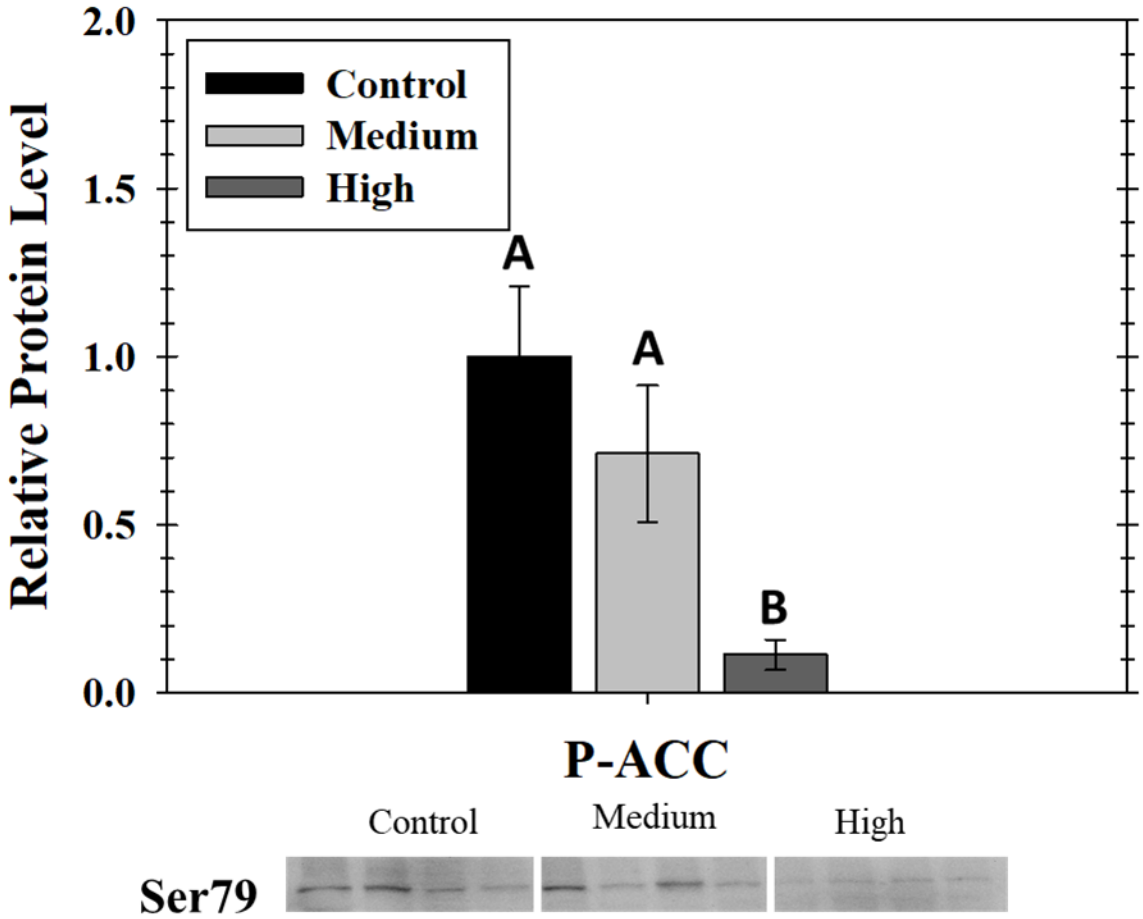

Figure 4.5: Relative protein expression levels of the phosphorylation of ACC1 on Ser79 in *X. laevis* skeletal muscle under control, medium dehydration, and high dehydration conditions. Other information as in Figure 4.2.

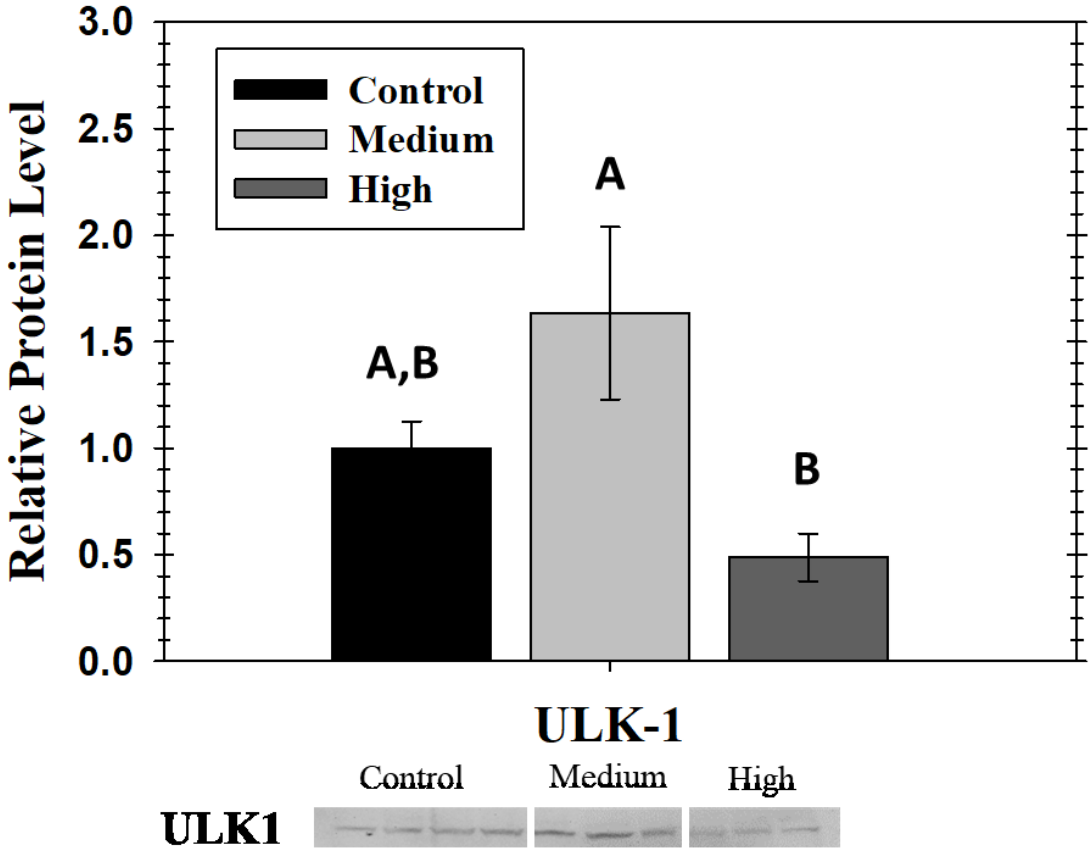

Figure 4.6: Relative protein expression levels of ULK1 in *X. laevis* skeletal muscle under control, medium dehydration, and high dehydration conditions. Other information as in Figure 4.2.

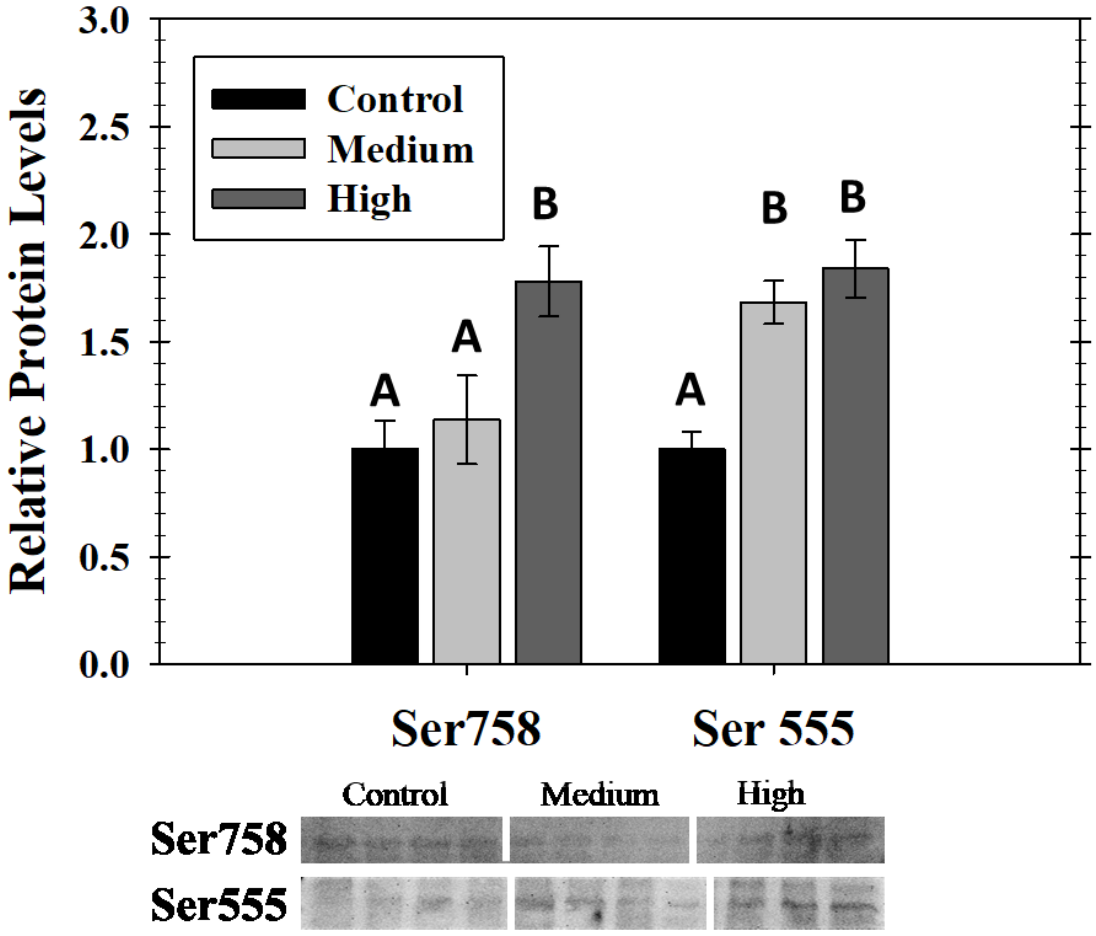

Figure 4.7: Relative protein expression levels of ULK1 phosphorylation on Ser758 and Ser555 in *X. laevis* skeletal muscle under control, medium dehydration, and high dehydration conditions. Other information as in Figure 4.2.

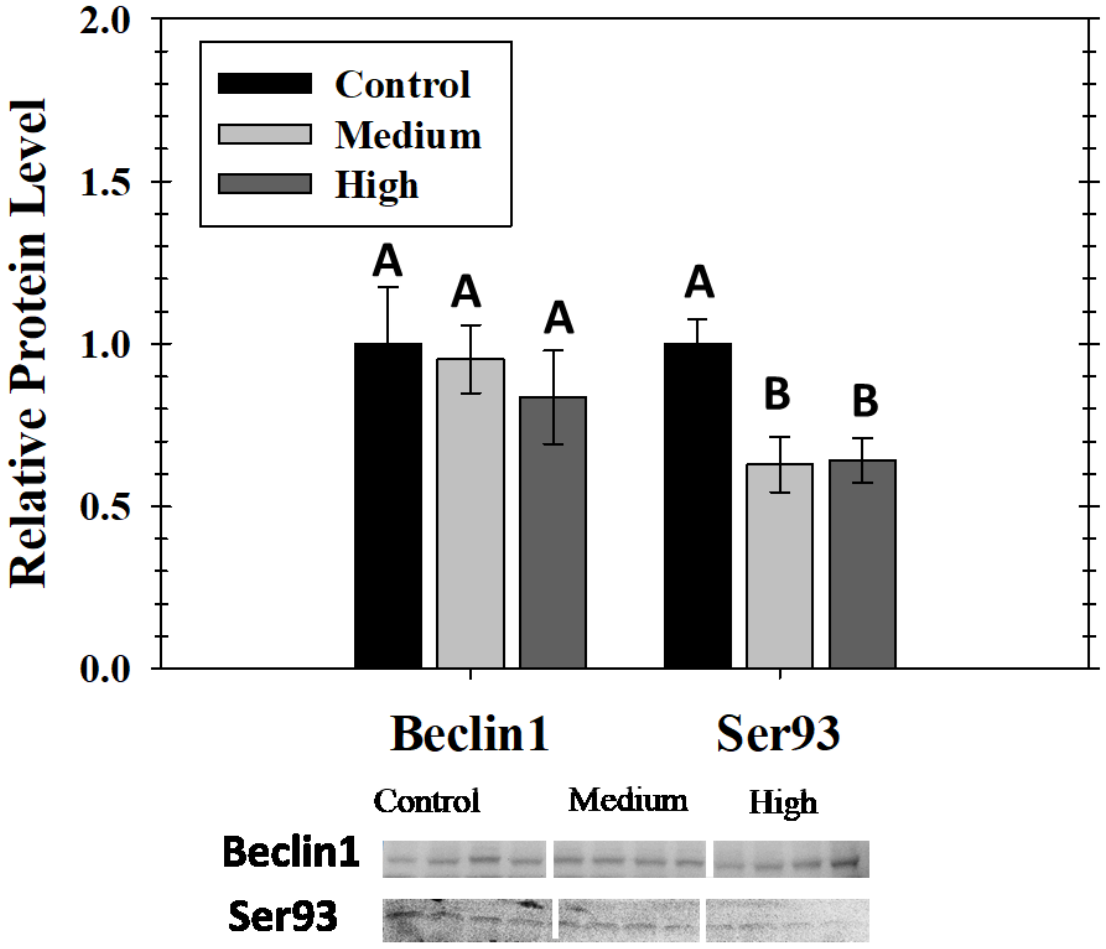

Figure 4.8: Relative protein expression levels of total beclin1 and the phosphorylation of beclin1 on Ser93 in *X. laevis* skeletal muscle under control, medium dehydration, and high dehydration conditions. Other information as in Figure 4.2.

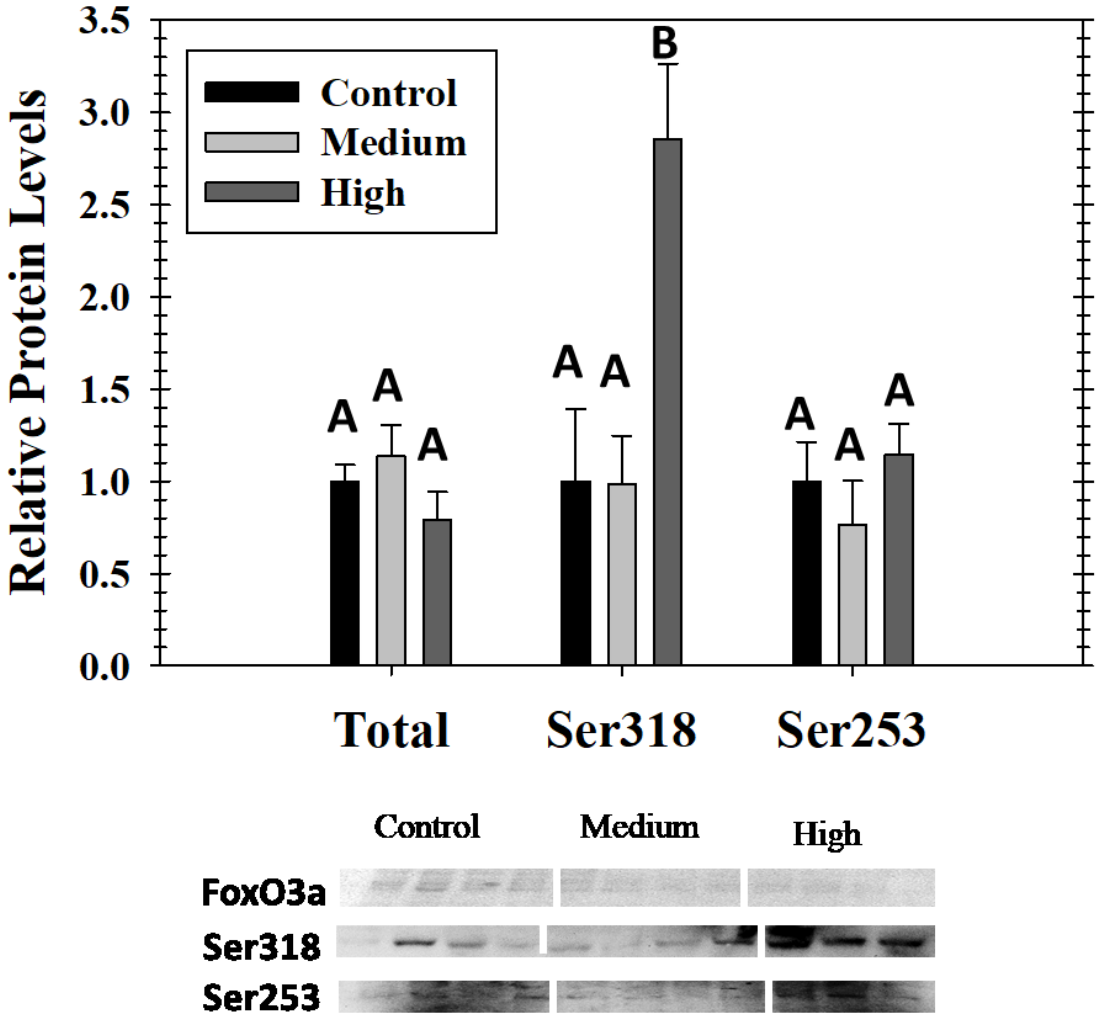

Figure 4.9: Relative protein expression levels of total FoxO3a and the phosphorylation of FoxO3a on Ser318 and Ser253 in *X. laevis* skeletal muscle under control, medium dehydration, and high dehydration conditions. Other information as in Figure 4.2.

4.6 Tables

Table 4.11: Antibody catalogue numbers for each target.

Target	*Company*	*Cataloge Number*
AMPK β	**Transduction Labs**	**610802**
AMPK alpha 1	**R&D**	**AF3197**
AMPK alpha 2	**R&D**	**AF2850**
AMPK- T172/183	**Boster**	**P01420-2**
AMPK- S496	**Boster**	**P00994-1**
ACC – S79	**Genetex**	**GTX30764**
Foxo3a	**Genetex**	**GTX82877**
FOXO3a – S318	**Cell Signalling**	**#9465**
FOXO3a – S253	**Cell Signalling**	**#9466**
ULK	**Genetex**	**GTX16974**
ULK1 – S555	**Abclonal**	**AP0760**
ULK1- S758	**Genetex**	**GTX132654**
Beclin- S93	**Cell Signalling**	**#14717**
Beclin total	**Cell signalling**	**#3738**

Chapter 5: Purification and characterization of NADP-dependent isocitrate dehydrogenase in relation to dehydration in the African clawed frog, *Xenopus laevis*.

5.1 Introduction

African clawed frogs, *X. laevis*, can survive significant loss of body water during arid summers. Critical consequences occur from the thickening of blood due to dehydration that leads to an interruption of regular blood circulation and oxygen delivery (Hillman 1978a). This thesis shows that an interruption of regular circulation leads to adjusted metabolic enzyme function and altered energy stress signalling in skeletal muscle (Hillman 1978a; Hillman and Sommerfeldt 1981; Childers and Storey 2016, 2019). Previously, Luu (2018) demonstrated that important proteins involved in fatty acid oxidation were suppressed in skeletal muscle, along with glycolytic genes and pyruvate dehydrogenase kinases. Furthermore, this thesis demonstrates that the stress signalling is regulated to promote fatty acid synthesis through reduced ACC1 phosphorylation (Chapter 4). Cytosolic $NADP^+$-dependent isocitrate dehydrogenase (IDH1; EC 1.1.1.42), catalyzes the oxidative decarboxylation of isocitrate, reversibly producing alpha-ketoglutarate (α-KG) and CO_2 and vice versa (Shechter et al. 2003):

$$\text{Isocitrate} + Mg^{2+} + NADP^+ \leftrightarrow \alpha\text{-KG} + CO_2 + NADPH$$

α-KG serves as a substrate for a variety of lipid synthetic and energy-yielding pathways whereas NADPH is a main source of reducing equivalents for biosynthetic reactions along with many antioxidant reactions. Since it has been suggested that the contribution of IDH1 to NADPH production may be significant, it is possible that regulation of IDH1 expression and enzymatic activity may have an indirect effect on lipid metabolism in *X. laevis* (Shechter et al. 2003; Kim et al. 2012).

In naturally estivating *X. laevis*, ammonium ion in the thigh muscle increases from 0.8 to 2.5 mmol/g wet wt. along with ammonium ion concentrations in blood plasma (Balinsky et al. 1967; Unsworth and Crook 1967). To produce this ammonia however, there would be an equal amount of α-KG made through the glutamate dehydrogenase (GDH) reaction and previous evidence has demonstrated that GDH has a lower glutamate K_m and an increased K_m for α-KG (Appendix1) in muscle from dehydrated *X. laevis*. This indicates that the GDH reaction is poised towards amino acid metabolism and α-KG/ammonia production, which concurs with known increases in urea cycle enzymes and urea production in the animal during dehydration (Balinsky et al. 1967). The fate of α-KG in *X. laevis* tissues however is not clearly known, as α-KG can be used in many ways such as: a) transported into the cytosol to be used by IDH1 to create isocitrate and citrate (for fatty acid synthesis or glycolytic inhibition), b) it can be used as a TCA cycle intermediate to further aerobic energy production or c) it can be used in a critical reaction that removes a potent PPARα agonist and thus reduce β-oxidation signalling during dehydration (Unsworth and Crook 1967; Shechter et al. 2003; Chinopoulos 2013; Iacobazzi and Infantino 2014) (See Figure 5.1).

Interrupted circulation can also result in interrupted oxygen deliver and the potential for oxidative damage. NADPH is often necessary in various antioxidant reactions making the regulation of its production critically important in frog muscle as circulation is reduced (Hillman 1978b; Koh et al. 2004). Accordingly, previous work on *X. laevis* muscle indicated that dehydration exposure increased some antioxidant defenses. For example, the nuclear content of nuclear factor erythroid 2-related factor 2 (Nrf2) increased by 4.3-fold in the muscle of *X. laevis* during dehydration, which

correlates with the upregulation of multiple downstream antioxidant proteins (Malik and Storey 2009b). Nrf2 also targets many cytoprotective proteins and protects aerobic cells from reactive oxygen intermediates (Baird and Dinkova-Kostova 2011). Previous work focused on the response to oxidative stress, demonstrated no downstream changes in manganese-dependent superoxide dismutase (MnSOD) in skeletal muscle of *X. laevis* but did show an increase in catalase in response to dehydration (Malik and Storey 2011). As an enzyme though to contribute to buffering NADPH reserves, IDH1 is often found in tissues that require high levels of cellular defense against oxidative damage. Certainly, knockdown studies of IDH1 in mouse melanocytes resulted in increased apoptosis with a lower ratio of reduced to oxidized glutathione which was attributed to the importance of IDH1 in antioxidant capacity and cell survival (Kim et al. 2012). Furthermore, the upregulation of IDH1 in LLC-PK1 cells protected cells against hydrogen peroxide assault causing an increase in the GSSG/(GSH+GSSG) ratio, supporting the protective potential of IDH1 (Kim et al. 2009). The role of IDH1 in skeletal muscle as either antioxidant or lipid metabolism support, however, is unknown. The present study of *X. laevis* IDH therefore analyzes the posttranslational phosphorylation of IDH1 that could be involved in enzyme control with respect to the needs for dehydration survival in skeletal muscle from the African clawed frog.

5.2 Methods

Animals

See Chapter 2.

NADP-dependent Isocitrate Dehydrogenase Assay

IDH activity was assayed using a Thermo Labsystems Multiskan Spectrum microplate spectrophotometer and Multiskan software. IDH activity was measured by monitoring the consumption or production of NADPH at 340 nm at room temperature (23°C). The optimum assay conditions for the NADPH producing forward reaction for muscle IDH from both control and dehydrated frogs were 1.5 mM $NADP^+$, 50 mM DL-isocitrate, 1.0 mM Mg^{2+}, 20 mM HEPES, pH 7.5 in a total volume of 200 µl with 15 µl of muscle extract used per assay.

NADP-dependent Isocitrate Dehydrogenase Isolation

Frozen thigh muscle samples were homogenized 1:5 w:v, using a Diamed Pro 200 homogenizer, in cold homogenization buffer (Buffer A) containing 20 mM K_2PO_4, 10 mM 2-mercaptoethanol, 1 mM EGTA, 1 mM EDTA, 10 mM β-GP and 10% v:v glycerol, pH 8.0. A few crystals of PMSF were added at the time of homogenization. Homogenates were centrifuged for 30 min at 13,500 × g at 4°C. The resulting supernatant was decanted and held on ice until use. IDH1 was isolated from muscle of both control and dehydrated frogs using a combination of ion-exchange and dye-ligand affinity. Crude muscle extracts were applied to a DEAE column (1.5 cm x 7 cm) equilibrated in buffer A. The column was then washed with 15 ml of buffer A. Aliquots from each fraction were assayed and fractions with high IDH activity were identified and pooled. The pooled fractions were applied to a Cibacron blue column (1.5 x 4 cm) equilibrated in buffer A. The Cibacron column was washed with 30 ml of buffer A and then eluted with 80 ml of buffer A with 100 mM isocitrate:Mg^{2+} added. Fractions (~1.4 mL) were collected and assayed and

those with the most activity were pooled. These pooled fractions were diluted 10 times in buffer A before being loaded onto an identical second Cibacron column. The second Cibacron column was washed with 30 ml of buffer A before the enzyme was eluted with a 0-1M KCl gradient made in buffer A. The gradient fractions were assayed, and peak fractions were run on an SDS PAGE gel to determine the quality of the isolated protein. Isolated fractions were pooled for analytical studies.

SDS-polyacrylamide gel electrophoresis

For analysis of isolated skeletal muscle IDH1, enzyme samples from the different isolations steps were mixed 1:1 v:v with SDS loading buffer as done in Chapter 2. In brief, samples from each of the isolation steps were mixed 1:1 v:v with SDS loading buffer, boiled for 5 min and stored at -20°C until use. Lanes of 10% SDS-PAGE gels were loaded with 5-15 µl of sample and electrophoresis was carried out at 180 V for 60 min in running buffer. Coomassie brilliant blue protein stain was used to stain the gels and a ChemiGenius instrument was used for imaging as in Chapter 2 (SynGene, Frederick, MD). For analysis of posttranslational modifications, 15 µl of isolated enzyme from control and dehydrated preparations were run on 10% SDS-PAGE and electrophoresis was also carried out for 50min. For analysis of total protein, skeletal muscle extracts were prepared as described in chapter 2. Each lane of 10% SDS-PAGE gels was loaded with 20 µg of total protein and electrophoresis was carried out at 180 V for 70 min.

Protein Quantification

Total protein concentrations were measured using the Bradford method with reagents from BioRad and bovine serum albumin as the protein standard (Bradford 1976).

Immunoblotting

For both total protein and protein phosphorylation SDS PAGE gels, proteins were transferred to PVDF membranes at 160 mA for 90 min as in Chapter 2. Membranes were then blocked and washed as in Chapter 2. Antibodies used were the rabbit anti-phosphoserine (Cat #618100), rabbit anti-phosphothreonine (Cat. #718200), and mouse anti-phosphotyrosine (Cat #700286); all from Invitrogen (Carlsbad, CA, USA) and rabbit anti-IDH1 from Cell Signaling (Cat#3997). The primary antibody was left to incubate at 4°C overnight. Unbound primary antibody was removed with three 5-min washes with TBST and the membrane was then incubated with HRP-conjugated anti-rabbit secondary antibody or anti-mouse secondary antibody (BioShop, both diluted 1:4000 v:v in TBST) for 40 min and then washed again with 3×5 min washes of TBST. Immunoreactive bands were visualized by enhanced chemiluminescence and visualized on the ChemiGenius Bioimaging System (Syngene, Frederick, MD). IDH1 band intensities were quantified using GeneTools software. Isolated IDH1 phosphorylation intensities were standardized against the corresponding Coomassie brilliant blue stained band to correct for any variations in sample loading. Total protein membranes were also re-stained using Coomassie brilliant blue and samples were standardized against the total protein amount loaded as in Chapter 2.

Kinetic Studies

Substrate affinity constants (K_m values) were determined from the Michaelis-Menten equation using a nonlinear least squares regression computer program (Brooks 1992). The concentrations of inhibitors that decrease enzyme velocity by 50% (I_{50} values) were determined using plots of initial velocity vs [inhibitor]. Plots were constructed for frog IDH1 by measuring enzyme activities under standard assay conditions (20 mM HEPES, pH 7.5 at 23 ℃, with 1.5 mM $NADP^+$, 50 mM DL-isocitrate, 1.0 mM Mg^{2+}). All kinetic parameters are means ±SEM for n=4–5 determinations.

In vitro incubation to stimulate protein kinases and phosphatases

To determine if the activation of protein kinases or protein phosphatases affected IDH1 kinetic parameters, incubation studies were conducted as described in Chapter 2 with some alterations. The incubation buffer was (20 mM K_2PO_4, 10 mM 2-mercaptoethanol, and 10% v:v glycerol, pH 8.0). Aliquots of the filtered supernatants were incubated for 24 h at ~4°C with specific stimulators of either protein kinases or protein phosphatases as described in Macdonald and Storey (1999). Each aliquot was mixed 1:3 v:v with the appropriate additions (made in incubation buffer) that were designed to stimulate the following:

G. OPEN conditions (control for unaccounted for changes to the enzyme during the incubation period): no additions to incubation buffer.

H. STOP condition (same as Buffer A) was designed to inhibit all protein kinases and phosphatases. Incubation buffer plus, 1 mM EGTA, 1 mM EDTA, 10 mM β-GP.

I. General Endogenous Protein Phosphatases: Incubation buffer plus

   a. no ions (thus no PP2B or PP2C activity) + 30 mM Na_3VO_4 stimulates protein phosphatase 2A (PP2A);

   b. + 30 mM NaF, stimulates tyrosine phosphatases only (PTPs);

   c. 5 mM $CaCl_2$ + 2 mM EDTA (chelates Mg^{2+}, inhibits PP2C) + 1 μM okadaic acid (inhibits PP1/PP2A) + 5 mM Na_3VO_4 stimulates protein phosphatase 2B (PP2B)

   d. All of the above and 5 mM $MgCl_2$ + 5 mM $CaCl_2$ + 5 mM Na_3VO_4 to stimulate total serine/threonine phosphatases (Total Ppase)

J. Endogenous Protein Kinases: buffer B plus 5 mM Mg·ATP, 30 mM β-GP and either:

   a. 1.3 mM $CaCl_2$ + 7 μg/mL phorbol myristate acetate (PMA) to stimulate protein kinase C (PKC)

   b. 1 U of calmodulin + 1.3 mM $CaCl_2$ to stimulate calcium–calmodulin kinase activity (CaMK)

   c. 1 mM cAMP, to stimulate protein kinase A (PKA)

   d. 1 mM, AMP (stimulate AMPK), 1 mM cGMP (to stimulate PKG) plus all the components in (a)-(d) above to stimulate total protein kinases.

After incubation overnight, samples were mixed 1:1 with STOP buffer to halt kinase or phosphatase reactions before the samples were assayed as above with varying

isocitrate concentrations to determine the changes to the K_m or relative V_{max} of the preparations. Open and Stop conditions were compared for any unaccounted-for changes in IDH1 activity. These values were not found to be different and thus were averaged and used for comparison to the treated values under the title 'OPEN'.

Kinase in Silico predictions and homology modelling

The IDH FASTA sequence (XP_018094513.1) taken from the NCBI database was used to predict the most likely protein kinase interactions through the online software from Netphos3.1 server (http://www.cbs.dtu.dk/services/NetPhos/). Serine, threonine and tyrosine residues were selected individually with threshold values set to 0.75. The same IDH sequence was then run through a simple homology modelling server (https://swissmodel.expasy.org/), using 5yfn.1.A from human isocitrate dehydrogenase 1 bound with isocitrate (Nordlund, P. et al. To be published), to view the location of the predicted phosphorylation sites and compare *X. laevis* IDH1 structure to the human template.

Differential Scanning Fluorimetry (DSF)

IDH protein unfolding was measured using a Bio-Rad IQ PCR instrument. Isolated IDH was combined with DSF buffer (Biggar et al. 2012), 40× diluted SYPRO orange dye (Invitrogen) and any additional reagents to a 20 µl final volume in thin-walled PCR plates. The plates were placed in the IQ and fluorescence was measured as described by Bigger et al. (2012). OriginPro 8.5. was used to analyze fluorescence

intensity using the Boltzmann distribution curve, which calculated the T_m (Biggar et al. 2012).

Data and statistical analysis

As in Chapter 2, the MPA program was used to analyze enzyme rates and kinetic parameters were determined using Kinetics 3.51 (Brooks, 1992; Brooks, 1994). Statistical analysis of two conditions (control vs. dehydrated) were carried out with a Student's t test (SigmaPlot 12.0 statistical package) with a P value < 0.05 considered significant. Immunoblott data are expressed as means ± SEM, n = 3-4 independent samples from different animals. Differences between control and dehydrated samples were analyzed using SigmaPlot software and considered statistically significant when the one-way ANOVA with the Tukey's post-hoc test yielded a result of $p < 0.05$.

5.3 Results

The steps for the isolation of *X. laevis* IDH from control frogs are summarized in Table 5.1. The specific activity of IDH in crude muscle extracts was 33.8 U/mg protein. The first step in the isolation was ion-exchange chromatography on DEAE Sephadex where 29% IDH eluted in the initial run-through. The DEAE Sephadex fractions containing IDH activity were pooled and loaded onto a Cibacron Blue column that was eluted with 100 mM isocitrate: Mg^{2+}. After this step IDH specific activity increased to 214.8 U/mg protein, providing a 6.36-fold isolation compared to the crude extract and an 20.97 % overall yield. The fractions eluted from the Cibacron column that had the most IDH activity were then pooled and diluted 10x in homogenization buffer before being

loaded onto a fresh Cibacron column equilibrated in the same buffer. IDH was then eluted with a 0-1M KCl gradient resulting in a final specific activity of 329.2 U/mg and a final fold isolation of 9.75 (Table 5.1). IDH from muscle of dehydrated *X. laevis* was isolated with the same scheme and had a similar yield.

Isolation results for control and dehydrated IDH are shown on 10% SDS-PAGE gels (Figure 5.2). The fractions containing IDH activity off the final Cibacron blue step showed an enriched band for IDH at ~39 kD. This is lower than the predicted monomer molecular weight (IDH is a dimer) calculated from the predicted amino acid sequence which was 46.9 kD (NCBI Reference Sequence: XP_018094513.1: https://web.expasy.org/compute_pi/). The total protein immunoblotting however, revealed a band that also lined up to approximately 39 kD. Figure 5.2 demonstrates the isolations for both control and dehydrated frogs; Lane A is the molecular weight ladder, lane B shows the isolated control IDH, land C is molecular weight ladder and lane D is the isolated IDH from dehydrated frogs.

Western blotting with antibodies that detect different phosphorylated amino acid residues was used to assess relative changes in posttranslational modifications to IDH between control and dehydrated conditions. Relative phosphorylation on threonine and tyrosine residues was 1.79-fold and 1.26-fold higher ($P < 0.05$) for dehydrated IDH as compared to control IDH whereas phosphorylation of serine residues on IDH from dehydrated frogs was not significantly different from control phosphorylation levels (Figure 5.3). Immunoblotting was used to evaluate the relative amount of IDH protein in muscle from control, medium and high dehydrated *X. laevis*. Antibodies detecting

mammalian IDH showed no significant change in IDH protein in response to dehydration (Figure 5.4).

K_m values for $NADP^+$, isocitrate and Mg^{2+} were measured at saturating co-substrate concentrations. K_m values for $NADP^+$ (~0.4 mM) and isocitrate (~0.095 mM) for skeletal muscle IDH1 from control versus dehydrated frogs were not significantly different (Figure 5.5, Table 5.2). However, the K_m for Mg^{2+} for IDH from dehydrated frogs was just 43% of the K_m of control IDH1 and the V_{max} was 48.6% of the control IDH1 value ($p<0.05$, Figure 5.5 and Table 5.2). Muscle IDH1 from control and dehydrated *X. laevis* showed no differences in I_{50} values for urea, citrate or guanidine hydrochloride (Figures 5.5 and 5.6; Table 5.2). However, IDH1 from dehydrated frogs had a lactate I_{50} that was just 71.75% of the control IDH1 value ($p<0.05$, Figure 5.5, Table 5.2). DSF was used to test the thermal stability of isolated IDH1 from control and dehydrated frogs. However, there was no significant difference in the thermal stability between control and dehydrated IDH1 stability with both forms having a T_m value (melting temperature) of 54°C (Figure 5.7; Table 5.2).

To determine if *X. laevis* muscle IDH was subject to reversible protein phosphorylation and whether this could account for the stable kinetic differences between control and dehydration conditions, *in vitro* incubation studies were conducted. Crude muscle extracts were incubated with small molecule activators or inhibitors of specific endogenous protein phosphatases or protein kinases and the effects of these incubations on the K_m (Table 5.3) and V_{max} (Table 5.4) for isocitrate were analyzed for muscle IDH1 from control and dehydrated frogs. Incubation conditions that inhibited both kinases and

phosphatases (STOP) resulted in a higher K_m isocitrate for control IDH (0.11±0.01mM) and a significantly lower one for the enzyme from dehydrated frogs (0.07±0.01 mM, p=0.013). In extracts of dehydrated skeletal muscle, however, there was no significant change in the K_m of isocitrate when kinases were stimulated, but the K_m of isocitrate increased significantly by 1.6-fold when total phosphatases were stimulated and decreased by 42.9% when only PP2A was stimulated (Table 5.3). In control muscle homogenates there were many significant changes in the K_m of isocitrate when kinases were stimulated. When CAMK and PKC were stimulated the K_m isocitrate was raised 1.81- and 2-fold, respectively, whereas stimulation of PKA and total kinases lowered the K_m isocitrate by 45.5% and 63.6% (Table 5.3). Furthermore, stimulation of total phosphatases, PP2A, PP2B, and PTPs lowered the K_m isocitrate by 54.5%, 72.7%, 45.5% and 72.7%, respectively (Table 5.3). Relative Vmax values were compared to the OPEN incubation condition. In the crude samples from control frogs stimulating PP2A, PTPS, CAMK or PKC reduced the relative V_{max} IDH1, 28%, 29%, 86% and 98% respectively. Only the stimulation of PKA significantly increased the relative V_{max} (1.53-fold) with the stimulation total kinases or phosphatases not significantly altering the relative V_{max} of IDH1 (Table 5.4, $p<0.05$). In dehydrated crude samples, PP2A, PP2B, PTPs, CAMK, PKC and PKA all reduced the relative V_{max} of IDH1 (47%, 21%, 32%, 31%, 31%, and 32% respectively) as compared to the OPEN incubation (Table 5. 4, $p<0.05$). Stimulation of total kinases and total phosphatases again had no significant impact on the V_{max} of IDH1 (Table 5. 4).

Using the predicted IDH1 protein sequence (XP_018094513.1), PKC was the only kinase that met the 0.75 threshold for phosphorylating IDH1 (Table 5.5). The

highest score (0.85) for phosphorylating IDH1 at Ser2, followed by PKC on Thr313 a score 0.84 (Table 5.5). The same IDH sequence was then run through a simple homology modelling server using human IDH as the template which resulted in a sequence identity of 88.32%. The two sites predicted to be phosphorylated by PKC were highlighted to demonstrate their exposure on the quaternary structure (Figure 5.9).

5.4 Discussion

To determine how IDH1 is regulated during whole animal dehydration *X. laevis* muscle IDH1 was isolated using a combination of ion-exchange and affinity chromatography (Table 5.1). The apparent monomer subunit molecular weight, ~ 39 kDa determined by SDS-PAGE corresponded well with the IDH1 band molecular weight in the total protein determination and with the subunit molecular weight reported for IDH1 from various other vertebrate species (Xu et al. 2004; Zera et al. 2011) (Figure 5. 2). This molecular weight was smaller than the predicted molecular weight from the amino acid sequence, which suggests that IDH1 in *X. laevis* is truncated *in vivo*, however structural research is needed to determine if this is the case. The presented isolation scheme produced enzyme preparations that were purified 9.8-fold with a final specific activity of 329.3 mU/mg (Table 5.1). Thus, the isolation procedure presented here is an effective way of separating IDH1 from *X. laevis* muscle.

The present study demonstrates that IDH1 from dehydrated frogs has a significantly decreased V_{max} (44%) and a significant increase in substrate affinity for Mg^{2+} (42% lower K_m) when compared to the control enzyme. This indicates that IDH1 activity is suppressed overall in skeletal muscle during whole body dehydration and that

the production of NADPH and α-KG is favored. Solute concentrations would naturally be increased during dehydration thus the impact of magnesium concentrations would be elevated in *X. laevis* during dehydration. This change in magnesium affinity could be a mechanism of poising IDH to favor the conversion of isocitrate into α-KG as dehydration progresses (Hillman 1978b). However, this may not necessarily be to increase the production of α-KG and could rather be a mechanism of directing citrate to isocitrate through the removal of any product of the aconitase reaction during dehydration. Citrate can exit the mitochondria in exchange for malate and generate oxaloacetate and acetyl-CoA through an energy expensive reaction, which then supports other pathways such as fatty acid synthesis through ACC1 activity (Icard et al. 2012). ACC is dephosphorylated during high dehydration which suggests that it could use acetyl-coA derived from citrate to increase fatty acid synthesis. The IDH1 increase in affinity for Mg^{2+} could provide a competing direction for citrate to flow through aconitase and IDH1 (Chapter 4)(Icard et al. 2012). Mg^{2+} was thought to have no allosteric effect on IDH, demonstrated in porcine cardiac muscle, and therefore the increase in affinity could be a specific mechanism to support the isocitrate-using reaction during *X. laevis* dehydration (Murakami et al. 1997). Inhibition studies, however, indicate that IDH1 is also more sensitive to lactate during dehydration with a 28 % decrease in lactate I_{50} to 85 mM (Figure 5.6). Lactate in rested vs exercised *X. laevis* muscle can range from 0.58 to 2.54 mg/g muscle, potentially allowing the increase in lactate to inhibit IDH1 function as the frog dehydration continues (Miller and Camilliere 1981). The interaction of magnesium affinity and lactate inhibition on IDH activity *in vivo* needs further study.

Ultimately, IDH1 appears to favor the continued production of α-KG and NADPH at a reduced overall velocity during high dehydration in *X. laevis*. This agrees with current signalling information since α-KG is required as a substrate for the phytanoyl-CoA α-hydroxylase reaction. This reaction is required for the catabolic removal of phytanic acid, a known agonist to the transcription factor, peroxisome proliferator activated receptors α (PPARα) (pathway described in Shechter et al. 2003). PPARα supports the transcription of β-oxidation genes and has been shown to have decreased transcript levels in dehydrated skeletal muscle (Luu, 2018). The regulation of IDH1 to favor the production of α-KG could support the removal of the PPARα agonist and further suppress its transcription activity and thus β-oxidation during dehydration (Luu, 2018). Conversely, NADPH is required for catalase to form active tetramers. Since catalase is known to be upregulated during high dehydration in *X. laevis,* some production of NADPH is still necessary (Lee et al. 2002; Malik and Storey 2009b). Therefore, further studies are needed to determine if NADPH is sufficiently produced through the reduced kinetic function of IDH1 or if other sources of NADPH are required.

It is well known that reversible phosphorylation of enzymes is a major mechanism allowing for the plasticity and regulation of metabolic reactions when animals respond to environmental stress. Stress-responsive reversible protein phosphorylation (involving protein kinases and phosphatases) has been studied extensively for many enzymes in many animal models but relatively little is known about reversible phosphorylation control of vertebrate IDH1 or about this enzyme in an amphibian model of dehydration (Hurley et al. 1989; Lee et al. 1995; Humphrey et al. 2015). Currently, glutathionylation is the only posttranslational modification known to regulation IDH1 function. In a human

embryonic kidney cell line, the addition of a glutathione group on the reactive cysteine completely abolished IDH function (Shin et al. 2009). The present study demonstrates that IDH1 from dehydrated skeletal muscle is 1.8-fold and 1.2-fold more phosphorylated on threonine and tyrosine residues, respectively, when compared to control IDH1 enzyme (Figure 5.3). This phosphorylation correlates with the reduced V_{max} of IDH1 but has no effect on the enzyme's overall stability since chemical destabilizers and thermal unfolding were not changed (Figure 5.7 and 5.8).

The use of *in vitro* incubations with endogenous protein kinases and phosphatases demonstrates the effects of varying the phosphorylation state of *X. laevis* IDH1 on its affinity for isocitrate (Tables 5.3 and 5.4). The enzyme from dehydrated muscle was only sensitive to the stimulation of phosphatases with the enzyme affinity for isocitrate being lowered after PP2A was stimulated (Table 5.4). PP2A is a serine/threonine phosphatase which has a highly conserved binding sequence, therefore this kinetic change is likely due to the removal of phosphorylation at PP2A specific sites (Kong et al. 2009). PP2A can mediate the glucose inhibition of AMPK, the central cellular energy gauge, through its dephosphorylation (Ravnskjaer et al. 2006). This could be a mechanism for the on/off phosphorylation of IDH1 as well in response to changing energy availability as *X. laevis* moves through dehydration. In the hydrated muscle extracts, phosphorylation stimulated by CAMK or PKC lowered the enzyme's affinity for isocitrate whereas the stimulation of PKA or total kinases raised the affinity for isocitrate (Table 5.3). Furthermore, hydrated samples that were artificially phosphorylated by CAMK and PKC demonstrated a reduction in IDH1 V_{max}, which makes the *in vivo* kinetics likely due to the increasing threonine phosphorylation (Table 5.4). Since the *in silico* results also suggest that PKC is

a likely kinase to act on IDH1 (Table 5) and the action of PKC mimicked the *in vivo* reduction in V_{max} (Table 5.4), the predicted Thr313 is likely a site of phosphorylation regulation for *X. laevis* IDH1. Thr313 is proximal to the active site, likely allowing the addition or removal of a phosphate to impact substrate binding (Figure 5.9). The impact of changes to phosphorylation on IDH1, on both tyrosine and threonine residues, requires further investigation to detail the effect of individual sites on dehydration survival.

In conclusion, the present data show that IDH1 from *X. laevis* muscle undergoes stable changes in its enzymatic properties in response to dehydration. A concurrent increase in protein phosphorylation, which can be mimicked through stimulation with PP2A or PKC, implicates this PTM as the mechanism underlying IDH1 kinetic inhibition. The physiological consequences of dehydration-induced IDH1 regulation is a reduction in enzyme maximal velocity and a bias towards the use of isocitrate and magnesium. This serves to slow the production of NADPH and α-KG during dehydration in the African clawed frog perhaps to avoid the upstream buildup of citrate or perhaps to allow for a reduced but continual production of NADPH.

5.5 Figures

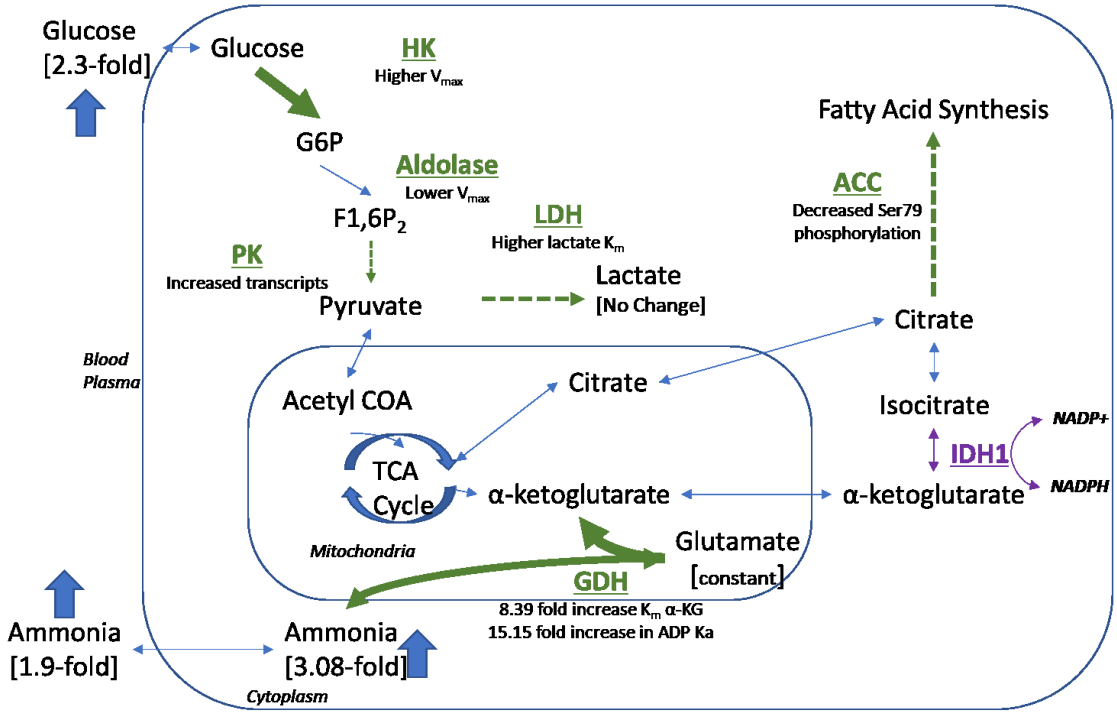

Figure 5.1: Role of IDH1 in the metabolic pathway of dehydrated *X. laevis* skeletal muscle. Green arrows indicate direction of reactions with green arrows indicating known directional biases based on K_m information. Solid blue lines are known reaction directions based on pooled substrates and increased affinities, dotted green lines have decreased V_{max} values but are poised to favor that direction. HK has a higher V_{max} increasing the consumption of glucose (Childers and Storey 2016). Aldolase has a decreased V_{max} which seems to slow glycolysis (Chapter 2). LDH is poised to continue in the forward direction at a lower Vmax (Childers and Storey 2019). There is evidence to support promotion of fatty acid synthesis through ACC1 dephosphorylation (Chapter 4). GDH is known to favor the production of α-KG from glutamate during high dehydration (*GDH reaction occurs in the mitochondria) (Appendix 1). IDH1 (in purple) interconverts isocitrate and α-KG in the cytoplasm while converting $NADP^+$ to NADPH.

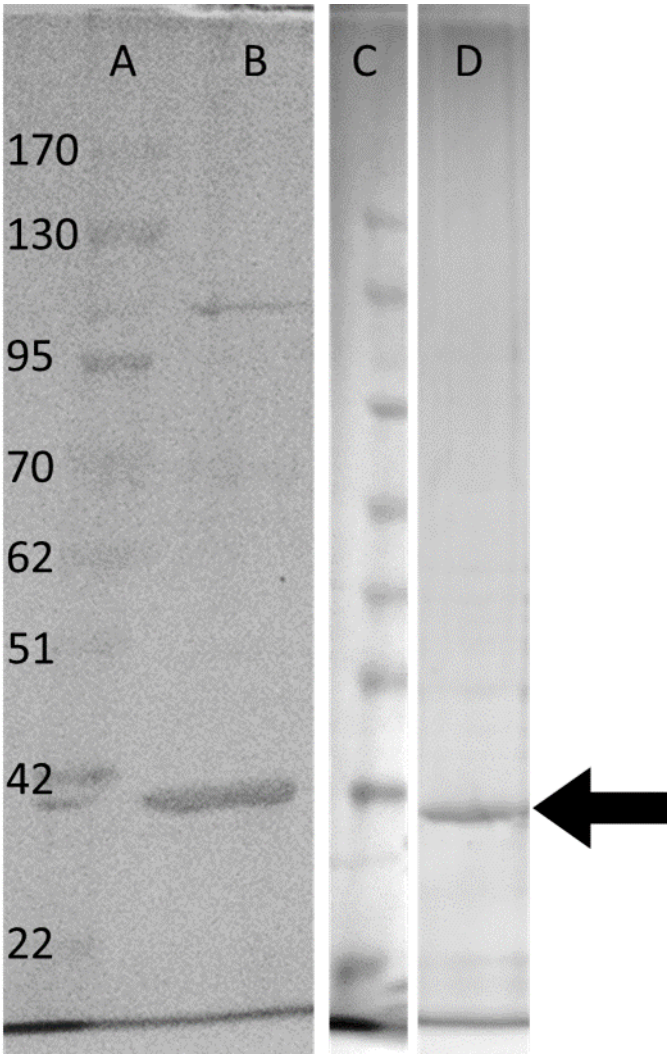

Figure 5.2: Isolation of muscle IDH from control and dehydrated *X. laevis*. Electrophoretic analysis on a Coomassie stained 10 % SDS-PAGE gels shows the result of the isolation steps. Lane A: molecular weight ladder with kDa sizes indicated on the left. Lane B: Pooled control IDH fractions after 0-1M KCl gradient elution off Cibacron Blue. Lane C: Molecular weight ladder cut from the dehydrated gel that had Lane D: Pooled dehydrated IDH fractions after 0-1M KCl gradient elution off Cibacron Blue. A black arrow indicates the band that corresponding to the immunoblot band for IDH.

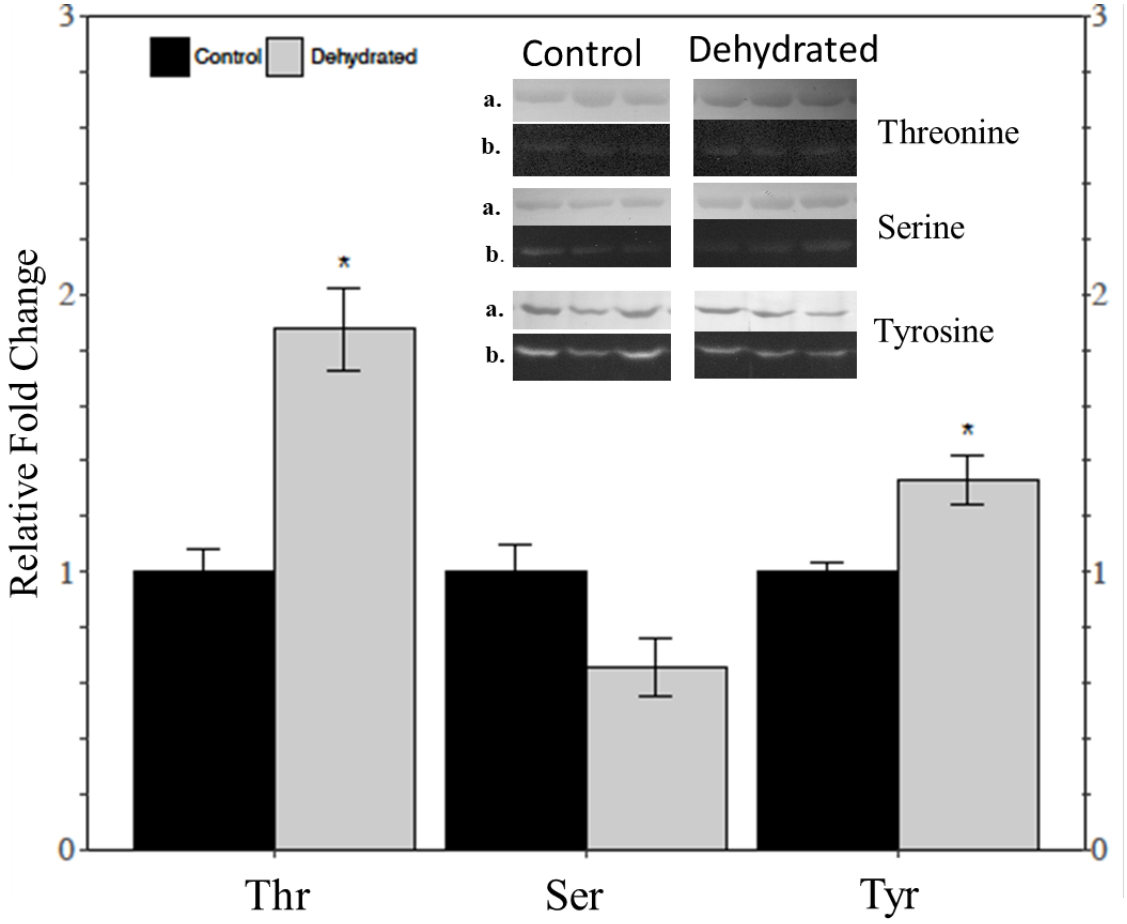

Figure 5.3: Immunoblot analysis of phosphorylation on threonine, serine or tyrosine residues of isolated *X. laevis* muscle IDH from control and dehydrated frogs. Chemiluminescent images (a) and subsequent Coomassie brilliant blue stained images of the same blots (b) are imbedded above the histogram bars. Relative amounts of phosphorylated residues were standardized against the corresponding blue stained band. Data are relative intensities, means ± SEM, n = 3. *Significantly different from the corresponding control value using the Student's t test, $p < 0.05$.

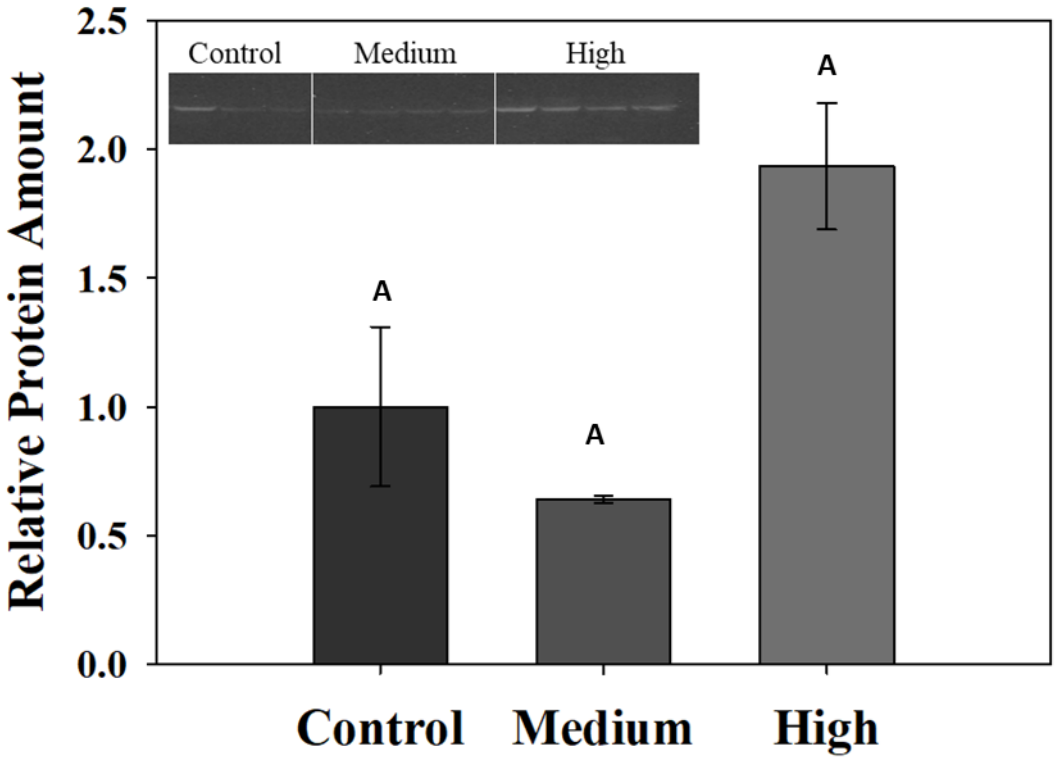

Figure 5.4: Relative total IDH protein in total protein extracts of skeletal muscle from control, medium and high dehydrated *X. laevis* skeletal muscle as assessed by immunoblotting. Data are means ± SEM, n = 3-4 independent determinations.

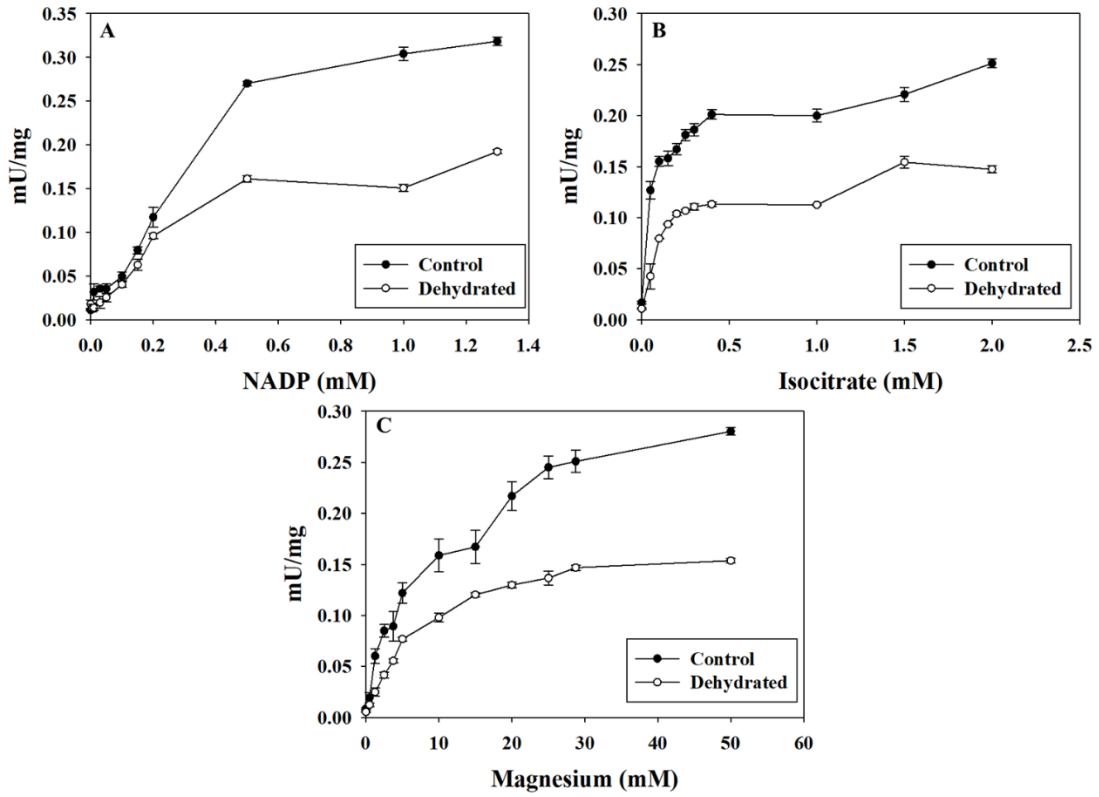

Figure 5.5: Graphical results of kinetic analysis of substrate affinities for isolated NADP$^+$-isocitrate dehydrogenase. V vs [substrate] plots of untransformed initial rates with increasing amounts of (A) NADP, (B) Isocitrate or (C) Magnesium with respective co-substrates held at constant saturating concentrations. Velocities are means ± SEM for n=3-4.

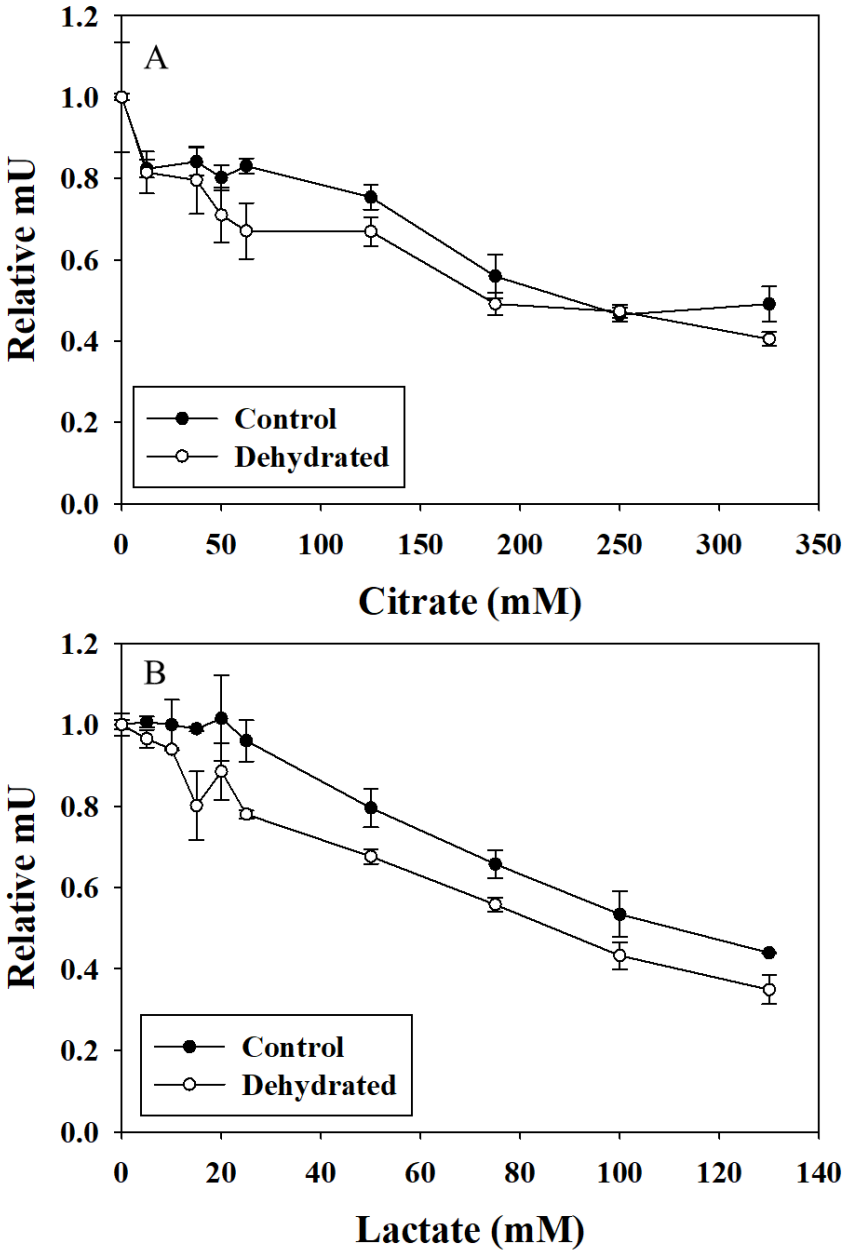

Figure 5.6: Graphical results assessing inhibition of isolated NADP$^+$-isocitrate dehydrogenase by A) citrate or B) lactate. These acidic additives were made in assay buffer (pH 7.5).V vs [inhibitor] plots of untransformed initial rates with increasing amounts of inhibitor at saturating co substrate concentrations. Velocity points are n=3-4, mean ±SEM.

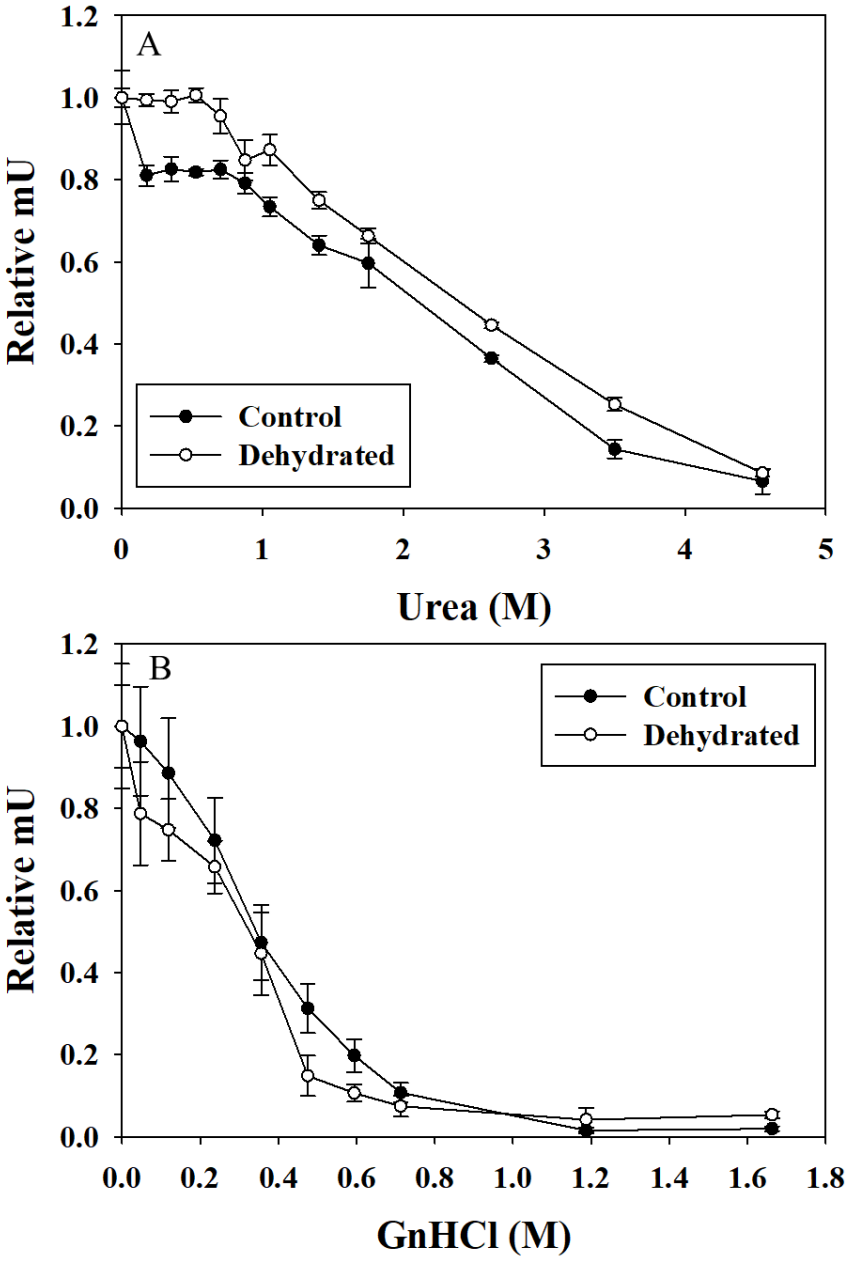

Figure 5.7: Graphical results showing inhibition of isolated NADP$^+$-isocitrate dehydrogenase by A) guanidine hydrochloride or B) urea. Additives were made in assay buffer (pH 7.5).V vs [inhibitor] plots untransformed initial rates with increasing amounts of inhibitor. Velocity points are n=3-4, mean ±SEM.

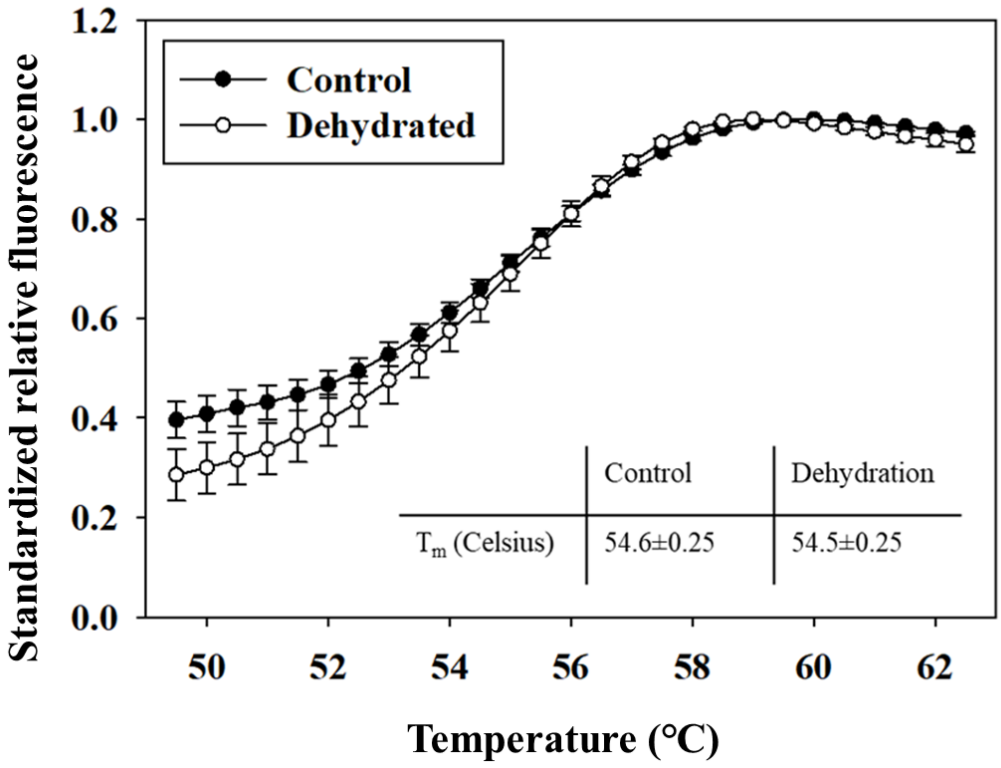

Figure 5.8: Thermal stability of IDH1 from both control and dehydrated skeletal muscle measured using differential scanning fluorimetry. Typical melt curves for isolated IDH1 from control and dehydrated skeletal muscle are shown and indicate no change in the T_m (54.6 ± 0.25°C) between the two physiological states. The average values for control and dehydrated are inset with data being mean ± SEM, n=4.

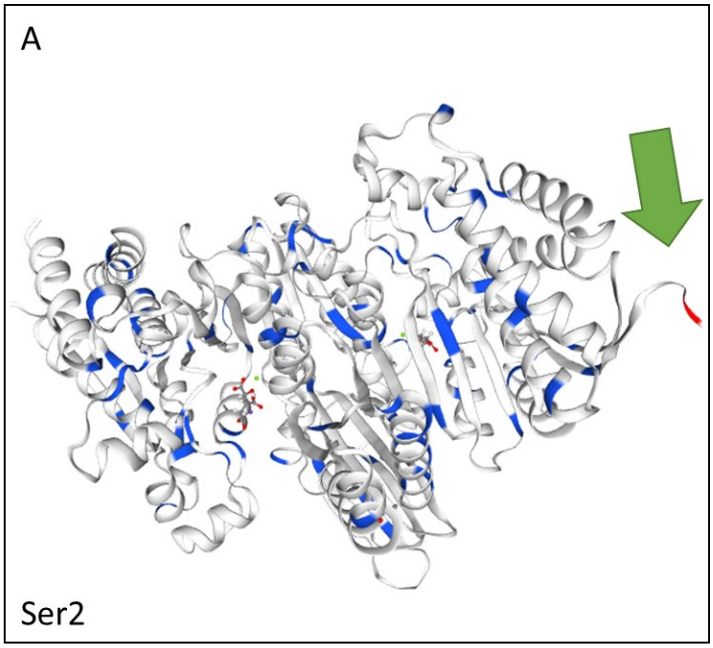

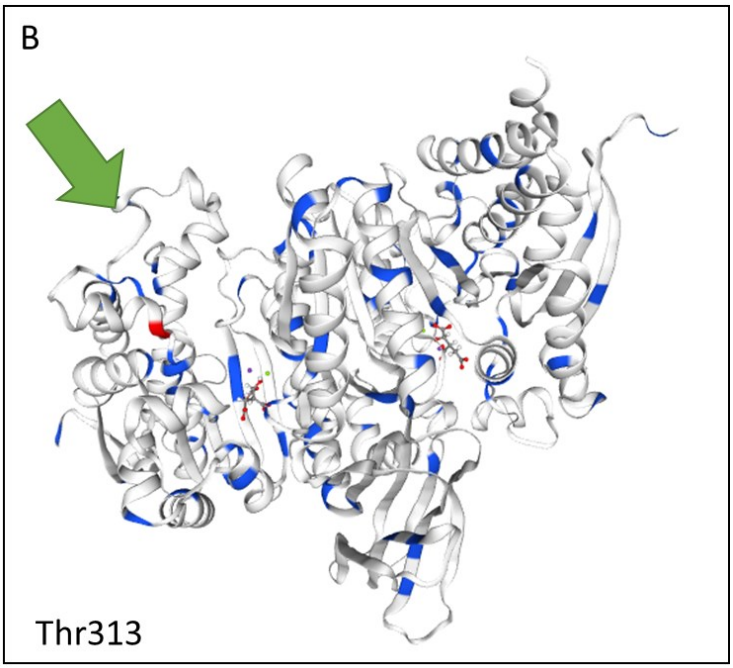

Figure 5.9: Homology models of *X. laevis* muscle IDH1 indicating the predicted phosphorylation sites: (A) Ser2 and (B) Thr313. Green arrows point to the red amino acid sites predicted by NetPhos3.1. A) Ser2 and B) Thr313.

5.6 Tables

Table 5.1: Isolation steps of control IDH from skeletal muscle of *X. laevis*.

Step	Total protein (mg)	Total activity (mU)	Yield (%)	Specific activity (mU/mg)	Fold isolation
Crude	29.89	1009.17		33.77	
DEAE	25.72	912.54	90.43	35.48	1.05
Cibacron (Iso/Mg^{2+})	0.99	211.60	20.97	214.77	6.36
Cibacron (0-1M KCl)	0.31	101.23	10.03	329.31	9.75

Table 5.2: Summary of enzyme kinetic parameters for isolated IDH from muscle of control and dehydrated frogs assayed at 23 °C. Data are mean ± SEM, n = 4-5. Statistically significant differences are marked with an asterisk.

Condition	Control	Dehydrated
K_m $NADP^+$ (mM)	0.33±0.01	0.47±0.06
K_m Isocitrate (mM)	0.08±0.01	0.11±0.02
K_m Mg^{2+} (mM)	15.38±0.67	6.61±0.18*
V_{max} (mU/mg)	0.37±0.007	0.19±0.03*
I_{50} GuHCl (M)	0.35±0.01	0.26±0.1
I_{50} Urea (M)	1.48±0.28	2.13±0.16
I_{50} Citrate (mM)	322±24	262±53
I_{50} Lactate (mM)	118±5.6	85±10*

Table 5.3: IDH1 K_m values for isocitrate (mM) after incubations to stimulate the activities of native protein phosphatases or kinases. The p-values are for comparisons to control or dehydrated OPEN conditions. Data are means ± SEM, n=4. "*" indicates a significant difference between the incubation condition and the OPEN condition of the same sample using a Student's t test.

	Control K_m	p-Value	Dehydrated K_m	p-Value
OPEN	0.11±0.01		0.07±0.01	
Total PPase	0.05±0.005*	0.002	0.11±0.01*	0.03
PP2A	0.03±0.005*	0.0003	0.04±0.002*	0.02
PP2B	0.06±0.014*	0.03	0.07±0.004	0.36
PTPs	0.03±0.005*	0.0003	0.05±0.01	0.15
CAMK	0.20±0.03*	0.03	0.08±0.01	0.06
PKC	0.22±0.01*	0.0004	0.05±0.01	0.12
PKA	0.06±0.01*	0.02	0.05±0.01	0.26
Total Kinase	0.04±0.002*	0.0006	0.13±0.03	0.07

Table 5.4: IDH1 relative V_{max} values for isocitrate (mM) after incubations to stimulate the activities of native protein phosphatases or kinases. The p-values are for comparisons to control or dehydrated OPEN conditions which are set to 1. Data are means ± SEM, n=4. "*" indicates a significant difference between the incubation condition and the OPEN condition of the same sample using a Student's t test.

	Control V_{max}	p-values	Dehydrated V_{max}	p-values
OPEN	1.00±0.1		1.00±0.05	
Total Ppase	0.76±0.04	0.05	0.93±0.03	0.26
PP2A	0.72±0.04*	0.03	0.53±0.17	0.06
PP2B	0.90±0.08	0.40	0.79±0.02*	0.02
PTPs	0.71±0.04*	0.03	0.68±0.03*	0.00
CAMK	0.14±0.1*	0.00	0.69±0.02*	0.00
PKC	0.02±0.02*	0.00	0.69±0.01*	0.01
PKA	1.53±0.04*	0.02	0.68±0.04*	0.00
Total Kinases	1.31±0.03	0.06	1.01±0.09	0.95

Table 5.5: *In silico* kinase binding site prediction from the NetpPhos 3.1 server for *X. laevis* IDH (Accession#: XP_018094513.1) that scored higher than 0.75.

Residue	Context	Score	Kinase
Ser2	---M**S**KKIN	0.847	PKC
Thr313	HGTV**T**RHYR	0.809	PKC

Chapter 6: General Discussion

Xenopus laevis has been used as a model amphibian for a number of studies of the physiological and behavioral effects of dehydration, a very relevant environmental stress for amphibians that have highly water-permeable skin. However, less is known about the cellular, metabolic and enzymatic responses involved in amphibian endurance of dehydration stress. In the general introduction (**Chapter 1**) of this thesis, the physiological conditions experienced by *X. laevis* during whole body dehydration are described. When enduring whole body dehydration these frogs show a decrease in plasma volume, which elevates hematocrit and blood viscosity, and ultimately causes restriction of oxygen delivery to the frogs' peripheral tissues (Hillman 1978b; Hillman and Sommerfeldt 1981). Instead of entering a state of hypometabolism, as many other dehydration tolerant species do, *X. laevis* increase their resting heart rate to compensate for a deteriorating capacity of the circulatory system as hematocrit increases (Hillman 1978b; Storey and Storey 2012). This continues as dehydration progresses until the limits of tolerance are reached, at which time the resting and maximal heart rates are equivalent, returning blood oxygen is zero and whole-animal lactate levels rise (Hillman 1978b).

Previous work on the effects of whole-body dehydration on *X. laevis* have provided preliminary evidence to describe the role that reversible protein phosphorylation has in the molecular response to this stress. It has been shown that reversible protein phosphorylation affects a broad range of processes including transcription factor binding and enzyme kinetic properties in *X. laevis* (Childers and Storey, 2016; Dawson et al., 2018; Katzenback et al., 2014; Malik and Storey, 2011, 2009). However, reversible protein phosphorylation are known to be ubiquitous and the results of these modifications are often tissue-specific (Olsen et al. 2006; Humphrey et al. 2015). In this thesis, the role

of reversible phosphorylation in regulating enzyme function and intracellular signaling in response to dehydration was investigated in *X. laevis* skeletal muscle. Skeletal muscle is of particular interest because *X. laevis* is known to restrict blood circulation to this tissue under dehydrating conditions in order to conserve oxygen for delivery to higher order tissues like the brain (Hillman and Sommerfeldt 1981). Furthermore, the processes investigated in this thesis include pathways that have been shown previously to be regulated in other animal models in response to environmental stress (Horman et al. 2005; Abnous and Storey 2007; Dieni and Storey 2009; Dawson et al. 2013). However, these models commonly use whole animal metabolic rate depression as a major component of their strategy for dealing with worsening environmental conditions (Storey and Storey 2005; Storey 2010). The molecular responses in an animal that does not have this coping mechanism, such as *X. laevis,* would be useful for comparison and for future discoveries about strategies of metabolic regulation.

With respect to skeletal muscle glucose catabolism, it is important to realize that glycolysis is crucial to survival under high dehydration conditions, since oxidative phosphorylation becomes increasingly compromised as blood thickens and blood flow slows restricting access to oxygen delivery. Indeed, during dehydration, glucose concentrations in the blood plasma increase to support an increased reliance on this fuel use during this time of stress (Malik and Storey 2009a). The fact that glycolysis is critical for survival during dehydration is corroborated by the lactate concentrations that increase dramatically as soon as dehydration reaches a point where oxygen delivery is compromised (Hillman 1978b). Indeed, transcript levels and activities of PK are also maintained likely to ensure that PK activities stay high in dehydrating tissue to sustain the

glycolytic pathway and supply pyruvate to LDH (Dawson et al. 2018). Indeed, a study on locomotion during dehydration in these frogs indicates that the loss of water causes a decline in skeletal muscle ability to synthesize ATP by aerobic means, which further signals that dehydrated *X. laevis* has an increased dependence on glycolysis for energy production (Gatten 1987).

The fact that glycolytic substrate and product concentration are in flux during high dehydration, and that a continual degradation or synthesis of glycolytic enzymes would be energetically uneconomical, it is practical that the reactions of glycolysis could be simply regulated at the enzyme level through control mechanisms that can be quickly and reversibly applied when environmental conditions are severe or when conditions improve. Indeed, many years of research have identified reversible protein phosphorylation as a major mechanism for making adaptive changes to metabolic pathways in response to environmental stress (Storey and Storey 1990, 2007, 2010, 2012; Storey 2004). Furthermore, a recent phosphoproteome study revealed that the abundance of phosphopeptides retrieved from nine glycolytic enzymes in the liver of the freeze tolerant wood frog, *Rana sylvatica*, suggested that dehydration has a unique pattern of protein phosphorylation as compared to the responses to anoxia or freezing stresses (Hawkins et al. 2019). Certainly, within *X. laevis* skeletal muscle, preliminary results of glycolytic regulation via reversible phosphorylation have been demonstrated. Critically, the first enzyme of glycolysis, HK, is phosphorylated to mediate an increase in its maximal velocity under high dehydration (to support glucose intake), whereas the terminal enzyme of anaerobic glycolysis, LDH, is regulated to support forward glycolytic flux (Childers and Storey 2016, 2019).

The present thesis found that the coordinated regulation of enzyme activity within the glycolytic pathway was not just at the "bookending" regulatory points but also includes the intermediate steps, evidenced by the regulation of aldolase. In **Chapter 2,** the relative phosphorylation and activity of aldolase was quantified in skeletal muscle from control and dehydrated *X. laevis.* It was initially reasoned that if glycolysis was being relied upon and was already regulated to take in more carbohydrates, then the rest of glycolysis may need a similar up-regulation to support glycolytic ATP production. However, the kinetic properties of aldolase suggested that glycolytic flux may be reduced during dehydration by a constricted flow of $F1,6P_2$ into GAP by aldolase. This kinetic alteration was mediated through reversible phosphorylation in line with a rapid and reversible stress response. This corroborates the trend indicated by the regulation of LDH in this tissue, which indicated that the glycolytic rate is slowed within skeletal muscle during dehydration. Furthermore, these results suggest that there is a global mechanism of phosphorylation of glycolytic enzymes that is used to quickly coordinate the pathway to adapt to stress as tissue water decreases.

Specific Hypothesis 1 revisited: Aldolase, is regulated by reversible phosphorylation to reduce glycolytic flux during whole animal dehydration and may contribute to a tissue-specific glycolytic regulation.

Previous work and the evidence from Chapter 2 indicate that even though glycolysis is increasingly relied upon during dehydration in *X. laevis*, the production of ATP is likely reduced, requiring the animal to adapt to a lower capacity for energy production. This leaves an important question open. If glycolysis is now a main source of ATP how is

skeletal muscle maintaining an adenylate ratio during dehydration? One enzyme that is crucial to provide a rapid response to falling ATP levels in skeletal muscle is CK. CK acts to regenerate ATP by gating the use of P-Cr reserves that can be used to quickly produce ATP and creatine when adenylates are low. Previously, CK has been shown to be upregulated by increased protein phosphorylation in another frog species , *Rana sylvatica* (Dieni and Storey 2009). Increased relative phosphorylation had activating effects in this species and, as a result, CK maximal activity was elevated along with an increase in affinity for its substrates (Dieni and Storey 2009). In **Chapter 3**, an analysis of *X. laevis* CK demonstrated a somewhat similar trend in that the removal of phosphorylation caused a decrease in overall maximal activity of CK when assayed at the control maximal $MgCl_2$ concentration. However, this reduction in maximal activity was dependent on the concentration of $MgCl_2$, with the enzyme from dehydrated frogs having a higher V_{max} than its control counterpart when assayed at increased concentrations of $MgCl_2$ (measured up to 4 mM). Therefore, dehydration-induced CK regulation appears to limit the use of P-Cr until intracellular magnesium concentrations naturally increase as a consequence of dehydration. This is a similar mechanism of regulation to that demonstrated for LDH which is urea sensitive in multiple *X. laevis* tissues (Katzenback et al. 2014; Childers and Storey 2019). These frogs may leverage natural increases in key solutes to contingently regulate the activities of enzymes involved in energy homeostasis. Interestingly, during dehydration of *X. laevis* muscle, the tissue appears to slow the replenishment of ATP from P-Cr stores as well as slow the rate of glycolysis as seen in Chapter 2. The reduction in CK V_{max} suggests that during dehydration, although there is a reduced glycolytic rate, there is also an apparent saving of P-Cr. This could perhaps be a

preparatory mechanism, as dehydration in the natural environment of African clawed frogs could signal the beginning of a long drought that could last for months. Dehydration could therefore be the beginning of slower entry into longer term metabolic adaptions required for estivation. Thus, although metabolic processes are regulated to continue ATP production by non-oxygen dependent pathways (glycolysis, phosphagen stores), they are seemingly also contributing to lowering of ATP production, perhaps to adapt for long term survival.

Specific Hypothesis 2 revisited: Creatine kinase is regulated by phosphorylation to decrease any p-Cr production. Creatine kinase is also regulated to favor the conversion of p-Cr to ATP at a reduced maximal velocity until magnesium concentrations increase activating the production of ATP as dehydration increases.

If modes of synthesizing ATP are reduced, then adenylate ratios may be in flux during dehydration stress. This could cause some interesting consequences for cellular energy signaling as the AMPK is canonically responsive to adenylate ratios and can become activated as a result. One downstream influence of AMPK is to promote the use of alternative fuels to restore the cells energy balance. Thus, the effect of dehydration on the activation state of AMPK and its downstream targets involved in fat metabolism and autophagy were investigated. Immunoblotting data reported in **Chapter 4** indicated that there was no significant increase in signaling through AMPK in response to energy stress signals in muscle of dehydrated *X. laevis* as evidenced by no change in Thr172 phosphorylation and reduced phosphorylation on Ser496. Therefore, it is proposed that although these experimental frogs were experiencing high dehydration, they may not be

taxed to an extent that required the recruitment of alternative energy sources. ACC1 and ULK1 phosphorylation was also investigated to determine the downstream signaling. The phosphorylation patterns of these proteins did not suggest that an activation of β-oxidation or autophagy was occurring. This is ultimately understandable since the activation of β-oxidation would require further oxygen using reactions. Curiously, there was a dual increase of ULK1 phosphorylation on sites specific to AMPK and mTOR, which highlights the importance of dephosphorylation as a key mediator in the response to environmental stress. It is known that mTOR phosphorylation, and thus its activity, is reduced during high dehydration in *X. laevis* (Luu 2011). Chapter 4 however, reveals that the degradation of mTOR-mediated phosphorylation on ULK1 is not reduced relative to control and is surprisingly relatively increased during high dehydration. This sustained phosphorylation perhaps is maintained by the remaining mTOR or another kinase in order to block AMPK autophagy stimulation. Further study into the kinases able to act on this site are needed. The consistent phosphorylation of AMPK on Thr172 therefore, may still serve to prepare the tissue for autophagy recruitment once mTOR phospho-signaling is removed.

***Specific Hypothesis 3 revisited*:** AMPK is not activated during dehydration in *X. laevis* skeletal muscle and the regulation of its downstream targets through reversible phosphorylation poise this tissue to suppress fatty acid β-oxidation and autophagy signals.

The regulation of isocitrate dehydrogenase 1 (IDH1) was investigated because it has been previously demonstrated that NADPH production by this enzyme can be a major

source of reducing power for the cell (Shechter et al. 2003). This reducing power can support many biosynthesis pathways as well as antioxidant reactions. However, the reactions that draw on α-KG and isocitrate as substrates are perhaps more intriguing. **Chapter 5** demonstrated that IDH1 maximal velocity is suppressed through reversible phosphorylation, continuing a theme of reduced metabolic processing in *X. laevis* under dehydrating conditions in general. The enzyme appears to favor the production of α-KG since IDH1, like CK, also has an increased affinity for Mg^{2+}during dehydration. As discussed for CK, this would only become significant when dehydration naturally increased cellular concentrations of ions and other solutes and would serve to reduce the concentration of isocitrate (and possibly also citrate) in the cytosol during dehydration. Cytosolic citrate is inhibitory of glycolysis as it is a key inhibitor of phosphofructokinase and can feed into many cell growth pathways, such as fatty acid biosynthesis (Wise et al. 2011; Icard et al. 2012). Avoiding a buildup of cytosolic citrate may be the goal of IDH1 regulation as it can control the flux of citrate to isocitrate through a constant conversion of isocitrate to α-KG. Furthermore, the reduced V_{max} of IDH1 suggests that this enzyme is not activated to increase NADPH production during dehydration and thus IDH does not seem to be crucial to the support of antioxidant capacity under these conditions. Therefore, perhaps these frogs can sufficiently defend against reactive oxygen species on a lower NADPH concentration in the cytosol or rely on other NADPH-producing enzymes such as glucose-6-phosphate dehydrogenase.

Specific Hypothesis 4 revisited: IDH1 is regulated by reversible phosphorylation to favor α-KG production at a much reduced maximal velocity during whole animal dehydration.

Conclusion

In conclusion, this thesis demonstrates that skeletal muscle is relying on a reduced glycolytic capacity under high dehydration conditions to sustain ATP production for muscle cells. Furthermore, the stress of dehydration alone is not enough to recruit AMPK activation or the metabolic signaling that AMPK can provide to recruit alternative energy pathways. A main mechanism that is altering the overall energy state of skeletal muscle is reversible protein phosphorylation, as evidenced by the changes to enzyme kinetic properties after artificial stimulation of the activities of endogenous protein kinases and protein phosphatases. AMPK and IDH1 regulation both poise this tissue to reduce fat metabolism under dehydrating conditions through a reduction of ACC1 phosphorylation and lower yet continued production of α-KG by IDH1. This is sensible since β-oxidation would require oxygen which is in limited supply during high dehydration in *X. laevis*. Aldolase and CK regulation poise these enzymes to slow the production of ATP during dehydration, perhaps in preparation of a natural longer estivation. Overall, this thesis demonstrates a wide-ranging regulation of metabolism through reversible protein phosphorylation to serve the energy balancing processes needed in the skeletal muscle of *Xenopus laevis* during whole animal dehydration.

Future Directions

Reversible protein phosphorylation is a crucial mode of regulating cellular energetics in animal cells in response to stress signaling as clearly documented here for *X. laevis* skeletal muscle. Future studies should focus on other potentially key protein kinases that can mediate stress signaling. The protein kinase C (PKC) family is one example protein

that could prove interesting for many phosphor-signaling networks. The PKC family of kinases is known to participate in many biological responses including the regulation of insulin sensitivity and lipid metabolism (Nishizuka 1995). Furthermore, it is has been shown to be strongly reduced in response to freezing in another frog species (Dieni and Storey 2014) In this thesis, *in silico* methods of predicting phosphorylation sites concluded that all enzymes isolated in this thesis were likely regulated by PKC in some capacity. Kinetic alterations were demonstrated after incubations that stimulated endogenous PKC that resulted in decreased substrate K_m values for aldolase, CK and IDH. Stimulation of PKC activity also had no effect on the V_{max} for aldolase or CK but drastically reduced the V_{max} for IDH. Therefore, the phosphorylation on PKC sites seems to promote carbohydrate metabolism while inhibiting enzymes involved in fatty acid metabolism. Free fatty acids have been shown to stimulate insulin resistance through the activation of PKC and therefore the reduction in fat oxidation may be part of the mechanism to promote PKC activity and alter skeletal muscle energy production (Griffin et al. 1999). However, this is based on a small sample of metabolic enzymes and therefore future studies on the role of PKC in metabolic regulation during dehydration are needed to determine the role it plays in *X. laevis*. Furthermore, future work should investigate related phosphatases and the signaling that stimulates dephosphorylation, since the lack of phosphatase activity seems to play a critical role in blocking energy stress signaling as evidenced by the maintenance of mTOR phosphorylation on ULK1 (Luu 2018).

All enzymes in this study were assessed in control animals, which had not been dehydrated, as well as animals that had been dehydrated for about 48 hours as they

reached ~30% dehydration (31.18 ± 0.83%). The reasoning was that any metabolic changes should be in full effect after high dehydration. However, some enzymes could be differentially regulated at different time points over the course of increasing dehydration over the hours or days or weeks of natural dehydration in the native environment of these frogs, durations that would also involve a halt to feeding by *X. laevis* (Merkle and Hanke 1988a, c; Merkle 1989). Dehydration in natural models of *X. laevis* does not happen in a short time frame as depicted in our laboratory model of dehydration (Balinsky et al. 1961; Merkle and Hanke 1988a). The long-term nature of natural aestivation includes the variables of a longer duration and the associated starvation that can require a modified energy metabolism to allow these animals to survive. Future studies could include time course studies to determine the influence of long-term studies of food deprivation (without dehydration) or time course studies of more extended periods of dehydration to determine when/if dehydration can stimulate molecular regulation of energy stress related pathways, like AMPK, and the associated pathways discussed in this thesis. It would be interesting to determine when different protein kinases and phosphatases become activated during dehydration versus starvation to alter the balance of signals between nutrient signaling and energy stress.

Appendices

Appendix 1: GDH isolation and activity from skeletal muscle of dehydrated *X. laevis*.

Table A1: Purification of GDH from leg muscle of dehydrated *X. laevis*.

Step	Total Protein (mg)	Total Activity (mU)	Specific Activity (mU/mg)	Yield %	Fold purification
Crude	38.7	107.7	2.78	-	-
$DEAE^{+}$ Sephadex	0.736	26.52	36.0	24.62	12.9
Cibacron Blue	0.204	15.79	77.6	14.66	27.8
GTP-Agarose	0.026	9.91	376.8	9.20	135.3

Table A2: Comparison of kinetic parameters of purified GDH from muscle of control and dehydrated frogs assayed at 23 °C in both the forward and reverse directions. K_m and K_a data are means ± SEM, n = 6 independent determinations on purified enzyme. When K_m was measured in the presence of ADP, the ADP concentration was 1.5 mM. * - Significantly different from the corresponding control value using the Students t-test, $p<0.05$.

Forward reaction	**Control GDH**	**Dehydrated GDH**
K_m glutamate, mM	18.7 ± 1.11	3.59 ± 1.35*
K_m glutamate with ADP, mM	3.34 ± 0.31	2.42 ± 0.41
K_m NAD^+, mM	1.31 ± 0.10	1.29 ± 0.25
K_m NAD^+ with ADP, mM	0.75 ± 0.23	0.22 ± 0.026
K_a ADP, μM	35.5 ± 6.3	20 ± 9

Reverse reaction	**Control GDH**	**Dehydrated GDH**
K_m α-ketoglutarate, mM	0.028 ± 0.005	0.235 ± 0.023*
K_m α-ketoglutarate with ADP, mM	0.61 ± 0.07	1.50 ± 0.28*
K_m NH_4^+, mM	79.9 ± 14.0	94.2 ± 10.4
K_m NH_4^+, with ADP, mM	15.2 ± 1.49	21.0 ± 2.29
K_a ADP, μM	13.0 ± 1.3	197 ± 40*

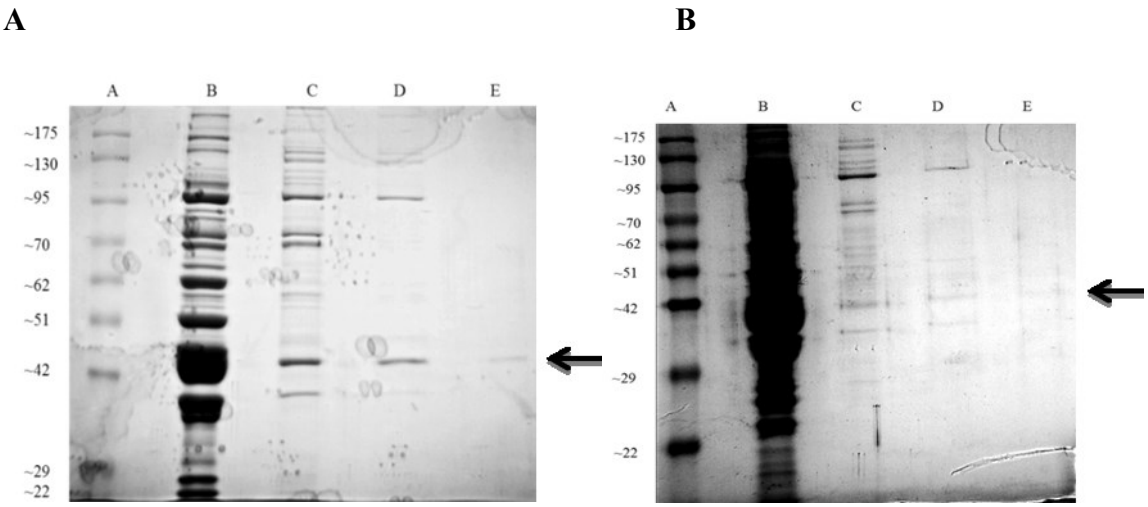

Figure A1: **A**) Purification of skeletal muscle GDH from control frogs; 10% SDS-PAGE gel shows samples from each of the purification steps. Protein was stained with Coomassie blue. Lane A – FroggaBio molecular weight ladder with the approximate molecular weights indicated to the left; Lane B – crude muscle extract; Lane C – pooled peak fractions eluted from DEAE Sephadex; Lane D – pooled peak fractions eluted from Cibacron Blue; Lane E – pooled peak fractions eluted from GTP-agarose. **B)** Purification of skeletal muscle GDH from dehydrated frogs showing purification steps on a 12% SDS-PAGE gel stained with Coomassie blue on. Lanes are as described above. Arrows shows the position of the final purified GDH.

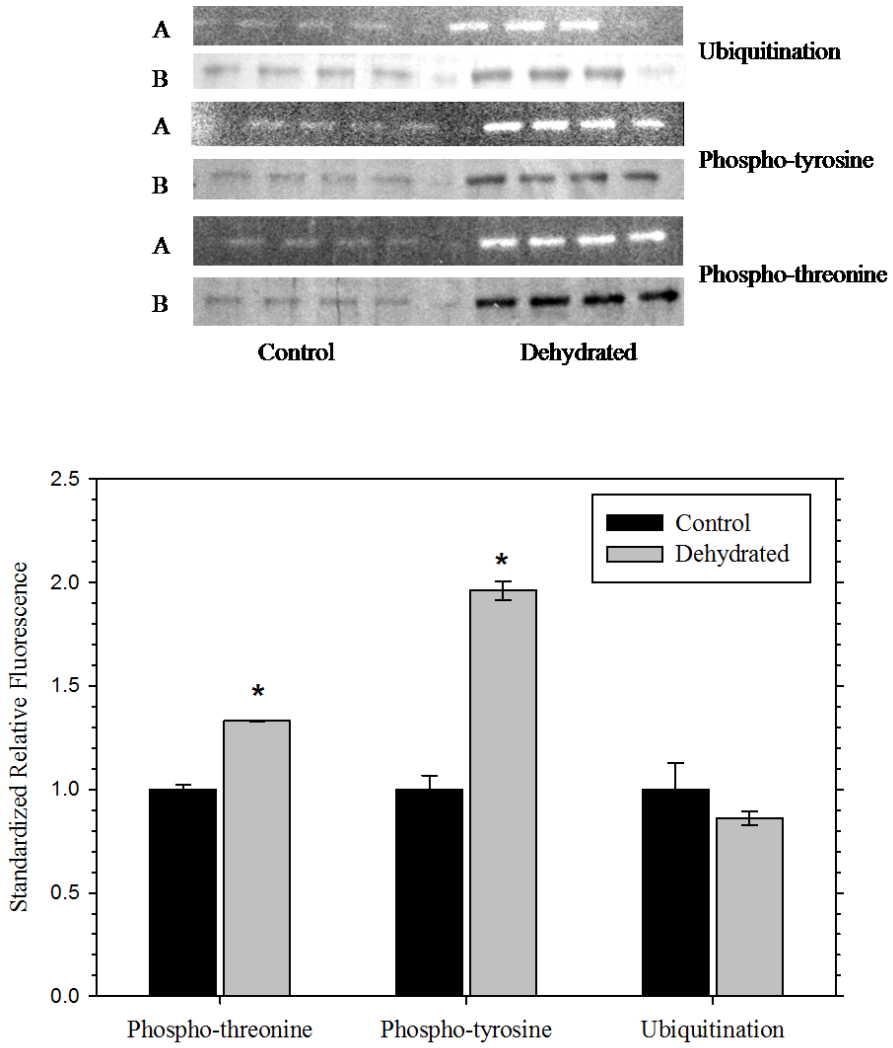

***Figure A2**: Relative post-translational modifications on purified muscle GDH from control and dehydrated frogs: ubiquitination, phospho-threonine, and phospho-tyrosine. Immunoblot band density in each lane was standardized against the density of the same band when re-stained with Coomassie blue. The histogram shows standardized relative band intensities, mean ± SEM, n = 4 independent determinations. * - Significantly different from the corresponding control value by the Student's t-test, $p<0.05$. Images labeled "A" show the immunoblot chemiluminescence; images labeled "B" show the corresponding Coomassie blue stained bands.*

Appendix 2: Curve Fitting: Storey Lab custom kinetics software

Analysis of kinetic data is typically performed using a statistical program designed for the Storey lab, published in BioTechniques (Brooks, 1992). The program allows the input of X-Y scatter points, pertaining to activity versus the concentration of a biomolecule which affects the enzyme (a substrate, inhibitor, or activator). The program is designed with appropriate equations for determining kinetic parameters. The equations are as follows:

Michaelis-Menten equation: The standard velocity versus substrate curve with hyperbolic kinetics. Will calculate V_{max} and K_m.

*Mainly used in this thesis.

Hill equation with h > 0: This is used as a starting point for curve fitting. It fits a velocity versus substrate curve with sigmoidal, cooperative kinetics. This equation leaves open the possibility that the Hill coefficient is greater than 0 but less that one, indicating negatively cooperative kinetics. $S_{0.5}$ is used instead of K_m as a half-saturation constant.

Hill equation with h > 1: This is a velocity versus substrate curve with sigmoidal, positively cooperative kinetics. It should be used only with certainty that positively cooperative kinetics are present.

Activator equation with h > 0: This is a velocity versus an allosteric activator, when dealing with an activator that has a cooperative mechanism. This leaves open the possibility that activation may be negatively cooperative. Activator equations calculate

the activation constant K_a, a V_{max} which is the maximum activated rate of reaction, and V_0, the rate of reaction in the absence of inhibitor. In order to use any activation equations, the plotted activity in the absence of activator must not be zero.

Activator equation with h > 1: This is a velocity versus an allosteric activator, when dealing with an activator that has a positive cooperative mechanism.

Activator equation with h = 1: This is a velocity versus an allosteric activator, when dealing with an activator that has a Michaelis-Menten-like mechanism.

Linear inhibition equation: This is for analysis of velocity versus [inhibitor]. As its name implies, the correlation between inhibition and inhibitor concentration is a linear one. This equation calculates the concentration of inhibitor at which activity is 50% of the activity in the absence of inhibitor, I_{50}. In order to use any inhibitor equations, the plotted activity in the absence of inhibitor must not be zero.

Non-linear inhibition equation: This is velocity versus an inhibitor. As its name implies, the correlation between inhibition and inhibitor concentration is not a linear one and is based on the Hill equation. Depending on the equation used, one can calculate I_{50} or K_{50}, which is the apparent affinity constant for an inhibitor typically seen in competitive inhibition, and not necessarily equivalent to I_{50}.

Appendix 3: List of Publications

- **Childers CL,** Tessier SN, Storey KB. (2019). The heart of a hibernator: EGFR and MAPK signaling in cardiac muscle during the hibernation of thirteen-lined ground squirrels, *Ictidomys tridecemlineatus*. PeerJ 7:e7587
- Le Tri D, **Childers CL**, Adam MK, Ben RN, Storey KB, Biggar KK (2019). Characterization of ice recrystallization inhibition activity in the novel freeze-responsive protein Fr10 from freeze-tolerant wood frogs, *Rana sylvatica*. *Journal of Thermal Biology*, 84, 426-30.
- **Childers CL**, Storey KB (2019). Purification and characterization of a urea sensitive lactate dehydrogenase from skeletal muscle of the African clawed frog, *Xenopus laevis*. *Journal of Comparative Biology: Part B*, 189(2), 271-281.
- Mattice AMS, MacLean IA, **Childers CL**, Storey KB (2018). Characterization of pyruvate kinase from the anoxia tolerant turtle, *Trachemys scripta elegans*: a potential role for enzyme methylation during metabolic rate depression. *PeerJ*, e4918.
- Luu BE, Green SR, **Childers CL**, Holahan MR, Storey KB (2017). The roles of hippocampal microRNAs in response to acute postnatal exposure to di(2-ethylhexyl) phthalate in female and male rats. *Neurotoxicology,* 59, 98-104.
- Ruberto AA, **Childers CL,** Storey KB (2016). Purification and properties of glycerol-3-phosphate dehydrogenase from the liver of the hibernating ground squirrel, *Urocitellus richardsonii*. *Comparative Biochemistry and Physiology Part B: Biochemistry and Molecular Biology*, 202:48-55.

- **Childers CL,** Green SR, Dawson NJ, Storey KB (2016). Native denaturation differential scanning fluorimetry: Determining the effect of urea using a quantitative real-time thermocycler. *Analytical Biochemistry*, 508:114-117.
- **Childers CL**, Storey KB (2016). Post-translational regulation of hexokinase function and protein stability in the aestivating frog *Xenopus laevis*. *The Protein Journal,* 35(1):61-71.
- Katzenback BA, Holden HA, Farlardeau J, **Childers CL,** Hadj-Moussa H, Avis TJ, Storey KB (2014). Regulation of the *Rana sylvatica* brevinin-1SY antimicrobial peptide during development and in dorsal and ventral skin in response to freezing, anoxia, and dehydration. *Journal of Experimental Biology*, 217(8):1392-401.

Appendix 4: Animal Care Standard Operating Procedure

Romeo Protocol Number: 106936

Purpose

To provide information about the general care and holding conditions for clawed frogs, *Xenopus*.

Responsibilities

- Responsible personnel: KB Storey or JM Storey

Materials

- Current animal supplier: Science Animal Support Services, CW401 Biological Sciences Building, University of Alberta, Edmonton T6G 2E9
- Food: CU Adult Frog Diet, PMI Nutrition International (supplied with frogs by U. Alberta)
- Aquarium tap water conditioner: standard pet trade grade for detoxification of chloramine-treated Ottawa city water. For example, Aquarium Pharmaceuticals Tap Water Conditioner

Procedures

1. For holding and acclimation, *Xenopus* are held in Steacie Room 502 or 503 in large opaque plastic containers (15x22x12 inches, 80 L) or buckets (20 L). Choice of container size depends on the total number of frogs to be housed and

the body masses; for example, a bucket can accommodate 4-5 small frogs (~20-30 g) or 2-3 large frogs (40-50 g). Containers are loosely covered with lids since Xenopus may be startled by overhead movement/shadows.

2. Pre-experimental acclimation is 1-2 weeks in water at room temperature (20°C) and with a depth of about 6 inches. It is recommended that Xenopus be able to reach the surface to breathe by stretching upwards, not swimming.
3. Monitoring: Frogs are monitored daily Monday to Friday to check for any signs of disease or injury and once on weekends (either Saturday or Sunday). If discovered, any problematic frog is transferred to a separate individual container and further monitored. If disease is suspected, other frogs in same container (Steacie) will be kept separate in a labeled container and monitored; neither frogs nor containers will be mixed with other frogs. In our experience, Xenopus are extremely hardy due to powerful antimicrobial peptides in their skin that protect them in their natural swampy tropical environments and, to date, we have never encountered a disease situation with any animal purchased from a commercial Xenopus breeder.

   Concerns or emergencies at any time: Contact Ken Storey or Jan Storey for instructions at (613) 225-9015 or by email at kenneth_storey@carleton.ca or jan_storey@carleton.ca

4. Feeding: Frogs are fed Monday, Wednesday and Friday mornings with Xenopus adult frog diet. Feeding is 2-3 kernals of food per animal depending on body size (e.g. 2 kernals for 20-30 g frogs; 3 for larger).

5. Cleaning: For frogs, water is changed Monday, Wednesday and Friday afternoons about 6 hours after feeding. Fresh tap water is treated with commercial aquarium water conditioner in the amount specified for the detoxification of chloramines (e.g. 3 drops per 4 liters if using Aquarium Pharmaceuticals Tap Water Conditioner) and is allowed to sit overnight to equilibrate to room temperature before use. Animals are gently netted and transferred to a new container; old containers are rinsed for reuse. No detergents or cleansers are used on containers.
6. Enrichment: One or more section of plastic pipe is added into the water in which the animals can hide. Containers are also loosely covered. Xenopus are startled by overhead shadows (such as from predatory wading birds in their natural environment) and like to hide.
7. Euthanasia of diseased or badly injured frogs: Should it be necessary to euthanize an animal or animals due to disease or injury that is deemed untreatable, then euthanasia will be conducted by prolonged immersion in a buffered MS-222 solution (10 g/L). This has never occurred to date.

References

Abboud J, Storey KB (2013) Novel control of lactate dehydrogenase from the freeze tolerant wood frog: role of posttranslational modifications. PeerJ 1:e12. doi: 10.7717/peerj.12

Abnous K, Storey KB (2007) Regulation of skeletal muscle creatine kinase from a hibernating mammal. Arch Biochem Biophys 467:10–19. doi: 10.1016/J.ABB.2007.07.025

Alers S, Löffler AS, Wesselborg S, Stork B (2012) Role of AMPK-mTOR-Ulk1/2 in the regulation of autophagy: cross talk, shortcuts, and feedbacks. Mol Cell Biol 32:2–11. doi: 10.1128/MCB.06159-11

Alexander SS, Bellerby CW (1938) Experimental studies on the sexual cycle of the South African clawed toad (*Xenopus laevis*). I. J Exp Biol 15:74–81

Bach M, Larance M, James DE, Ramm G (2011) The serine/threonine kinase ULK1 is a target of multiple phosphorylation events. Biochem J 440:283–91. doi: 10.1042/BJ20101894

Baird L, Dinkova-Kostova AT (2011) The cytoprotective role of the Keap1–Nrf2 pathway. Arch Toxicol 85:241–272. doi: 10.1007/s00204-011-0674-5

Balinsky JB, Choritz EL, Coe CGL, van der Schans GS (1967) Amino acid metabolism and urea synthesis in naturally aestivating *Xenopus laevis*. Comp Biochem Physiol 22:59–68. doi: 10.1016/0010-406X(67)90166-1

Balinsky JB, Cragg MM, Baldwin E (1961) The adaptation of amphibian waste nitrogen excretion to dehydration. Comp Biochem Physiol 3:236–244. doi: 10.1016/0010-406X(61)90009-3

Bellerby CW (1938) Experimental studies on the sexual cycle of the South African Clawed Toad (*Xenopus laevis*). II. J exp Biol London 15:82–90

Biggar K, Dawson N, Storey K (2012) Real-time protein unfolding: a method for determining the kinetics of native protein denaturation using a quantitative real-time thermocycler. Biotechniques 53:231–8. doi: 10.2144/0000113922

Bradford MM (1976) A rapid and sensitive method for the quantitation of microgram quantities of protein utilizing the principle of protein-dye binding. Anal Biochem 72:248–254. doi: 10.1016/0003-2697(76)90527-3

Brewster LM (2018) Creatine kinase, energy reserve, and hypertension: from bench to bedside. Ann Transl Med 6:292–308. doi: 10.21037/atm.2018.07.15

Brooks SP (1992) A simple computer program with statistical tests for the analysis of enzyme kinetics. Biotechniques 13:906–11

Carling D, Thornton C, Woods A, Sanders MJ (2012) AMP-activated protein kinase: new regulation, new roles? Biochem J 445:11–27. doi: 10.1042/BJ20120546

Chiacchiera F, Simone C (2010) The AMPK-FoxO3A axis as a target for cancer treatment. Cell Cycle 9:1091–1096. doi: 10.4161/cc.9.6.11035

Chida K, Kasahara K, Tsunenaga M, et al. (1990a) Purification and identification of creatine phosphokinase B as a substrate of protein kinase C in mouse skin in vivo. Biochem Biophys Res Commun 173:351–357. doi: 10.1016/S0006-291X(05)81064-2

Chida K, Tsunenaga M, Kasahara K, et al. (1990b) Regulation of creatine phosphokinase B activity by protein kinase C. Biochem Biophys Res Commun 173:346–350. doi: 10.1016/S0006-291X(05)81063-0

Childers CL, Storey KB (2016) Post-translational regulation of hexokinase function and protein stability in the aestivating frog *Xenopus laevis*. Protein J 35:61–71. doi: 10.1007/s10930-016-9647-0

Childers CL, Storey KB (2019) Purification and characterization of a urea sensitive lactate dehydrogenase from skeletal muscle of the African clawed frog, *Xenopus laevis* . J Comp Physiol B 189:271–281. doi: 10.1007/s00360-018-1200-3

Chinopoulos C (2013) Which way does the citric acid cycle turn during hypoxia? The critical role of α-ketoglutarate dehydrogenase complex. J Neurosci Res 91:1030–1043. doi: 10.1002/jnr.23196

Cortright RN, Azevedo JL, Zhou Q, et al. (2000) Protein kinase C modulates insulin action in human skeletal muscle. Am J Physiol Metab 278:E553–E562. doi:

10.1152/ajpendo.2000.278.3.E553

Coughlan KA, Valentine RJ, Sudit BS, et al. (2016) PKD1 Inhibits AMPKα2 through Phosphorylation of Serine 491 and Impairs Insulin Signaling in Skeletal Muscle Cells. J Biol Chem 291:5664–75. doi: 10.1074/jbc.M115.696849

Cox TM, O'Donnell MW, Camilleri M, Burghes AH (1983) Isolation and characterization of a mutant liver aldolase in adult hereditary fructose intolerance. Identification of the enzyme variant by radioassay in tissue biopsy specimens. J Clin Invest 72:201–13. doi: 10.1172/jci110958

Craig PM, Moyes CD, LeMoine CMR (2018) Sensing and responding to energetic stress: Evolution of the AMPK network. Comp Biochem Physiol Part B Biochem Mol Biol 224:156–169. doi: 10.1016/J.CBPB.2017.11.001

Dagon Y, Hur E, Zheng B, et al. (2012) p70S6 kinase phosphorylates AMPK on serine 491 to mediate leptin's effect on food intake. Cell Metab 16:104–12. doi: 10.1016/j.cmet.2012.05.010

Dawson NJ, Biggar KK, Storey KB (2013) Characterization of fructose-1,6-disphosphate aldolase during anoxia in the tolerant turtle, *Trachemys scripta elegans*: An assessment of enzyme activity, expression and structure. PLoS One 8:e68830. doi: 10.1371/journal.pone.0068830

Dawson NJ, Biggar Y, Malik AI, Storey KB (2018) Increased transcript levels and kinetic function of pyruvate kinase during severe dehydration in aestivating African clawed frogs, *Xenopus laevis*. Comp Biochem Physiol Part B Biochem Mol Biol. doi: 10.1016/J.CBPB.2018.01.003

Dieni CA, Storey KB (2009) Creatine kinase regulation by reversible phosphorylation in frog muscle. Comp Biochem Physiol Part B Biochem Mol Biol 152:405–412. doi: 10.1016/J.CBPB.2009.01.012

Dieni CA, Storey KB (2014) Protein kinase C in the wood frog, *Rana sylvatica* : reassessing the tissue-specific regulation of PKC isozymes during freezing. PeerJ 2:e558. doi: 10.7717/peerj.558

Eder M, Schlattner U, Wallimann T, et al. (2008) Crystal structure of brain-type creatine

kinase at 1.41 Å resolution. Protein Sci 8:2258–2269. doi: 10.1110/ps.8.11.2258

Egan D, Kim J, Shaw RJ, Guan K-L (2011) The autophagy initiating kinase ULK1 is regulated via opposing phosphorylation by AMPK and mTOR. Autophagy 7:643–644. doi: 10.4161/auto.7.6.15123

Eggert C, Fouquet A (2006) A preliminary biotelemetric study of a feral invasive *Xenopus laevis* population in France. Alytes 23:144–149

Fujiwara N, Usui T, Ohama T, Sato K (2016) Regulation of Beclin 1 Protein Phosphorylation and Autophagy by Protein Phosphatase 2A (PP2A) and Death-associated Protein Kinase 3 (DAPK3) *. doi: 10.1074/jbc.M115.704908

Gamblin SJ, Davies GJ, Grimes JM, et al. (1991) Activity and specificity of human aldolases. JMolBiol 219:573–576. doi: 10.2210/PDB1ALD/PDB

Gatten RE (1987) Activity metabolism of anuran amphibians: Tolerance to dehydration. Physiol Zool 60:576–585. doi: 10.1086/physzool.60.5.30156131

Gibbs AG (2002) Water balance in desert Drosophila: lessons from non-charismatic microfauna. Comp Biochem Physiol Part A Mol Integr Physiol 133:781–789. doi: 10.1016/S1095-6433(02)00208-8

Gowans GJ, Hawley SA, Ross FA, Hardie DG (2013) AMP Is a True Physiological Regulator of AMP-Activated Protein Kinase by Both Allosteric Activation and Enhancing Net Phosphorylation. Cell Metab 18:556–566. doi: 10.1016/J.CMET.2013.08.019

Griffin ME, Marcucci MJ, Cline GW, et al. (1999) Free fatty acid-induced insulin resistance is associated with activation of protein kinase C theta and alterations in the insulin signaling cascade. Diabetes 48:1270–4. doi: 10.2337/diabetes.48.6.1270

Guppy M, Withers P (1999) Metabolic depression in animals: Physiological perspectives and biochemical generalizations. Biol Rev 74:1–40

Hand SC, Menze MA (2015) Molecular approaches for improving desiccation tolerance: insights from the brine shrimp Artemia franciscana. Planta 242:379–388. doi: 10.1007/s00425-015-2281-9

Hardie DG (2011) AMP-activated protein kinase: an energy sensor that regulates all aspects of cell function. Genes Dev 25:1895–908. doi: 10.1101/gad.17420111

Hardie DG, Carling D (1997) The AMP-activated protein kinase. Fuel gauge of the mammalian cell? Eur J Biochem 246:259–273. doi: 10.1111/j.1432-1033.1997.00259.x

Hardie DG, Carling D, Carlson M (1998) The amp-activated/SNF1 protein kinase subfamily: Metabolic sensors of the eukaryotic cell? Annu Rev Biochem 67:821–855. doi: 10.1146/annurev.biochem.67.1.821

Hardie DG, Pan DA (2002) Regulation of fatty acid synthesis and oxidation by the AMP-activated protein kinase. Biochem Soc Trans 30:1064–70. doi: 10.1042/

Hardie DG, Ross FA, Hawley SA (2012) AMPK: a nutrient and energy sensor that maintains energy homeostasis. Nat Rev Mol Cell Biol 13:251–262. doi: 10.1038/nrm3311

Hawkins LJ, Wang M, Zhang B, et al. (2019) Glucose and urea metabolic enzymes are differentially phosphorylated during freezing, anoxia, and dehydration exposures in a freeze tolerant frog. Comp Biochem Physiol Part D Genomics Proteomics 30:1–13. doi: 10.1016/J.CBD.2019.01.009

Hillman SS (1978a) Some effects of dehydration on internal distributions of water and solutes in *Xenopus laevis* . Comp Biochem Physiol -- Part A Physiol 61:303–307. doi: 10.1016/0300-9629(78)90113-5

Hillman SS (1978b) The roles of oxygen delivery and electrolyte levels in the dehydrational death of *Xenopus laevis*. J Comp Physiol B 128:169–175. doi: 10.1007/BF00689481

Hillman SS, Sommerfeldt RW (1981) Microsphere studies of amphibian systemic blood flow redistribution during dehydration, hypovolemia, and salt load. J Exp Zool 218:305–308. doi: 10.1002/jez.1402180223

Holden CP, Storey KB (1994) Purification and characterization of aldolase from the cold hardy insect *Epiblema scudderiana*: Enzyme role in glycerol biosynthesis. Insect Biochem Mol Biol 24:265–270. doi: 10.1016/0965-1748(94)90006-X

Horman S, Hussain N, Dilworth SM, et al. (2005) Evaluation of the role of AMP-activated protein kinase and its downstream targets in mammalian hibernation. Comp Biochem Physiol Part B Biochem Mol Biol 142:374–382. doi: 10.1016/j.cbpb.2005.08.010

Humphrey SJ, James DE, Mann M (2015) Protein phosphorylation: A major switch mechanism for metabolic regulation protein phosphorylation: A pervasive regulator of cellular metabolism. Trends Endocrinol Metab 26:676–687. doi: 10.1016/j.tem.2015.09.013

Hurley JH, Thorsness PE, Ramalingam V, et al. (1989) Structure of a bacterial enzyme regulated by phosphorylation, isocitrate dehydrogenase. Proc Natl Acad Sci U S A 86:8635–8639. doi: 10.1073/pnas.86.22.8635

Iacobazzi V, Infantino V (2014) Citrate – new functions for an old metabolite. Biol Chem 395:387–399. doi: 10.1515/hsz-2013-0271

Icard P, Poulain L, Lincet H (2012) Understanding the central role of citrate in the metabolism of cancer cells. Biochim Biophys Acta - Rev Cancer 1825:111–116. doi: 10.1016/J.BBCAN.2011.10.007

Janssens PA, Cohen PP (2003) Biosynthesis of urea in the estivating African lungfish and in Xenopus laevis under conditions of water-shortage. Comp Biochem Physiol 24:887–898. doi: 10.1016/0010-406x(68)90800-1

Jokumsen A, Weber RE (1980) Haemoglobin-oxygen binding properties in the blood of *Xenopus laevis*, with special reference to the influences of aestivation and of temperature and salinity acclimation. J Exp Biol 86:19–37

Jørgensen CB (1997) Urea and amphibian water economy. Comp Biochem Physiol Part A Physiol 117:161–170. doi: 10.1016/S0300-9629(96)00356-8

Katzenback BA, Dawson NJ, Storey KB (2014) Purification and characterization of a urea sensitive lactate dehydrogenase from the liver of the African clawed frog, *Xenopus laevis*. J Comp Physiol B 184:601–611. doi: 10.1007/s00360-014-0824-1

Kim J, Kim KY, Jang H-S, et al. (2009) Role of cytosolic $NADP^+$-dependent isocitrate dehydrogenase in ischemia-reperfusion injury in mouse kidney. Am J Physiol

Physiol 296:F622–F633. doi: 10.1152/ajprenal.90566.2008

Kim J, Kim YC, Fang C, et al. (2013) Differential Regulation of Distinct Vps34 Complexes by AMPK in Nutrient Stress and Autophagy. Cell 152:290–303. doi: 10.1016/J.CELL.2012.12.016

Kim JY, Shin JY, Kim M, et al. (2012) Expression of cytosolic NADP+-dependent isocitrate dehydrogenase in melanocytes and its role as an antioxidant. J Dermatol Sci 65:118–125. doi: 10.1016/J.JDERMSCI.2011.12.007

Koh H-J, Lee S-M, Sohn B-G, et al. (2004) Cytosolic NADP +-dependent Isocitrate Dehydrogenase Plays a Key Role in Lipid Metabolism Downloaded from. JBC Papers in Press

Kong M, Ditsworth D, Lindsten T, Thompson CB (2009) α4 Is an Essential Regulator of PP2A Phosphatase Activity. Mol Cell 36:51–60. doi: 10.1016/J.MOLCEL.2009.09.025

Kong X, Manchester J, Salmon S, et al. (1994) Glucose transporters in single skeletal muscle fibers:Relationship to hexokinase and regulation by contractile activity. J Biol Chem 269:12963–12967

Krivoruchko A, Storey KB (2013) Anoxia-responsive regulation of the FoxO transcription factors in freshwater turtles, Trachemys scripta elegans. Biochim Biophys Acta - Gen Subj 1830:4990–4998. doi: 10.1016/J.BBAGEN.2013.06.034

Lam EW-F, Francis RE, Petkovic M (2006) FOXO transcription factors: key regulators of cell fate. Biochem Soc Trans 34:722–6. doi: 10.1042/BST0340722

Lee ME, Dyer DH, Klein OD, et al. (1995) Mutational analysis of the catalytic residues lysine 230 and tyrosine 160 in the NADP+-dependent isocitrate dehydrogenase from *Escherichia coli*. 34:378–384

Lee SM, Koh H-J, Park D-C, et al. (2002) Cytosolic NADP+-dependent isocitrate dehydrogenase status modulates oxidative damage to cells. Free Radic Biol Med 32:1185–1196. doi: 10.1016/S0891-5849(02)00815-8

Lipskaya TY (2001) The Physiological Role of the Creatine Kinase System: Evolution of Views. Biochem 66:115–129. doi: 10.1023/A:1002858311553

Luu BE (2018) Molecular responses to whole-body dehydration in a sequenced vertebrate, Xenopus laevis: Regulation of antioxidants and metabolism by the Sirtuin protein deacetylases. Carleton University

Luu BE (2011) Regulation of protein translation and cell cycle processes by reversible protein phosphorylation in response to dehydration in the African clawed frog. Carleton University

Luu BE, Wijenayake S, Malik AI, Storey KB (2018) The regulation of heat shock proteins in response to dehydration in Xenopus laevis. Cell Stress Chaperones 23:45–53. doi: 10.1007/s12192-017-0822-9

MacDonald JA, Storey KB (2002) Purification and characterization of fructose bisphosphate aldolase from the ground squirrel, *Spermophilus lateralis*: enzyme role in mammalian hibernation. Arch Biochem Biophys 408:279–285. doi: 10.1016/S0003-9861(02)00579-9

Malik AI, Storey KB (2009a) Activation of extracellular signal-regulated kinases during dehydration in the African clawed frog, *Xenopus laevis*. J Exp Biol 212:2595–2603. doi: 10.1242/jeb.030627

Malik AI, Storey KB (2011) Transcriptional regulation of antioxidant enzymes by FoxO1 under dehydration stress. Gene 485:114–119. doi: 10.1016/J.GENE.2011.06.014

Malik AI, Storey KB (2009b) Activation of antioxidant defense during dehydration stress in the African clawed frog. Gene 442:99–107. doi: 10.1016/J.GENE.2009.04.007

Mammucari C, Milan G, Romanello V, et al. (2007) FoxO3 Controls Autophagy in Skeletal Muscle In Vivo. Cell Metab 6:458–471. doi: 10.1016/J.CMET.2007.11.001

McGee SL, Hargreaves M (2010) AMPK-mediated regulation of transcription in skeletal muscle. Clin Sci (Lond) 118:507–18. doi: 10.1042/CS20090533

McLeish MJ, Kenyon GL (2005) Relating Structure to Mechanism in Creatine Kinase. Crit Rev Biochem Mol Biol 40:1–20. doi: 10.1080/10409230590918577

Measey G, Tinsley R (1998) Feral *Xenopus laevis* in south Wales. Herpetol J 8:23–28

Merkle S (1989) Long-term starvation in Xenopus laevis daudin—III. Effects on

enzymes in several tissues. Comp Biochem Physiol Part B Comp Biochem 94:783–788. doi: 10.1016/0305-0491(89)90166-1

Merkle S, Hanke W (1988a) Long-term starvation in Xenopus laevis daudin—I. Effects on general metabolism. Comp Biochem Physiol Part B Comp Biochem 89:719–730. doi: 10.1016/0305-0491(88)90314-8

Merkle S, Hanke W (1988b) Long-term starvation in Xenopus laevis Daudin--II. Effects on several organs. Comp Biochem Physiol A Comp Physiol 90:491–5

Merkle S, Hanke W (1988c) Long-term starvation in Xenopus laevis daudin—II. Effects on several organs. Comp Biochem Physiol Part A Physiol 90:491–495. doi: 10.1016/0300-9629(88)90225-3

Miller K, Camilliere JJ (1981) Physical Training Improves Swimming Performance of the African Clawed Frog Xenopus

Murakami K, Iwata S, Haneda Miyako, Yoshino Masataka (1997) Role of metal cations in the regulation of NADP-linked isocitrate dehydrogenase from porcine heart. 10:169–174

Niesen FH, Berglund H, Vedadi M (2007) The use of differential scanning fluorimetry to detect ligand interactions that promote protein stability. Nat Protoc 2:2212–2221. doi: 10.1038/nprot.2007.321

Nishizuka Y (1995) Protein kinase C and lipid signaling for sustained cellular responses. FASEB J 9:484–496. doi: 10.1096/fasebj.9.7.7737456

Oakhill JS, Rohan S, Zhi-Ping C, et al. (2011) AMPK is a direct adenylate charge-regulated protein kinase. Nat Rev Mol Cell Biol 332:1433–1435. doi: 10.1126/science.1204592

Oakhill JS, Scott JW, Kemp BE (2012) AMPK functions as an adenylate charge-regulated protein kinase. Trends Endocrinol Metab 23:125–132. doi: 10.1016/J.TEM.2011.12.006

Olsen J V., Blagoev B, Gnad F, et al. (2006) Global, In Vivo, and Site-Specific Phosphorylation Dynamics in Signaling Networks. Cell 127:635–648. doi: 10.1016/J.CELL.2006.09.026

Pasha ST, Salahuddin A (1977) Isolation of buffalo muscle aldolase and comparison of its properties with those of rabbit muscle aldolase. Biochim Biophys Acta - Enzymol 483:435–442. doi: 10.1016/0005-2744(77)90071-7

Pelosse M, Cottet-Rousselle C, Grichine A, et al. (2016) Genetically encoded fluorescent biosensors to explore AMPK signaling and energy metabolism. Springer, Cham, pp 491–523

Ponticos M, Lu QL, Morgan JE, et al. (1998) Dual regulation of the AMP-activated protein kinase provides a novel mechanism for the control of creatine kinase in skeletal muscle. EMBO J 17:1688–99. doi: 10.1093/emboj/17.6.1688

Pross N (2017) Effects of Dehydration on Brain Functioning: A Life-Span Perspective. Ann Nutr Metab 70:30–36. doi: 10.1159/000463060

Ravnskjaer K, Boergesen M, Dalgaard LT, Mandrup S (2006) Glucose-induced repression of PPARa gene expression in pancreateic B-cells involves PP2A activation and AMPK inactivation. J Mol Endocrinol 36:289–299. doi: https://doi.org/10.1677/jme.1.01965

Rellos P, Sygusch J, Cox TM (2000) Expression, purification, and characterization of natural mutants of human aldolase B. Role of quaternary structure in catalysis. J Biol Chem 275:1145–51. doi: 10.1074/jbc.275.2.1145

Rider MH (2016) Role of AMP-activated protein kinase in metabolic depression in animals. J Comp Physiol B 186:1–16. doi: 10.1007/s00360-015-0920-x

Roach PJ (2011) AMPK -> ULK1 -> autophagy. Mol Cell Biol 31:3082–4. doi: 10.1128/MCB.05565-11

Ross FA, MacKintosh C, Hardie DG (2016) AMP-activated protein kinase: a cellular energy sensor that comes in 12 flavours. FEBS J 283:2987–3001. doi: 10.1111/febs.13698

Salih DAM, Brunet A (2008) FoxO transcription factors in the maintenance of cellular homeostasis during aging. Curr Opin Cell Biol 20:126–36. doi: 10.1016/j.ceb.2008.02.005

Sanchez AM, Csibi A, Raibon A, et al. (2012) AMPK promotes skeletal muscle

autophagy through activation of forkhead FoxO3a and interaction with Ulk1. J Cell Biochem 113:695–710. doi: 10.1002/jcb.23399

Sawka MN, Cheuvront SN, Kenefick RW (2015) Hypohydration and Human Performance: Impact of Environment and Physiological Mechanisms. Sport Med 45:51–60. doi: 10.1007/s40279-015-0395-7

Seymour RS (1973) Energy Metabolism of Dormant Spadefoot Toads (Scaphiopus). Copeia 1973:435. doi: 10.2307/1443107

Shang L, Wang & X (2011) AMPK and mTOR coordinate the regulation of Ulk1 and mammalian autophagy initiation. doi: 10.4161/auto.7.8.15860

Shechter I, Dai P, Huo L, Guan G (2003) IDH1 gene transcription is sterol regulated and activated by SREBP-1a and SREBP-2 in human hepatoma HepG2 cells: evidence that IDH1 may regulate lipogenesis in hepatic cells. J Lipid Res 44:2169–2180. doi: 10.1194/jlr.M300285-JLR200

Shin SW, Shin SW, Oh CJ, et al. (2009) Glutathionylation regulates cytosolic NADP $^{+}$ -dependent isocitrate dehydrogenase activity. Free Radic Res 43:409–416. doi: 10.1080/10715760902801525

Sinclair BJ, Stinziano JR, Williams CM, et al. (2013) Real-time measurement of metabolic rate during freezing and thawing of the wood frog, *Rana sylvatica* : implications for overwinter energy use. J Exp Biol 216:292–302. doi: 10.1242/jeb.076331

Singh P, Salih M, Leddy JJ, Tuana BS (2004) The muscle-specific calmodulin-dependent protein kinase assembles with the glycolytic enzyme complex at the sarcoplasmic reticulum and modulates the activity of glyceraldehyde-3-phosphate dehydrogenase in a Ca2+/calmodulin-dependent manner. J Biol Chem 279:35176–82. doi: 10.1074/jbc.M402282200

Smith CM, Bryza J, Williamsony JR (1974) Regulation of mitochondrial α-ketoglutarate metabolism by product inhibition at α-ketoglutarate dehydrogenase. 249:1497–1505

Somme L (1993) Anhydrobiosis and cold tolerance in tardigrades. Eur J Entomol 93:349–357

Stefanski M, Gatten RE, Pough FH (1989) Activity Metabolism of Salamanders: Tolerance to Dehydration. J Herpetol 23:45. doi: 10.2307/1564315

Storey KB (1987) Organ-specific metabolism during freezing and thawing in a freeze-tolerant frog. Am J Physiol 253:R292-7. doi: 10.1152/ajpregu.1987.253.2.R292

Storey KB (2016) Comparative enzymology—new insights from studies of an "old" enzyme, lactate dehydrogenase. Comp Biochem Physiol Part B Biochem Mol Biol 199:13–20. doi: 10.1016/J.CBPB.2015.12.004

Storey KB (1980) Kinetic properties of purified aldolase from flight muscle of *Schistocerca americana gregaria*. Role of the enzyme in the transition from carbohydrate to lipid-fueled flight. Insect Biochem 10:647–655. doi: 10.1016/0020-1790(80)90054-2

Storey KB (2010) Out cold: biochemical regulation of mammalian hibernation - a mini-review. Gerontology 56:220–30. doi: 10.1159/000228829

Storey KB (Kenneth B. (2004) Functional metabolism : regulation and adaptation. John Wiley & Sons

Storey KB, Storey JM (1990) Metabolic rate depression and biochemical adaptation in anaerobiosis, hibernation and estivation. Q Rev Biol 65:145–174. doi: 10.1086/416717

Storey KB, Storey JM (1984) Biochemical adaption for freezing tolerance in the wood frog,Rana sylvatica. J Comp Physiol B 155:29–36. doi: 10.1007/BF00688788

Storey KB, Storey JM (2004) Metabolic rate depression in animals: transcriptional and translational controls. Biol Rev 79:207–233. doi: 10.1017/S1464793103006195

Storey KB, Storey JM (2005) Oxygen Limitation and Metabolic Rate Depression. In: Storey KB (ed) Functional Metabolism. John Wiley & Sons, Inc., Hoboken, NJ, USA, pp 415–442

Storey KB, Storey JM (2010) Metabolic Regulation and Gene Expression During Aestivation. Springer, Berlin, Heidelberg, pp 25–45

Storey KB, Storey JM (2012) Aestivation: signaling and hypometabolism. J Exp Biol

215:1425–33. doi: 10.1242/jeb.054403

Storey KB, Storey JM (1986) Freeze tolerant frogs: cryoprotectants and tissue metabolism during freeze-thaw cycles. Can J Zool 64:49–56

Storey KB, Storey JM (2007) Tribute to P. L. Lutz: putting life on 'pause'--molecular regulation of hypometabolism. J Exp Biol 210:1700–14. doi: 10.1242/jeb.02716

Suter M, Riek U, Tuerk R, et al. (2006) Dissecting the role of 5'-AMP for allosteric stimulation, activation, and deactivation of AMP-activated protein kinase. J Biol Chem 281:32207–16. doi: 10.1074/jbc.M606357200

Sygusch J, Beaudry D, Allaire M (1987) Molecular architecture of rabbit skeletal muscle aldolase at 2.7-A resolution. Proc Natl Acad Sci 84:7846–7850. doi: 10.1073/PNAS.84.22.7846

Thomson DM, Winder WW (2009) AMPK control of fat metabolism in skeletal muscle. Acta Physiol 196:147–154. doi: 10.1111/j.1748-1716.2009.01973.x

Tinsley RC, Kobel HR (1996) The biology of Xenopus. Published for the Zoological Society of London by Clarendon Press

Tong JF, Yan X, Zhu MJ, Du M (2009) AMP-activated protein kinase enhances the expression of muscle-specific ubiquitin ligases despite its activation of IGF-1/Akt signaling in C2C12 myotubes. J Cell Biochem 108:458–468. doi: 10.1002/jcb.22272

Uchiyama M, Konno N (2006) Hormonal regulation of ion and water transport in anuran amphibians. Gen Comp Endocrinol 147:54–61. doi: 10.1016/J.YGCEN.2005.12.018

Unsworth BR, Crook EM (1967) The effect water shortage on the nitrogen metabolism of xenopus laevis. Comp Biochem Physiol 23:831–845. doi: 10.1016/0010-406X(67)90345-3

Wallimann T (2015) The extended, dynamic mitochondrial reticulum in skeletal muscle and the creatine kinase (CK)/phosphocreatine (PCr) shuttle are working hand in hand for optimal energy provision. J Muscle Res Cell Motil 36:297–300. doi: 10.1007/s10974-015-9427-z

Wallimann T, Dolder M, Schlattner U, et al. (1998) Creatine kinase: An enzyme with a

central role in cellular energy metabolism. Magn Reson Mater Physics, Biol Med 6:116–119

Wallimann T, Wyss M, Brdiczka D, et al. (1992) Intracellular compartmentation, structure and function of creatine kinase isoenzymes in tissues with high and fluctuating energy demands: the “phosphocreatine circuit” for cellular energy homeostasis

Wang C, Ma J, Zhang N, et al. (2015) The acetyl-CoA carboxylase enzyme: a target for cancer therapy? Expert Rev Anticancer Ther 15:667–676. doi: 10.1586/14737140.2015.1038246

Wang Y-G, Han X-G, Yang Y, et al. (2016) Functional differences between AMPK α1 and α2 subunits in osteogenesis, osteoblast-associated induction of osteoclastogenesis, and adipogenesis. Sci Rep 6:32771. doi: 10.1038/srep32771

Winder WW, Hardie DG, Mustard KJ, et al. (2003) Long-term regulation of AMP-activated protein kinase and acetyl-CoA carboxylase in skeletal muscle. Biochem Soc Trans 31:182–5. doi: 10.1042/

Wise DR, Ward PS, Shay JES, et al. (2011) Hypoxia promotes isocitrate dehydrogenase-dependent carboxylation of -ketoglutarate to citrate to support cell growth and viability. Proc Natl Acad Sci 108:19611–19616. doi: 10.1073/pnas.1117773108

Withers P (1993) Metabolic Depression During Estivation in the Australian Frogs, Neobatrachus and Cyclorana. Aust J Zool 41:467. doi: 10.1071/ZO9930467

Wu C-W, Storey KB (2014) FoxO3a-mediated activation of stress responsive genes during early torpor in a mammalian hibernator. Mol Cell Biochem 390:185–195. doi: 10.1007/s11010-014-1969-7

Wyss M, Kaddurah-Daouk R, Hoffmann- F, Roche L (2000) Creatine and Creatinine Metabolism

Xiao B, Sanders MJ, Underwood E, et al. (2011) Structure of mammalian AMPK and its regulation by ADP. Nature 472:230–233. doi: 10.1038/nature09932

Xu X, Zhao J, Xu Z, et al. (2004) Structures of human cytosolic NADP-dependent isocitrate dehydrogenase reveal a novel self-regulatory mechanism of activity. doi:

10.1074/jbc.M404298200

Zera AJ, Newman S, Berkheim D, et al. (2011) Purification and characterization of cytoplasmic NADP+-isocitrate dehydrogenase, and amplification of the NADP+-IDH gene from the wing-dimorphic sand field cricket, *Gryllus firmus*. J Insect Sci 11:53. doi: 10.1673/031.011.5301

Zhao S, Feng J, Li C, et al. (2019) Phosphoproteome profiling revealed abnormally phosphorylated AMPK and ATF2 involved in glucose metabolism and tumorigenesis of GH-PAs. J Endocrinol Invest 42:137–148. doi: 10.1007/s40618-018-0890-4